Proton and Deuterium NMR Experiments in Zero Field

LBL--21260

DE86 009952

John M. Millar
Ph.D. Thesis

Lawrence Berkeley Laboratory
University of California
Berkeley, California 94720

February 1986

Proton and Deuterium NMR Experiments in Zero Field

John M. Millar

This work was supported by the Director, Office of Basic Energy Sciences, Materials Sciences Division of the US Department of Energy under Contract DE-AC03-76SF-000-98.

Proton and Deuterium NMR Experiments in Zero Field

John M. Millar

Abstract

High field solid-state NMR lineshapes suffer from inhomogeneous broadening since resonance frequencies are a function of molecular orientation. Time domain zero field NMR is a two-dimensional field-cycling technique which removes this broadening by probing the evolution of the spin system under zero applied field. The simplest version, the sudden transition experiment, induces zero field evolution by the sudden removal of the applied magnetic field. Theory and experimental results of this experiment and several variations using pulsed dc magnetic fields to initiate zero field evolution are presented. In particular, the pulsed indirect detection method allows detection of the zero field spectrum of one nuclear spin species via another (usually protons) by utilizing the level crossings which occur upon adiabatic demagnetization to zero field. Experimental examples of proton/deuteron systems are presented which demonstrate the method results in enhanced sensitivity relative to that obtained in sudden transition experiments performed directly on deuterium. High resolution ^{2}H NQR spectra of a series of benzoic acid derivatives are obtained using the sudden transition and indirect detection methods. Resolution of the ν_o lines allows assignment of the spectra; in some cases allowing assignment to specific molecular sites. Computer simulations of the dipolar perturbed ^{2}H NQR spectrum of the methylene group in diethyl terephthalate allow assignment of the EFG tensor orientations. Librational oscillations in the water molecules of barium chlorate monohydrate are studied using proton and deuterium ZF

experiments. A difference in the amplitude of the librational modes produces a nonaxially symmetric dipolar tensor which yields a three line ^{1}H spectrum, similar to that of a spin 1 where $\eta \neq 0$. ^{1}H ZF experiments are used to study the ordering of a solute dissolved in a nematic liquid crystal. The zero field order parameter is found to be equal to that in high field within experimental error. The distribution of intensities in the zero field spectrum indicates little disordering occurs in zero field on a timescale of ~.5 sec. Appendices discuss equivalence of EFG tensor orientations and preliminary ^{14}N and low temperature experiments.

Acknowledgements

I would like to thank Professor Alex Pines for his continued support and encouragement during the course of this work. I would also like to thank the steady stream of talented graduate students, post-docs and visiting scientists with whom it has been my pleasure to work. I also wish to thank the members of the Departmental Machine Shop and Electronics Shop for their dedication and skill. I also must acknowledge the technical expertise of A. Bielecki without whom these experiments would have been impossible. Finally, I especially wish to thank my coworker A.M. Thayer who collaborated on these experiments.

Table of Contents

Chapter One: Introduction

I. Introduction

This thesis will deal with the very broad topic of Zero Field NMR concentrating mainly on experimental results. Before even introducing this topic it is necessary to briefly review a few fundamentals so that the later description of the Zero Field experiment can flow more smoothly. All of what follows in this chapter is common knowledge in NMR and one can refer to the fundamental texts on the subject for a more complete treatment.[1-4]

II. Hamiltonians

A). Zeeman

One of the most important aspects of the physics of nuclear spins is the manner in which they interact with an applied magnetic field. The angular momentum of a nuclear spin is quantized in the direction of a strong magnetic field and the state of a single spin can be described by two quantum numbers; the total spin I, and the component of spin angular momentum along the field, I_z. We denote such a state for a single spin, i, by $|I,m_i\rangle$ where the quantum number m_i is defined through

$$I_z \, |I_i \; m_i\rangle = m_i |I_i \; m_i\rangle \qquad . \qquad (1.1)$$

The quantum number I is equal to 1/2 for protons and we note

$$I_i^2 \, |I_i \, m_i\rangle = I_i(I_i+1) \, |I_i \, m_i\rangle \qquad (1.2)$$

By strong magnetic field we mean one such that the magnitude of the spin interaction with the field is much greater than the magnitude of any of the other possible spin interactions, such as the dipolar or quadrupolar interactions (we shall discuss below). In some of the fields used in the zero field experiments, the nuclear spins may not be quantized along the direction of the applied field. We shall bring up this point again later.

The magnetic moment of a nuclear spin tends to align with a large enough applied magnetic field. This is expressed by the Zeeman Hamiltonian which is given by

$$H_z = - \vec{\mu} \cdot \vec{B} \qquad (1.3)$$

where B is the applied magnetic field conventionally defining the $\hat{z}$ axis of the laboratory frame. The magnetic moment, μ, is given by

$$\vec{\mu} = \gamma h \vec{I}/2\pi \qquad (1.4)$$

and the constant γ is the gyromagnetic ratio, the ratio of the magnetic moment and the spin angular momentum of the nuclear spin. In high field the magnitude of the Zeeman interaction is generally greater than that of all other possible spin interactions. In a typical NMR magnet (~ Tesla) the Zeeman energy corresponds to a frequency on the order of a hundred MHz.

B). Chemical Shift

The chemical environment of the nuclear spin can exert an

influence on the Zeeman interaction. Basically, electrons in a magnetic field produce magnetic fields which can add constructively or destructively to the applied magnetic field. This can be expressed

$$H = \vec{\mu}(1 - \vec{\sigma})\,\vec{B}_o$$

$$= H_z + H_{cs} \qquad (1.5)$$

thereby defining the chemical shift Hamiltonian, H_{cs}. Chemical shifts tend to be rather small perturbations of the Zeeman interaction, their ratio being roughly $\sim 10^{-5}$ to 10^{-6} for protons. Under the normal one-dimensional high field detection schemes used in zero field experiments one can ignore the effects of H_{cs}.

C). Dipolar Hamiltonian

The dipolar interaction is analagous to the classical interaction between bar magnets. Two nuclear spins with spin angular momentum designated by I_1 and I_2, respectively, have a dipolar interaction described by the dipolar Hamiltonian

$$H_D = \frac{\gamma_1\gamma_2\hbar^2}{r_{12}^3\,(2\pi)^2}\left[\vec{I}_1\cdot\vec{I}_2 - 3(\vec{I}_1\cdot\hat{r}_{12})(\vec{I}_2\cdot\hat{r}_{12})\right] \qquad (1.6)$$

where $\hat{r}_{12}$ is a unit vector parallel to the internuclear vector between the spins labelled 1 and 2. Proton dipolar interactions in organic solids are generally on the order of tens of kHz, considerably less than the magnitude quoted above for the Zeeman interaction. Two distinct cases arise when dealing with H_D, namely the cases of high field and zero field.

1). High Field. In high field the dipolar Hamiltonian is

merely a perturbation of the larger Zeeman Hamiltonian and is therefore truncated by it. That is, one need only consider that part of the dipolar Hamiltonian which commutes with H_z. This truncated or secular Hamiltonian is written H_D^o, and $[H_D^o, H_z] = 0$. For two homonuclear spins we have

$$H_D^o = \frac{\gamma^2 h^2}{8\pi^2 r_{12}^3} \left[3I_{1z}I_{2z} - \vec{I}_1 \cdot \vec{I}_2 \right] \cdot (1 - 3\cos^2\theta_{12}) \tag{1.7}$$

where θ_{12} is the angle between the internuclear vector r_{12} and the applied magnetic field, conventionally defined as the laboratory $\hat{z}$ axis. Use of H_D^o amounts to a perturbation approach where one retains only those terms which contribute to the energy in first order. A more physical picture can be obtained by expanding the full dipolar Hamiltonian H_D in the following manner.[1]

$$H_D = \frac{\gamma_1\gamma_2 h^2}{(2\pi)^2 r^3} \left[A + B + C + D + E + F \right] \tag{1.8}$$

where

$$A = I_{1z}I_{2z}(1-3\cos^2\theta)$$
$$B = (I_{1z}I_{2z} - I_1 \cdot I_2)(1 - 3\cos^2\theta)/2$$
$$C = (I_{1z}I_{2+} + I_{1+}I_{2z})(-\frac{3}{2} \sin\theta\cos\theta \exp(-i\theta))$$
$$D = C^*$$
$$E = -\frac{3}{2} \sin^2\theta \exp(-i2\phi) I_{1+}I_{2+}$$
$$F = E^*$$

Examining the nonzero matrix elements of H_D between states $|m_1\ m_2\rangle$, one notes that the terms A and B connect states where $\Delta m = \Delta(m_1 + m_2)$

= 0 whereas terms C,D and E,F connect terms where $\Delta m = \pm 1$ and ± 2, respectively. Since the $\Delta m \neq 0$ terms are not energy conserving in high field they are not allowed.

b). Zero Field. In zero applied magnetic field there is no truncation due to H_z. Truncation from other sources can arise however, for example because of a quadrupolar interaction much larger than the dipolar interaction or perhaps rapid motion about some axis. These examples would result in truncation of H_D with respect to the electric field gradient principal axis or the rotation axis, respectively. For now we assume no such truncation is present and then the zero field Hamiltonian would simply be the full dipolar Hamiltonian.

D). Quadrupolar Hamiltonian

Nuclei with a nonspherically symmetric distribution of nuclear charge possess an electric quadrupole moment which interacts with an electric field gradient present at that nucleus.[1] This occurs for spins $I > 1/2$ and can be written as

$$H_Q = \frac{eQ}{2I\,(2I-1)} \quad \vec{I} \cdot V \cdot \vec{I} \tag{1.9}$$

where the elements of the electric field gradient tensor V are given by

$$V_{ij} = \frac{\partial^2 V}{\partial x_i \partial_j} \qquad i,j = x,y,z \tag{1.10}$$

and V is the electric potential at the nucleus due to all charges excluding those of the nucleus. One notes that the tensor is symmetric and traceless, i.e.

$$V_{xx} + V_{yy} + V_{zz} = 0 \tag{1.11}$$

as a consequence of LaPlace's equation. Being symmetric, the tensor can be diagonalized by a unitary transformation into what is known as its principal axis system (PAS). This corresponds to a change of the coordinate system in which the tensor is defined. The elements in this PAS are conventionally ordered (with no loss of generality)[2]

$$|V_{zz}| \geq |V_{xx}| \geq |V_{yy}| \tag{1.12}$$

and one can write

$$V_{PAS} = \begin{bmatrix} V_{xx} & 0 & 0 \\ 0 & V_{yy} & 0 \\ 0 & 0 & V_{zz} \end{bmatrix} = eq \begin{bmatrix} -1/2(1-\eta) & 0 & 0 \\ 0 & -1/2(1+\eta) & 0 \\ 0 & 0 & 1 \end{bmatrix}$$

where we have defined $eq = V_{zz}$ and the asymmetry parameter η is defined by

$$\eta = \frac{V_{yy} - V_{xx}}{V_{zz}} \quad .$$

In this quadrupolar principal axis system one can write

$$H_Q = \frac{e^2qQ}{h4I(2I-I)} \left[3I_z^2 - I^2 + \eta(I_x^2 - I_y^2) \right] \quad . \tag{1.13}$$

The term eq is conventionally referred to[2] as the electric field gradient and the term e^2qQ/h as the quadrupole coupling constant. It is important to realize that H_Q in equation (13) is written in terms of its principal axis system and that the z direction of this frame does not generally coincide with the laboratory z axis. To describe a system with a Zeeman interaction and a quadrupolar interaction one

must either write the Zeeman part in the coordinate system of H_Q or vice versa. We describe such transformations of a Hamiltonian from one coordinate system to another in the next section.

Note that the quadrupole moment Q is a constant for a given isotope of the same element[5] and measures the deviation of the nuclear charge from spherical symmetry.[1,4] Generally Q increases in magnitude as the mass of the nucleus increases.[5] Strictly speaking, Poisson's equation applies rather than LaPlace's when there is a nonzero probability of finding an electron inside the nuclear volume, however this contribution has been shown to be rather slight and can be ignored.[6] Experimental evidence to date shows that the sign of Q and eq are both positive for deuterons bonded to carbon[7,11] which is the situation we will encounter in later chapters.

III. Transformation of Tensors

We consider transformation of a tensor T from one coordinate system (x,y,z) to another (x',y',z'). Let r be a vector expressed in system (x,y,z) and r' the same vector expressed in the system (x',y',z'). Now let R be the rotation matrix which transforms r into r'. We have

$$r' = R\, r \quad . \tag{1.14}$$

Transformation of T(x,y,z) to T(x',y',z') is accomplished by

$$T' = R\, T\, R^{-1} \quad . \tag{1.15}$$

If we represent r as a column vector, then the matrix corresponding to a 180^0 rotation about the z axis is simply

$$R = \begin{bmatrix} -1 & 0 & 0 \\ 0 & -1 & 0 \\ 0 & 0 & 1 \end{bmatrix} \quad . \qquad (1.16)$$

Transformations of one coordinate system to another are often described in terms of the Euler angles α,β,γ described in detail elsewhere[8,9] and illustrated in figure 1.1. The operator $R(\alpha\beta\gamma)$ applied to the coordinate system (xyz) amounts to rotation about the z axis by the angle α to produce the new system (x',y',z'). Next, one rotates by the angle β about the y' axis to form the system (x'',y'',z''). Finally one rotates by γ about the z'' axis to form the system (x''',y''',z'''). The operator $R(\alpha\beta\gamma)$ is written

$$R(\alpha\beta\gamma) = R(\gamma)_{z''}\, R(\beta)_{y'}\, R(\alpha)_{z} \qquad (1.17)$$

and the corresponding matrix is given by[12]

$$R = \begin{bmatrix} \cos\alpha\cos\beta\cos\gamma - \sin\alpha\sin\gamma & \sin\alpha\cos\beta\cos\gamma + \cos\alpha\sin\gamma & -\sin\beta\cos\gamma \\ -\cos\alpha\cos\beta\sin\gamma - \sin\alpha\cos\gamma & -\sin\alpha\cos\beta\sin\gamma + \cos\alpha\cos\gamma & \sin\beta\sin\gamma \\ \cos\alpha\sin\beta & \sin\alpha\sin\beta & \cos\beta \end{bmatrix} \quad . \qquad (1.18)$$

Note we follow the usual convention[8-10] that rotations of a coordinate system about an axis u_i are performed in such a way that when one looks out the axis a positive rotation moves the coordinate system in a clockwise manner.

IV. High Field Density Operator

The density operator applicable for a spin system in equilibrium

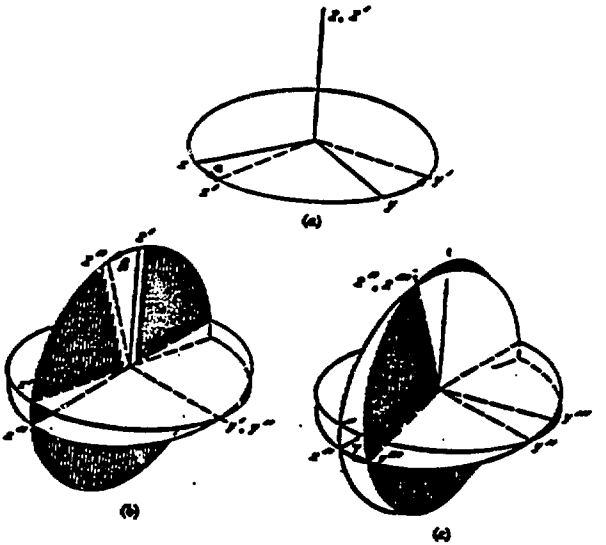

Figure 1.1 Transformation from coordinate system (x,y,z) to (x'',y'',z'') by use of Euler angles.

a) Rotation about z axis by angle α produces new system (x',y',z').

b) Next, one rotates by angle β about the y' axis to produce coordinate system (x'',y'',z'').

c) Finally, one rotates by angle γ about the z'' axis to produce (x''',y''',z''').

and at temperature T describable by a Hamiltonian H is given exactly by[4]

$$\rho = e^{H/kT} / \sum_i e^{H_i/kT} \tag{1.19}$$

which in the high temperature approximation ($H_i \ll kT$) becomes

$$\rho = (1 - H/kT) / \sum_i (1 - H_i/kT) \tag{1.20}$$

$$= (1 - H/kT) / \sum_i (1)$$

We note that the interaction energy of a single proton in a four Tesla field corresponds to a temperature of $\sim 10^{-2}$ K, thus the high temperature approximation should hold in nearly all commonly encountered situations. The first term in equation (20) is proportional to unity and will be invariant during any experiment. Therefore we will follow the common practice of defining a reduced density operator which omits this first term. We retain the same symbol for this reduced operator and write

$$\rho = cH \tag{1.21}$$

where the constant c follows from equation (20) and often will be omitted.

V. Chapter One References

1. A. Abragam, "The Principles of Nuclear Magnetism," (Oxford, London, 1961)
2. U. Haeberlen, "High Resolution NMR in Solids, Selective Averaging," Advances in Magnetic Resonance, J.S. Waugh, editor, (Academic, New York, 1976), Supplement I.
3. C.P. Slichter, "Principles of Magnetic Resonance," (Springer Verlag, Berlin, 1980).
5. R.S. Drago, "Physical Methods in Chemistry," (Saunders, Philadelphia, 1977).
6. M.H. Cohen and F. Reif, "Nuclear Quadrupole Effects in Nuclear Magnetic Resonance," Solid State Physics 5, 321(1957).
7. C. Muller, S. Idziak, N. Pislewski and U. Haeberlen, J.Magn. Reson. 47, 227(1982).
8. J. Mathews and R.L. Walker, "Mathematical Methods of Physics," (Benjamin, Menlo Park, 1970).
9. B. Silver, "Irreducible Tensor Methods," (Academic, New York, 1976).
10. A.R. Edmonds, "Angular Momentum in Quantum Mechanics," (Princeton, Princeton, 1974).
11. M. Rinne and J. Depireux in "Advances in Nuclear Qradrupole Resonance, J.A.S. Smith, editor, (Heyden, London, 1974) 1, 357.
12. M. Mehring, High Resolution NMR in Solids, (Springer-Verlag, Berlin, 1983), Second Edition.

Chapter Two. Introduction to the Zero Field Experiment

I. Introduction

High field solid state magnetic resonance involves the study of molecules by the perturbation that their internal interactions exert on the nuclear spin Zeeman interaction. These internal interactions e.g. dipolar and quadrupolar, are of great value since they allow one to probe the material at the molecular level and gain precise structural and bonding information. The resonance frequency of a particular molecule depends upon its orientation with respect to the applied field. Therefore the lineshapes of amorphous or polycrystalline materials can be quite broad, since their continuous range of molecular orientations produces a continuous range of frequencies which are superposed to form the "powder" spectrum. These linewidths, which are on the order of the internal interactions, are produced solely because of the inequivalence of molecular orientations in the applied field. This broadening presents a serious impediment to the use of NMR to study these samples because it produces a decrease in sensitivity and loss of spectral resolution. This broadening can be removed, however, simply by removal of the applied field. Without the applied field, the internal Hamiltonians become identical for all orientations of the molecular frame and the allowed transition frequencies directly reflect the internal interactions themselves rather than their perturbation of the Zeeman interaction. This is the basic idea of the time-domain zero field experiment which will be the subject of this thesis. There are several variations but

the two main branches, dipolar[1,2] and quadrupolar[3], are quite similar in their theory and concept. Therefore we begin with a qualitative description of the former. In this chapter we shall also discuss alternative methods of the experiment and touch upon related frequency domain experiments.

II. The Sudden Transition Zero Field Experiment

A). Qualitative Description

The experiment we describe is a field cycling variation of the two dimensional experiment;[3,4] the evolution of the spin system during one time period is probed indirectly during a second. A high magnetic field (~4 Tesla) is used to polarize the sample and create a magnetiztion M_z along the direction of the applied field. Schematically this field is removed "suddenly" and the sample previously in an eigenstate of the high field Hamiltonian finds itself under the influence of the zero field Hamiltonian. Since the high field eigenstates generally differ from those of zero field, the spin system evolves. For a dipolar system, this evolution corresponds to precession of M_z about the local fields. After a variable time, t_1, the field is replaced suddenly and $M_z(t_1)$ is recorded. The sequence of $M_z(t_1)$'s forms an interferogram which maps out the time evolution of the spin system during the time period t_1. Fourier transformation of this interferogram produces the zero field frequency spectrum.

B). The Sudden Transition Field Cycle

The technical details have been recently reviewed[5] and are also discussed in Appendix IV.2. The basic (slightly stylized) experi-

mental field cycle is shown in Figure 2.1. First the sample is polarized in high field for a time $\geq T_1$. The sample is then mechanically shuttled to an intermediate field B_{int} which fulfills the equation

$$|\gamma h I_z B_{int} / 2\pi| \gg H_{ZF} \tag{2.1}$$

where H_{ZF} is the zero field Hamiltonian. This intermediate field is switched off suddenly and the magnetization evolves under the zero field Hamiltonian for a variable time t_1 after which the intermediate field is switched back on suddenly. The sample is then returned to high field where the z component of the magenetization is measured as a function of t_1. The requirement of sudden switching of B_{int} at the initiation and conclusion of the zero field evolution period can be explicitly expressed as

$$|H_{ZF} t_{SW}| \ll 1 \tag{2.2}$$

where t_{SW} is the switching time of B_{int}. Physically this means that little or no spin evolution occurs during the switch-off or switch-on of B_{int}.

C). The Signal Function

In practice the samples move between the four Tesla B_o field to the 100 Gauss field in a time ~100 ms. With typical zero field frequencies ranging from 1 kHz to 150 kHz, this demagnetization can be considered quantum mechanically adiabatic.[6] Combined with the requirement of equation (2.1), this means the density operator describing the spin system in the field B_{int} will still be proportional to the high field Hamiltonian. Neglecting constants we have

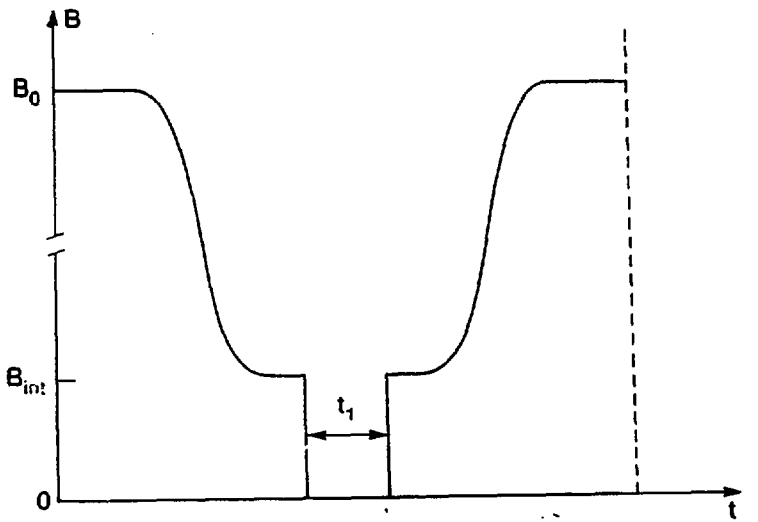

Figure 2.1). Idealized field cycle for the sudden-transition zero field experiment. Initially the sample is polarized in high magnetic field, here shown as 4 Tesla. After polarization, the sample is shuttled to an intermediate field, B_{int} ~.01 Tesla. At time t_1 = 0 B_{int} i suddenly switched off to initiate evolution in zero field. After the variable time period t_1 the field B_{int} is suddenly switched back on and the sample returned to high field where M_z is then measured as a function of t_1. The sequence of $M_z(t_1)$'s forms $S(t_1)$ which when Fourier transformed yields the zero field frequency spectrum.

$$\rho(t_1 = 0_-) = I_{z,lab} \tag{2.3}$$

where $t_1 = 0_-$ indicates the time just before the sudden switch-off of B_{int} and the operator $I_{z,lab}$ is the angular momentum operator referenced to the lab frame. The density operator a time t_1 after the switch-off of the field is given by

$$\rho(t_1) = U_{ZF}(t_1)\ I_{z,lab}\ U_{ZF}^{-1}(t_1) \tag{2.4}$$

where $U_{ZF}(t_1) = \exp(-iH_{ZF}t_1)$. Now at time t_1, B_{int} is suddenly switched on and the z component of the magnetization is "trapped" by the field. Adiabatic remagnetization of the sample to high field then allows detection of this magnetization (since the magnetization is invariant to an adiabatic demagnetization or remagnetization[7]). Therefore, the signal function is given by

$$S(t_1) = \langle I_{z,lab}(t_1) \rangle$$

$$= \mathrm{Tr}\left[I_{z,lab}\ U_{ZF}(t_1)\ I_{z,lab}\ U_{ZF}^{-1}(t_1) \right] \quad . \tag{2.5}$$

D). Example of Isolated Proton Pair

We now consider the effect of the zero field experiment on a single proton pair and then will generalize this to describe a powder sample. We start by defining a molecular frame whose z axis is defined by the internuclear vector of the proton pair. We can write $I_{z,lab}$ in terms of the molecular frame operators by

$$I_{z,lab} = I_{x,M}\sin\theta\cos\phi + I_{y,M}\sin\theta\sin\phi + I_{z,M}\cos\theta \qquad (2.6)$$

where now $I_{x,M}$, $I_{y,M}$ and $I_{z,M}$ refer to the spin variables of the molecular frame and θ,ϕ are the molecular frame spherical polar coordinates describing the orientation of a unit vector in the laboratory z direction. The full dipolar Hamiltonian describing the interaction between two protons in this frame is given by[8]

$$H_D = \frac{\gamma_1\gamma_2\hbar^2}{r_{12}^3\ (2\pi)^2}\left[I_{1,M}\cdot I_{2,M} - \frac{3(\vec{I}_{1,M}\cdot\vec{r}_{12})(\vec{I}_{2,M}\cdot\vec{r}_{12})}{r_{12}^2}\right] \qquad (2.7)$$

which reduces to

$$H_D = \frac{\gamma_1\gamma_2\hbar^2}{r_{12}^3}\left[I_{1,M}\cdot I_{2,M} - 3I_{1z,M}I_{2z,M}\right] \qquad (2.8)$$

since r_{12} is parallel to the molecular z axis. The eigenstates of H_D written in the product states $|I_{1z,M}\ I_{2z,M}>$ are given by

$$\begin{aligned} |1> &= |++> \\ |2> &= (|+-> + |-+>)/2^{1/2} \\ |3> &= |--> \\ |S> &= (|+-> - |-+>)/2^{1/2} \end{aligned} \qquad (2.9)$$

The expression for the high field signal is obtained using equations 2.5, 2.6 and 2.9. The normalized signal (ignoring constants is given by

$$S(t_1) = \frac{1}{2}\left[\cos^2\theta + \sin^2\theta\ \cos\omega_D t_1\right] \qquad (2.10)$$

where we have defined ω_D by

$$\omega_D = \frac{3\gamma^2 h}{4\pi r^3} \tag{2.11}$$

One calculates the normalized signal for a powder distribution as

$$S(t_1)_{powder} = \int_0^{2\pi} d\phi \int_0^{\pi} S(t_1) \sin\theta d\theta \Big/ \int_0^{2\pi} d\phi \int_0^{\pi} \sin\theta d\theta$$

$$= (1 + 2 \cos\omega_D t_1)/2 \tag{2.12}$$

which results in a frequency spectrum consisting of three equal intensity lines, one at zero frequency and one each at $\pm\nu_D = 3\gamma^2 h/4\pi r^3$.

E). Practical Considerations

The major factor determining the suitability of samples for the zero field experiment is the sample's T_1. More precisely the T_1 at all fields between B_o and zero field needs to be several times greater than the time necessary to perform one field cycle of the experiment. This consists of a trip to zero field (~100 ms) followed by the turn-on of the high inductance bucking coil (~50 ms) and finally a trip back to B_o (~100 ms) for a total of about 250 ms.

Another factor is the interpretability of the data. The isolated proton case described above is an example of a simple dipolar zero field experiment. As the number of coupled intermolecular and intramolecular coupled spins increases, so too does the complexity of the zero field spectrum. For n > 2, computer simulations are necessary for interpretation. Still some beautiful examples have been demonstrated where proton diplar zero field NMR can provide precise structural information.[1,2]

A related point is concerned with motion and the zero field experiment. As long as the system is static or in the limit where the correlation time of the motion is much greater than any zero field frequencies, the spectrum is easy to interpret or simulate. All other cases can be quite complex and require a stochastic Liouville treatment.[9] Thankfully the great majority of the samples we examine will fall into either the static or fast motion limits and we need not consider the matter.

F). The Real Field Cycle

To be completely correct in describing the experimental method we shall describe the actual field cycling method used, shown in Figure 2.2. The theory and description of the experiment do not change as long as equation (2.1) still holds. As in Figure 2, the sample is shuttled from B_o to a field B_{int} which is simply the fringe field of a superconducting magnet. One cannot turn off the fringe field so at least one additional field must be applied to cancel out the fringe field and produce the zero field region. In practice two extra fields are used, shown as B_1 and B_2 in Figure 2. We note the zero field experiment has two major technical requirements for the field cycle:

1) There must be a sudden transition from B_{int} to zero field. Stated simply, the inverse of the transition time or switching time must be much greater than any frequencies in the zero field spectrum. For protons, the maximum spectral frequency is ~40 kHz, so one needs $t_{sw} \ll 25\ \mu s$.

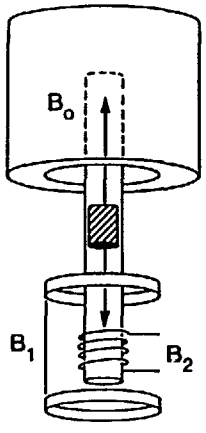

$$B = B_0 + B_1 + B_2$$

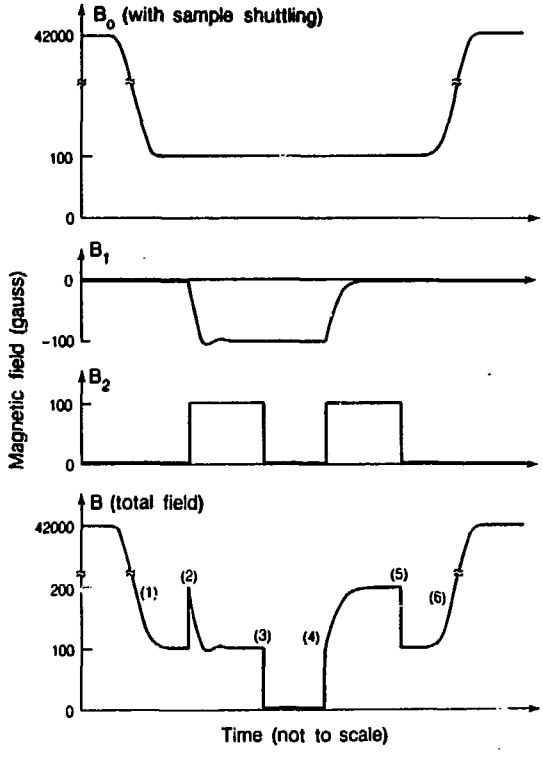

XBL 854-10155

Figure 2.2). Experimental field cycle and arrangement of field switching coils. The three fields shown here, B_o, B_1 and B_2 combine to form the zero field region. The sample is shuttled from the high field region to a region directly below it, which we call the zero field region. The fringe field there (produced by B_o) is -100 Gauss. After the sample arrives in the zero field region B_1 (the" bucking coil") and B_2(the intermediate field or "IF" coil) are switched on. B_2 reaches its maximum field much faster than B_1 since it has a much smaller inductive time constant and the resulant field is shown at bottom right. B_1 is a carefully regulated field designed to be as homogeneous as possible over the sample zero field region. B_2 is not carefully regulated and is relatively inhomogeneous. Use of the two coils B_1 and B_2 effectively separates out the requirements of good homogeneity and fast switching, making the electronics more manageable.

(This page inserted to preserve numbering)

2) The zero field region must be homogeneous over the sample.

One should recall that the time constant with which a magnetic field can be switched is given by $\tau = L/R$ where L is the inductance of the field coil and R its series resistance. Now the inductance scales roughly with the volume of the coil but so does its homogeneity. Since a small solenoid has a small inductance, it isoptimal for the first requirement but poor for the second. (Here small means close in dimensions to the sample itself.) A large solenoid is ideal for the second requirement but poor for the first. The problem can be solved by going to the coil system shown in Figure 2.2 because the two opposing requirements are "separated out." With this arrangement, after the sample is shuttled to the fringe field both B_1 and B_2 are turned on. B_2 reinforces the fringe field and B_1 opposes the fringe field. The time constants τ_1 and τ_2 are typically 20 ms and 0.1 μs respectively and the field cycle shown at bottom right in Figure 2.2 is produced. In the real field cycle, equation (2.1) should be interpretated using B_{fringe} in place of B_{int}. All ^1H zero field experiments used fringe fields of ~ 100 Gauss whose Zeeman frequency corresponds to 400 kHz. The ^2H sudden zero field NQR experiments used fringe fields of only 350 Gauss whose corresponding Zeeman frequency of 230 kHz is not much greater than the typical quadrupole frequencies of 150 kHz. The eigenstates of the 350 Gauss field are eigenstates of $H_Q + H_Z$ and so one expects a decrease in sensitivity and possible phase distortions in the zero field spectrum. For this reason one would like to go to even higher switching fields in the sudden transition experiments or perhaps use adiabatic demagnetization to

zero field followed by excitation of the zero field spectrum by large dc pulsed fields. (This method is described in Chapter 3.)

II. Related Field Cycling Methods and Possible Alternatives

A). Alternatives

There are several possible alternative methods by which one can perform the time domain zero field experiment which we shall briefly mention. First, the sudden transition experiment described above involves a net magnetization which oscillates during the evolution period t_1. In principle the evolution of this magnetization in zero field could be detected directly by use of an appropriately mounted coil. However, Faraday's Law states that the voltage induced in that coil would be proportional to the precession frequency of the magnetization. In the present experiments a substantial gain in sensitivity is then obtained by detection in a high magnetic field where the precession frequencies range from 20 MHz to 180 MHz rather than the 1 kHz to 150 kHz observed in the zero field spectra of proton dipolar systems and ^2H quadrupolar systems.

An alternative idea is to use a SQUID (Superconducting Quantum Interference Device) magnetometer as an ultralow noise preamp to detect the zero field signal in zero field. Recent NQR experiments using SQUID's have demonstrated the feasibility of this method.[10]

Another alternative method would be to perform the zero field experiment by switching off the B_0 field itself, thereby eliminating the need to mechanically shuttle the sample. One group performing relaxation measurements manages to switch fields of 1.5 T in times of ~25 ms.[11] Such switching times are insufficient for the sudden

experiment, but the experiment could be performed in conjunction with pulsed intermediate fields similar to those employed here. The obvious advantage with such switching fields is that the transition time from B_o to B_{int} would be cut significantly from that obtained with mechanical shuttling and the method would lessen the T_1 constraints which limit suitable samples.

B). Related Field Cycling Methods

Field cycling experiments are nothing new, and different versions have been reported as early as 1951. In that year, Ramsey and Pound[12] found that a sample of LiF polarized in a high field magnet would resonantly absorb energy in zero applied field. The absorption, due to spin 3/2 ^{7}Li, was the first example of a frequency domain field cycling NQR experiment. A complete review of the subject is beyond the scope of this work. These experiments and their double resonance analogues[13-15] are the subject of a vast amount of experimental work which has been reviewed elsewhere.[16] We note that the zero field indirect detection experiments described in Chapter III are the time domain version of Hahn's experiments[15] in which the NQR spectrum of the deuterons is detected by virtue of level crossings which occur during the field cycle. Field cycling techniques have also been used for the study of longitudinal relaxation in fields $\sim H_{local}$[17] and also for the study of T_1's as a function of applied field.[11,18,19]

IV.A Appendix - Experimental Details

1). Apparatus for Pulsed Magnetic Fields

a). Bucking Coils

Two pulsed coils were used for the sudden transition experiments. Both are situated in the fringe field under the superconducting magnet. They are referred to as the bucking coil and IF (intermediate field) coils and correspond to B_1 and B_2 respectively in Figure 2.2. Dimensions of each as well as construction details are given in reference (5). The B_1 coil used is ~11 cm in diameter and 13 cm in length. It is powered by a current regulating current pulser which is adjusted so that B_1 coil cancels or "bucks out" the fringe field as exactly as possible over the sample region. Regulation is estimated to be better than 0.1%. In practice the B_1 coil consists of a top and bottom loop of different lengths. This asymmetry produces a gradient designed to cancel the gradient of the fringe field. (An independent gradient shim coil provides further control.)

External inductors were added in series with the bucking coil itself to tailor the B_1 vs. time response. This was necessary because the level crossing experiments required a smooth slow transition through the level crossing of proton and deuteron energy levels. Two 20 mH inductors were typically used in series with the B_1 (bucking) coil. (These inductors were Triad C-48U "Filter Reactors", available at LBL.)

b). Intermediate Field "IF" Coil

The restrictions on regulation of the IF coil current and the homogeneity of the B_2 field thus produced are not so severe as those

on the bucking coil. All that is required is that equation 2.1 is held over all regions of the sample. This is because the IF coil is turned off during the zero field evolution period. One can estimate that the 100 Gauss system we used actually fluctuated by ~±5 Gauss. The 100 Gauss IF field was produced with a 25 Ω noninductive series resistance (Actually we used two 175 W/50 Ω resistors in series. These are stock # 2404 from Ohmite Mfg. Co., Skokie, Illinois 60076). Fields as high as 350 Gauss could be produced by change of the series resistor to ~6.2 Ω (produced using a combination of 10 Ω/12 W resistors, stock # 2051. Stock #2050, a 12W/5Ω resistor is also useful.) This represents the practical safe current limit because at this level one observes voltage spikes between the source and drain of the transistors used in the IF current pulser (Siliconix IF 450 or 451's) which approach the 400 volt maximum quoted by the manufacturer. Any higher risks (and usually results in) transistor burnout.

c). Current Pulsers and DC Supplies

All current pulsers (IF, Bucking, and those used for the transverse field of Chapter 7's liquid crystal experiments) and all high voltage unregulated IF power supplies were homebuilt from plans provided by A. Bielecki. The IF supplies drooped from 180 volts to as low as 140 depending upon the demands of the pulsed output. Commercial supplies were used for the bucking coils. At various times we employed a Sorenson "Nobatron" DCR 60-13 A or a Lambda LA 200-03BM. Upgrades for the high voltage IF supplies were obtained (Sorenson SRL 60-35, 60 V @ 35 amps) but have not been extensively tested. These upgrades could be run in series to obtain a 180 Volt 35 amp source which should produce virtually no droop over any zero field cycle.

A commercial high power current pulser for future experiments on low γ nuclei was obtained from Cober Electronics (Stamford, CT), model 606P capable of 1200 Volts at 5 amps. This has not been extensively tested at present.

d). Shims

A crude shim system was used with the 100 Gauss fringe field operation to "fine tune" the zero field region. Three coils were used, one in the lab x and y directions (defined as perpendicular to the applied field, B_o) plus a gradient coil in the lab z direction, all mounted on the bucking coil support. An old shim power supply was used, it was capable of up to 2.0 amps/channel. With good alignment of the bucking coil very little current was necessary in the x,y directions (< 10 mA) and usually $< .3$ A in the z gradient. The shim fields produced with maximum current were ≤ 2 Gauss in all cases.

2). Samples and Shuttling

The sample shuttling system has been described in detail elsewhere. Shuttles made of Kel-F of nylon (sample volume ~ .3 cm^3) traveled in a standard 10 mm o.d. glass tube. "True bore" tubing did not seem to offer any advantages. The glass tubes were remarkably free from breakage, generally we lost only one tube every few months or so under nearly continuous running (24 hr/day).

3. High Field Detection

a). RF Circuitry

i). Probe

All probes were homebuilt. All room temperature zero field

probes were built to accommodate the 10mm shuttle tubes. Ninety times of ~1.5 μs were typical using rf powers of 400-500 Watts. The schematic of a typical probe is shown in the Figure 2.3

ii). Pulsed Spin Locking

High field detection was accomplished by use of a pulsed spin locking sequence[20]:

$$90_x\text{-}\tau_1\text{-}90_y\text{-}(\tau_2\text{-}t_p\text{-}\tau_3\text{-}\theta_y)N$$

where t_p signifies a trigger pulse (TP1) sent to the data acquisition system, at these points the spectrometer basically samples the magnetization. Times for typical proton and deuteron systems are given in Table AI below. In practice we would usually optimize the θ

Table A.I Typical times for spinlocking sequence

	protons	deuterons
τ_1	20 μs	24.5 μs
τ_2	25 μs	31 μs
τ_3	15 μs	19 μs
t_{90}	6.2μs	6.2 μs
t_θ	5.8μs	5.6 μs

pulse length for each different compound, but nearly all showed this behavior that a pulse close to a ninety gave the largest, longest lived signal. The proton times quoted were found for barium chlorate

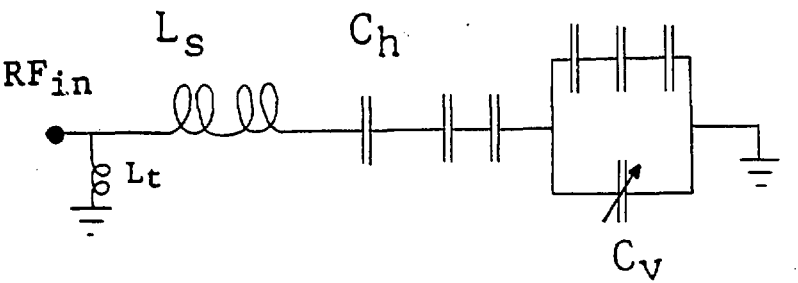

Figure 2.3). Schematic of typical zero field ^1H probe (tuned for 130 MHz). L_S is a Helmholtz, with 2 turns/side and ~1 cm in diameter. L_t is a matching inductor typically 1 turn with diameter of about 3 mm; adjustment is performed by mashing. C_h is a homebuilt capacitor made of ~1cm diameter brass tubing, teflon and center conductor from 1/4" rigid coax. The version we used was ~1 pf, and with it the probe could take well over 1 kW rf power over a 2048 pt pulsed spin locking cycle. We generally did not need to resort to homebuilt capacitors; this case was unusual in that we required an extremely high power capacitor with very low capacitance. The five unmarked capacitors in the figure are high voltage 20 pf Centralab capacitors (available LBL). C_v is a Voltronics variable capacitor, ~1 - 10 pf.

monohydrate, which is approximately an isolated two spin system. Coupled systems of more then two protons might behave more like the deuteron cases.

iii). RF Amplifiers

Protons

Proton work was conducted using an ENI 5100L to drive a Henry Radio 1001 which had been modified by Don Wilkinson of the UCB Department of Chemistry Electronics Shop. The AC input into the Henry was obtained from a voltage filter. An external DC supply (3.5 kV, 100 mA Drawing #7S1174) was used for the plate voltage as the voltage supplied by the Henry's internal supply was unregulated.

With careful tuning approximately 1 kW pulsed rf power could be obtained with the setup. Routine work used ~500 W for which we obtained ninety times of ~1.0 μs. Pulse shapes from the Henry were usually poor. The noisy output of the Henry required several diode boxes.

Deuterium

^{2}H rf was provided by a Drake L7 driven by an ENI 5100L. The Drake had been modified by D. Wilkinson and maximum power was ~1.5 kW, but typical was ~900 W with which we obtained ninety degree pulse times of ~6 μs.

b). Data Collection

i). Temp Routine

The Temp routine was written by D. Zax in order to facilitate the zero field experiments. The program was able to run an entire zero field experiment and collect data in high field. The command is

executed in operating system of the spectrometers (program "Spec") by typing:

Temp &1 &2 &3 &4 &5 &6 &7 &8 &9 &10

where &n represents an argument described in Table AII below.

Table AII. Temp Routine Arguments

Argument	
&1	points inthe t_1 fid (zero field fid)
&2	initial point number for t_1 fid
&3	first value for pulse programmer register FA (this defines the zero field evolution time)
&4	FA increment (units of μs)
&5	lower bound for average in high field fid
&6	upper bound for average in high field fid
&7	phase cycling option: 1 = x only 2 = x then -x, stored at 2049 and 6145, respectively 3 = (x)-(-x) stored at 2049
&8	NFID in high field
&9	number of times to run average over each t_1 point
&10	scope update option; update after each shot 0=yes 1=no

ii). Signal Processing

In general we felt that the t_1=0 point of a zero field fid should not be included in the Fourier transform because of imperfections in

the field switching. To obtain better signal to noise one could take the zero field fid and use the spectrometer MX (mix) command to put all the signal in one buffer. Then clearing the "no signal" buffer and Fourier transforming the single nonzeroed buffer resulted in a $2^{1/2}$ improvement in signal to noise. The resulting frequency spectrum is an even function of frequency and so spurious signals appear identical at positive and negative frequencies. Therefore we limited the practice to those cases where the spectrum was reasonably well characterized.

iii). Drift - Use of Phase Cycling

The baseline of the zero field fids exhibited severe drift, usually over the time scale of hours. We took great pains to eliminate factors under our control which might contribute to this problem, but often problems were sporadic and difficult to diagnose. Some factors which contribute to drift are listed below

1) tuning drift of probe - usually caused by the variable capacitor; exacerbated by the collision of the shuttle into the sample stop in high field. To combat this problem we rigidly fastened the variable capacitor's external tuning.

2) irregular shuttling - caused by old shuttle, irregular shuttle tube , air pressure variation. Scotch tape affixed to the shuttle helped with the first two of these, the third was rarely a problem as we generally used ≥2 pressure regulators on the Chemistry Departments 100 p.s.i. compressed air line. (These regulators ["Speedaire" Model 4Z028, Dayton Electric Mfg. Co., Chicago, Il. 60848] also

served as traps for the the grease, water and oil found in that line. We did not feel it necessary to further filter or dry the compressed air.)

3) drift of rf amplifiers - so far impossible to fix. Rf amps can drift because of their tuning or because of drifting plate voltage, tube temperature, etc. Tuning drift can be reduced by reducing the Q of the amplifier, but this reduces the output power of the amp. A new amplifier ordered from IFI (Instruments for Industry) should help with these problems.

4) spectrometer drift - most likely due to amplifiers in receiver section (rf to audio)

5) A/D Converters - These really don't drift in the usual sense but occasionally overheat due to failure of their fans, or extremes in weather. When either of these occur, one notices spikes in the data.

A reasonable solution was to use phase cycling. This simply amounts to performing two zero field cycles for each t_1 evolution period. Alternate cycles would initiate the pulse spin locking cycle with either a 90_x pulse or 90_{-x} pulse. The signal from successive shots of the same t_1 value were then subtracted. This could be accomplished automatically by the Temp routine and eliminated any drift occuring on a time scale much slower than a few field cycles. We found that choosing the pulse delays τ_2 and τ_3 too short amplified

the drift problem because rf pulses could leak into the preamp and saturate the receiver. Waiting an insufficient time meant that the receiver could not recover into the linear regime. Perhaps just as important, the amplitude of the rf pulse leak through depended upon the drift in the rf pulse amplitude.

IV.B Appendix - Technical Details Cross-Reference

In this Appendix I shall attempt to list several important categories of technical details relating to the spectrometers and where one can go for documentation. I cannot hope to be complete in this endeavor and I apologize in advance to anyone who feels their contributions have been slighted. The categories in the listing are Spectrometer (general), RF section, Receiver and Data Acquisition, Probes, Pulse Programmer, Display Scope, Computers(Data General), Magnets and Zero Field. (In what follows theses are abbreviated DW = Dave Wemmer, GD = Gary Drobney, JG = Joel Garbow, SS = Steve Sinton, JMM = J.M. Millar)

1). Computer (Data General)

a) Computer Filters. DG Part #118-000-511, ~$90/ea available from Computer Parts Exchange

b) Diagnostics. We possess a copy of a DG diagnostics pack capable of memory checking, disk exercise, fast formatting of fixed and/or removable packs plus more. Documentation is in the JMM Computer file.

c) Disk Drives. Replacements available used from MCE for ≤$1600 ea(price falling though); also have used floppy drives.

d) Floppy Drives. Available used MCE.

e) Memory Boards. Available used from MCE, compatible copies from Plessy, or new from DG (at unreasonably high prices).

f) Memory Compatibility. Currently lab owns a Nova 2, 3, 4, and two 820's. Memory boards and CPU's are not generally

interchangeable and extreme damage can result to boards and computer should interchange be performed. Consult with DG or MCE.

g) Repairs. Usually on-site repair is several times more expensive than shipping to MCE or DG. On-site repairmen (from DG and also CALTEK) generally lack the necessary parts and expertise to repair the ancient computers we possess. Therefore we are charged for multiple visits. In addition DG has two price structures for parts. The "full price" is what we are charged if the item is replaced on-site. These prices are vastly inflated, e.g. $3000 for a disk controller board when we can get the same board used (from MCE) for about $150. DG has two repair facilities, one in Colorado and the other in Massachusetts, each dealing with only specific models. However they offer complete refurbishing of old computers for fixed prices and for slightly higher prices can offer turn-around in 10 days or less.

h) Vendors

i) Caltek (Rahim Morid- Fremont CA 490-2043). Private repair firm dealing with DG computers. Service in the past has been less than satisfactory in cases involving serious repairs (e.g. replacement of disk drive heads or loss of ready status in disk drives.) Probably ok for small jobs.

ii) Computer Parts Exchange(Northridge, CA; 213-341-3783). Deals in small things such as computer air filters for β,γ,δ.

iii) DG (Data General- Oakland Office 569-0867; Colorado Repair Depot, 800-525-9295; Massachusetts Repair Depot 800-343-3768).

iv) MCE (Mini Computer Exhange, Sunnyvale CA. John

McFarlane 408-733-4400). Deals in used DG equipment and repair of same. Probably better than DG on both scores.

v) MDB (Orange, CA). Sell memory boards and "blank" interface boards of the type used to construct the scope interface.

2). Display Scope.

-Display scope interface boards were built from MDB blank interface boards using schematics available in group archives. Beta (1/85) and Data Station interface boards(~9/85) and the boxes mounted on the spectrometer were built from same design but cables, inputs, and outputs are not standardized, therfore the systems are interchangeable only as entire systems. Delta and gamma were built from design incorporating all functions on the interface board residing in spectrometer computer. Note: software for scope is a function of the display scope itself (e.g. H.P. or Tektronix) and the interface board/spectrometer box. Compare Spec program listings for differences.

3). Magnets

a) Charging. The group possesses two charging supplies.

i). Bruker B-CN 40/60. Essentially donated to us. Their ex-engineer ("Constantine") left it with us after a magnet charge in ~1983. At that time he complained about it, saying it was old and probably malfunctioning. Since then it has been used by Craig Bradley to charge and shim the delta (late 1983, same day Weitekamp left for Delft). He made similar complaints. Not recommended for use.

ii). HP 6259B (12V @ 50-60 V). Fitted with a piggy-back box for magnet charging. Last used ~1984 to charge Gamma (JMM/AMT). Quite adequate but not as easy to use as the automated Bruker versions.

b) Schematics. For β and γ currently kept near β. Craig Bradley (Cryomagnet Systems, Indianapolis, Indiana) was involved in building either one or both of them and he is extremely familiar with all facets of their design, maintenance and repair.

c) Stands. Old α supercon magnet stand carted off to UC's Richmond Storage facility in ~1983. Many consider this facility to be the world's first known black hole.

d)Shim Supplies. Old α shims were given to J.A. Reimer in Chemical Engineering in ~1984. He since gave the magnet to another Chem.E. group who may or may not need its three shim supplies.

4. Probes		SS DW JG JMM
5. Pulse Programmers		
a) Hardware		GD SS DW
b) Softwar		GD
c) μ-code listing		GD
d) Schematics	Group archives +	GD
VI. Receiver and Data Acquisition		
a) Receiver		DW JG GD
b) Preamps/IF Cain		GD SS

c) Phase Sensitive Detect GD

d) Data Acquisition GD SS DW JG

7. RF Sectio.. (high and low power)

a) RF Generator (low power GD SS DW JG

b) Phase Shifter (digitally controlled) GD

c) RF Amps GD SS DW JG JMM

8. Spectrometer, General GD

9. Zero Field Equipment

Review article by A. Bielecki et. al (Rev.Sci.Instrum. 1986) is quite comprehensive and chocked full of circuit diagrams. Schematics of new improved versions of current pulsers (including the bidirectional pulser) will or should be in the Electronics Shop archives and/or A.Bielecki's Ph.D thesis. The JMM thesis contains some documentation of everyday use and our contributions to the technical side.

V. Chapter Two References

1. a) D.P. Weitekamp, A. Bielecki, D. Zax, K. Zilm and A. Pines, Phys.Rev.Lett., 50, 1807(1983).
   b) D.B. Zax, A. Bielecki, K.W. Zilm, A. Pines and D.P. Weitekamp, J.Chem.Phys. 83, 4877(1985).
2. D.B. Zax, A. Bielecki, M.A. Kulzick, E.L. Mutterties and A. Pines, in press J.Phys.Chem.
3. A. Bielecki, J.B. Murdoch, D.P. Weitekamp, D.B. Zax, K.W. Zilm, H. Zimmermann and A. Pines, J.Chem.Phys. 80, 2232(1984).
4. a) J. Jeener, Ampere International Summer School, Basko Polje, Yugoslavia(1971), unpublished.
   b) W.P. Aue, E. Bartholdi and R.R. Ernst, J.Chem.Phys. 64, 2229(1976).
5. A. Bielecki, D.B. Zax, K.W. Zilm and A. Pines, in press Rev.Sci. Instrum.
6. L.I. Schiff, Quantum Mechanics, (McGraw, New York, 1968) Third edition.
7. M. Goldman, Spin temperature and NMR in Solids, (Oxford, London, 1970).
8. A. Abragam, The Principles of Nuclear Magnetism, (Oxford, London, 1961).
9. a) J.W. Hennel, A. Birczynski, S.F. Sannowski and M. Stachurowa, Z.Phys. Condensed Matter, 60, 49(1985); b) P. Jonsen et al., Poster Presentation ENC 1986, Baltimore, Maryland.
10. C. Hilbert, J.C. Clarke, T. Sleator, and E.L. Hahn,Appl.Phys. Lett. 47 637(1985).
11. R.D. Brown and S.H. Koenig, I.B.M. Research Report, RC6712 (#28906) 8/31/71.
12. N.F. Ramsey and R.V. Pound, Phys.Rev. 81, 278(1951).
13. R.F. Slusher and E.L. Hahn, ,12, 246(1964).
14. A.G. Redfield, Phys.Rev. 130, 589(1963).
15. J.C. Koo and Y.N. Hsieh, Chem.Phys.Lett. 9,239(1971); J.C. Koo and E.L. Hahn, Bull.Am.Phys.Soc. Series 11, 13 356(1968).

J.C. Koo, Ph.D. Thesis, University of California,Berkeley,(1969).

16. D.T. Edmonds, Phys.Rep. 29, 233(1979).
17. R.L. Strombotne and E.L. Hahn, Phys.Rev. 133A, 1616(1964).
18. S.H. Koenig, R.D. Brown III, D. Adams, D. Emerson and C.G. Harrison, presented at Thirty-first Annual Meeting, Association of University Radiologists, Mobile, AL, March 1983.
19. M. Stohrer and F. Noack, J.Chem.Phys. 67, 3729(1977) and references therein.
20. E.D. Ostroff and J.S. Waugh, Phys.Rev.Lett. 16, 1097(1966).; W.K. Rhim, D.P. Burum and D.D. Elleman, Phys.Rev.Let. 37, 1764(1976; D. Suwelack and J.S. Waugh, Phys.Rev.B 22, 5110(1980); M. Matti Maricq, Phys.Rev.B 25, 6622(1982).

Chapter Three - Indirect Detection

Time domain zero field techniques have recently been applied to polycrystalline solids,[1] extending the field cycling experiments of Hahn et. al.[2] and others.[3-6] In the original zero field experiment, evolution was initiated by sudden field switching. In this Chapter we introduce a variation which relies on the pulsed application of a dc magnetic field after demagnetization to initiate evolution in zero field. This pulsed method can be used to selectively irradiate isotopic species (e.g. protons and deuterons) in zero field and can also be adapted to exploit the advantages of indirect detection for sensitivity enhancement and extended ranges of relaxation times. The pulsed method also greatly enhances the ability of the experimentalist to coherently manipulate the spin system and allows application of composite and multiple pulse techniques to zero field experiments.

First, we briefly describe the original zero field experiment. The sudden switched version, Figure 3.1, is performed by shuttling a sample from a large polarizing field B_o to a collinear intermediate field which is then switched off suddenly to initiate evolution under the zero field Hamiltonian. The spin eigenfunctions in the field B_i differ from those in zero field; thus, when B_i is suddenly switched off, the system which was originally in high field eigenstates will evolve under the zero field Hamiltonian. After an evolution period t_1, B_i is suddenly switched on and the sample shuttled back to high field where evolution during t_1 is probed at a later time as in two-dimensional NMR.[7] The z component of the magnetization at time t_1 is

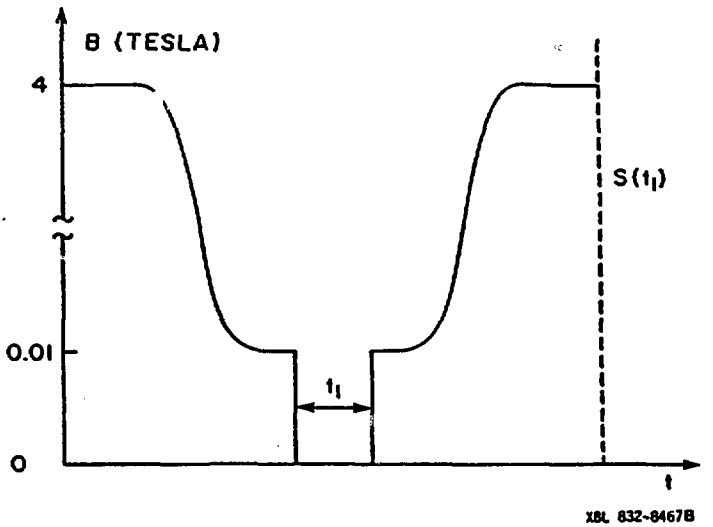

Figure 3.1. Field cycle for the sudden zero field experiment. The sample is shuttled adiabatically from the magnetic field B_o to an intermediate field B_1, illustrated here as 0.01 Tesla. Sudden removal of the intermediate field initiates zero field evolution for a time t_1 after which B_1 is reapplied and the sample is returned to high field. The magnetization is detected for regularly incremented values of t_1 forming the interferogram $S(t_1)$ which when Fourier transformed produces the zero field spectrum.

measured using pulsed spin locking[8] or for quadrupolar systems, multiple echoes, to enhance the detection sensitivity. The integral of this signal is recorded as a function of t_1 forming an interferogram which when Fourier transformed yields the zero field spectrum.

We consider a case in which the spin system consists of two isotopic species, e.g. protons and deuterons. The sudden experiment initiates evolution for all spin species, as long as the spin interaction with the switching field is large compared with the zero field interactions, i.e. dipolar and quadrupolar interactions. Thus any evolution of the spin system present in the detected signal will produce a zero field spectrum containing both dipolar and quadrupolar frequencies. Even if the deuteron evolution could be detected through the protons, it may often be obscured by the signal from the protons, which can occur over all or part of the range of 0 - 50 kHz. It is thus worth considering pulsed experiments on completely demagnetized states[9] which are better suited for indirect experiments as level crossings will occur during the field cycle.

II. Effects of dc Pulsed Magnetic Fields

A). Density Operator of the Demagnetized State.

Neglecting the heteronuclear dipolar coupling between a system of protons and deuterons, the density operator for a system demagnetized from high field to zero field can be written in the molecular frame as

$$\rho_M(0) = \rho_I + \rho_S \qquad (3.1)$$

where

$$\left[\rho_M(0),\ H_{ZF} \right] = 0 \tag{3.2}$$

and I and S corresponding to the protons and deuterons, respectively, and H_{ZF} is the pure dipolar Hamiltonian for protons and the quadrupolar Hamiltonian for deuterons in zero field. It will be necessary to evaluate the effect of applied dc pulsed in a fixed laboratory frame where the density operator becomes

$$\rho_L(0) = R(\alpha,\beta,\gamma)^{-1}\ \rho_M(0)\ R(\alpha,\beta,\gamma) \tag{3.3}$$

where $R(\alpha,\beta,\gamma)$ is the rotation operator relating the laboratory to the molecular axes in terms of the Euler angles α, β, and γ. A similar expression transforms the zero field Hamiltonian into the laboratory frame:

$$H_{ZF}^{L} = R(\alpha,\beta,\gamma)^{-1}\ H_{ZF}\ R(\alpha,\beta,\gamma)\ . \tag{3.4}$$

At time t=0, consider the application of a dc pulsed magnetic field which is turned on for a time τ. The density operator $\rho_L(\tau)$ is then written

$$\rho_L(\tau) = \exp\ (-iH_{DC}\ \tau)\ \rho_L\ \exp\ (iH_{DC}\tau)\ .$$

Choosing the laboratory z axis parallel to the pulsed dc field, then

$$\begin{aligned}\rho_L(\tau) = {} & \exp\ (-i\gamma_I I_z B_{DC}\tau)\ \rho_{IL}\ \exp\ (i\gamma_I I_z B_{DC}\tau) \\ & + \exp\ (-i\gamma_S S_z B_{DC}\tau)\ \rho_{SL}\ \exp\ (i\gamma_S S_z B_{DC}\tau)\end{aligned} \tag{3.5}$$

where $H_{DC} = [\gamma_I I_z + \gamma_S S_z]B_{DC}$ and describes the dc pulsed field, such that pulse angles of $\theta_I = \gamma_I B_{DC}$ and $\theta_S = \gamma_S B_{DC}$ may be defined, and we have assumed

$$|H_{DC}| >> |H_{ZF}| \quad . \tag{3.6}$$

Since the effective pulse angle is different for the protons and deuterons, it allows a selective means for their manipulation since H_{DC} depends on their gyromagnetic ratios. In general, the effect of a pulse depends on the relative orientation of the spin system and field; however, for any particular species a 2π pulse given by $\theta = \gamma B_{DC}\tau$ will leave the density operator unchanged.

B). A Simple Test - Calibration of the Pulsed dc Field.

As a simple test of these ideas consider the following experiment[Figure 3.2(a)] performed on the protons in polycrystalline $Ba(ClO_3)_2 \cdot H_2O$. The sample, initially in high field, is shuttled to zero field where it is subjected to a single dc pulse of varying length, then shuttled back to high field where its proton pulsed spin locking signal is recorded. The high field signal for a pulse of length τ is given by

$$S(\tau) = Tr[\rho_L(0)\ \exp(-iH_{DC}\tau)\ \rho_L(0)\ \exp(iH_{DC}\tau)] \quad . \tag{3.7}$$

For a powder sample, equation (3.7) must be averaged over all possible orientations, i.e., over all α, β and γ of equation (3.3).

Figure 3.2(b) shows that the experimental response is periodic and that the signal magnitude for $\theta = 2\pi$ is nearly equal to that for $\theta = 0$. This experimental result is for a dipolar system consisting of nearly isolated water molecules but the same behavior has been observed in deuterium systems. Assuming isolated ^1H spin pairs and that a single spin temperature describes the demagnetized state,

Figure 3.2. Field cycle for application of a single dc magnetic field pulse (a) and high field magnetization as a function of dc pulse length (b). The pulse angle is given by $\theta = \gamma_H B_{dc} \tau$ where τ is on the order of a few μs and $B_{dc} \gg B_{local}$. The magnitude of the proton magnetization from a sample of $Ba(ClO_3)_2 \cdot H_2O$ is detected as a function of the dc pulse applied after demagnetizing the sample to zero field. The detected signal is periodic as given by Eq. (3.8) and after a 2π pulse the magnetization is nearly equal to its initial value. The damping may be attributed to imperfections in pulsed field homogeneity.

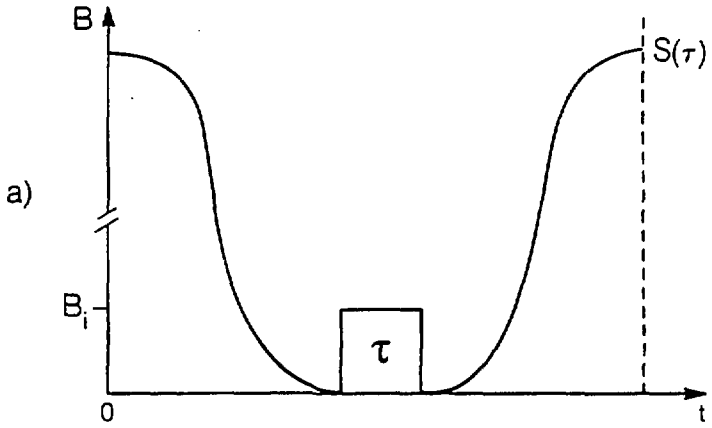

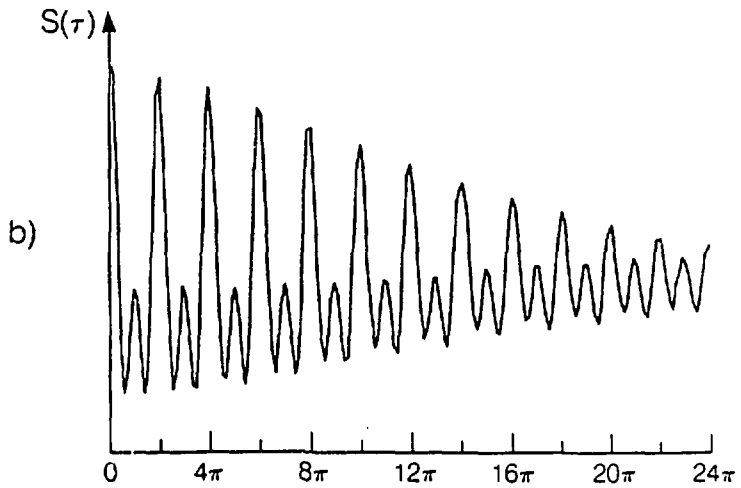

$\theta_H = \gamma_H B_i \tau$ (radians)

XBL 853-8832

$$\rho_M(0) = \beta_D H_D$$

and performing the integration over the presumed powder distribution, the signal function calculated from equation (3.7) is

$$S(\tau) = 1/5[1 + 2\cos(\gamma_I B_{DC}\tau) + 2\cos(2\gamma_I B_{DC}\tau)]S(\tau=0) \quad . \qquad (3.8)$$

This agree with the experimental results showing local maxima at $n\pi$, but predicts no signal decay. The decay may be explained by the inhomogeneity of the pulsed fields together with evolution and relaxation which occur during the dc pulse. Inhomogeneous pulsed fields indeed result in a more severe damping effect on the observed signal. Evidence for evolution under the internal Hamiltonian during the dc pulse may be seen in quadrupolar systems in which the damping effect is more pronounced as the condition in equation (3.6) is not stringently met.

In what follows, we deal with two situations arising from the above considerations. First, in a homonuclear system one can initiate evolution under the zero field Hamiltonian by simply pulsing a system which is initially in a stationary (diagonal) state in zero field, as consistent with equation (3.2). Secondly in a heteronuclear system by using a pulsed field which acts as an identity rotation for one spin species it is possible to effectively rotate that part of the total density matrix corresponding to only one and not the other species. Thus in a system of deuterons and protons one should be able to selectively excite and induce evolution for the deuterons since the deuteron-proton dipolar coupling is essentially quenched in zero field.[10] Similarly, a 2π pulse for protons is a $\pi/2$ pulse for ^{13}C in heteronuclear zero field NMR. Clearly, such selective pulses can be

applied to spin decoupling in zero field.

III. Pulsed Zero Field Detection

A). Possible Schemes

To apply dc magnetic field pulses in obtaining zero field spectra, many schemes are possible. Two simple examples of the field cycles and pulse sequences are shown in Figure 3.3. After demagnetization to zero field the reduced density matrix is diagonal in the zero field basis set and therefore is proportional to second rank tensors only. The form of the initial state in zero field will depend on the dynamics of the demagnetization. This aspect will be treated in detail in a later paper.[12] The initial dc pulse results in off-diagonal terms which evolve for a time t_1 under the zero field Hamiltonian. Detection of the zero field evolution may be accomplished by application of a suddenly switched field in the same direction as the first pulse(in this case, the lab z direction) and remagnetization to high field where the z component of the magnetization is sampled as described above. This field cycle is illustrated in Figure 3.3(a) and the high field signal is formally given by

$$S(t_1) = \mathrm{Tr}\ \{\ I_z \exp(-iH_{ZF}^{L}t_1)\ \exp(-i\theta I_z)\ \rho_L(0) \cdot \exp(i\theta I_z)\ \exp(iH_{ZF}t_1)\ \} \qquad (3.9)$$

where for simplicity we are considering a homonuclear system of spins, I, where I refers to any isotopic species. This is analogous to directly detected magnetization in a pulsed NQR experiment where the signal is sinusoidal and begins with zero intensity. This is due to

Figure 3.3. Schematics of the field cycles used for pulsed zero field NMR and NQR. The sample is demagnetized by removal of the sample to a region of zero applied field. The spin system after demagnetization is in eigenstates of the zero field Hamiltonian and evolution may be initiated by the application of the first dc pulsed field (θ). After the evolution period t_1, which is incremented in successive field cycles, evolution is terminated by the application of a suddenly switched magnetic field as in (a) or by a second dc pulse (θ') as in (b). The sample is then remagnetized and the high field signal is recorded.

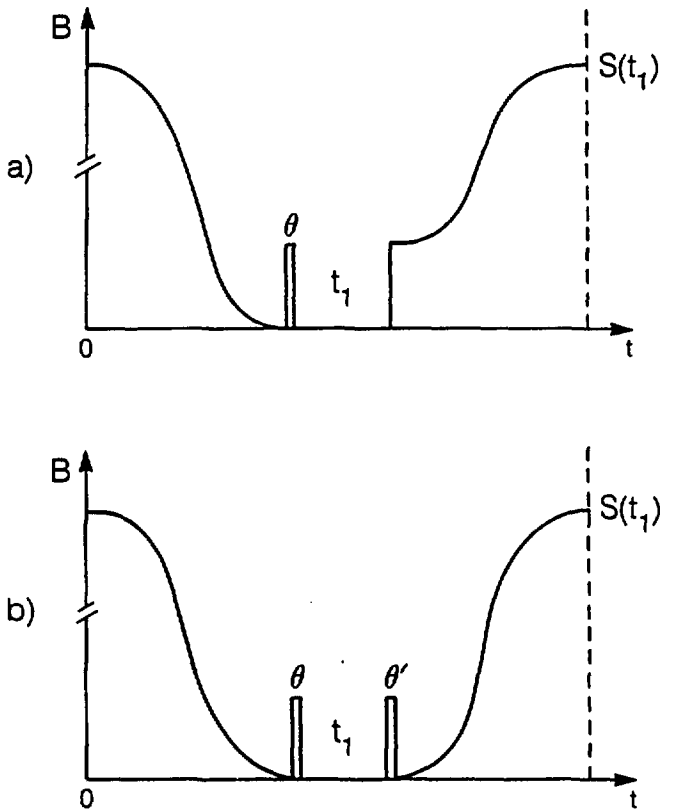

XBL 853-8828

the orthogonality of second rank (the initial density matrix) and first rank tensors (the detected operator). Alternatively, to detect zero field evolution a second pulse applied after the t_1 period will return a portion of the off-diagonal elements to the diagonal. Upon remagnetization these population differences are measurable by standard high field pulse sequences. In these experiments it is not possible to find pulse angles which excite complete evolution for all crystallite orientations. Thus the signal is necessarily somewhat reduced from the previously described experiment (Figure 3.1) as only a portion of the total spin order evolves in zero field. Figure 3.3(b) illustrates this field cycle and zero field pulse sequence, and the high field signal is now given by

$$S(t_1) = \mathrm{Tr}\left[\rho_L(0)\, \exp(-i\theta' I_z)\, \exp(-iH^L_{ZF} t_1)\, \exp(-i\theta I_z) \cdot \rho_L(0)\, \exp(i\theta I_z)\, \exp(iH^L_{ZF} t_1)\, \exp(i\theta' I_z) \right] . \qquad (3.10)$$

B). Results of Different Zero Field Pulse Sequences.

Figures 3.4(a) and 3.4(b) illustrate our results for the sudden transition field cycle (as seen in Figure 3.1), and the demagnetization and pulsed direct detection zero field experiments [Figure 3.3(b)] done on perdeuterated 1,4-dimethoxybenzene. As expected, the frequencies obtained in both are identical and the linewidths agree within experimental error. Comparison of the two experiments is reasonably straightforward, but we defer this to a later section.

Figure 3.4. Zero field NQR spectra of 1,4-dimethoxybenzene ($CH_3OC_6H_4OCH_3$). (a) Sudden transition zero field spectrum of perdeuterated dimethoxybenzene obtained using the field cycle described in Figure 3.1. Peaks at frequencies corresponding to the methyl and aromatic deuterons are resolved. (b). Pulsed direct detection zero field spectrum of perdeuterate dimethoxybenzene obtained using the field cycle of Figure 3(b). As the magnitude of the observed magnetization is dependent of the dc pulse lengths used, peak intensities are now scaled differently with respect to (a). Relaxation effects occuring during the different length field cycles in the sudden and pulsed experiments are manifested in the different relative methyl and aromatic signal intensities of (a) and (b). (c). Indirect detection via protons of the deuterium NQR spectrum in 60% - 70% aromatic deuterated 1,4-dimethoxybenzene. (Note that in this sample the methyl groups were not deuterated.) Clearly resolved ν_+, ν_-, and ν_0 transitions are observed with no evidence of proton signal. Signal-to-noise for the aromatic deuterons is improved relative to the sudden and pulsed zero field methods.

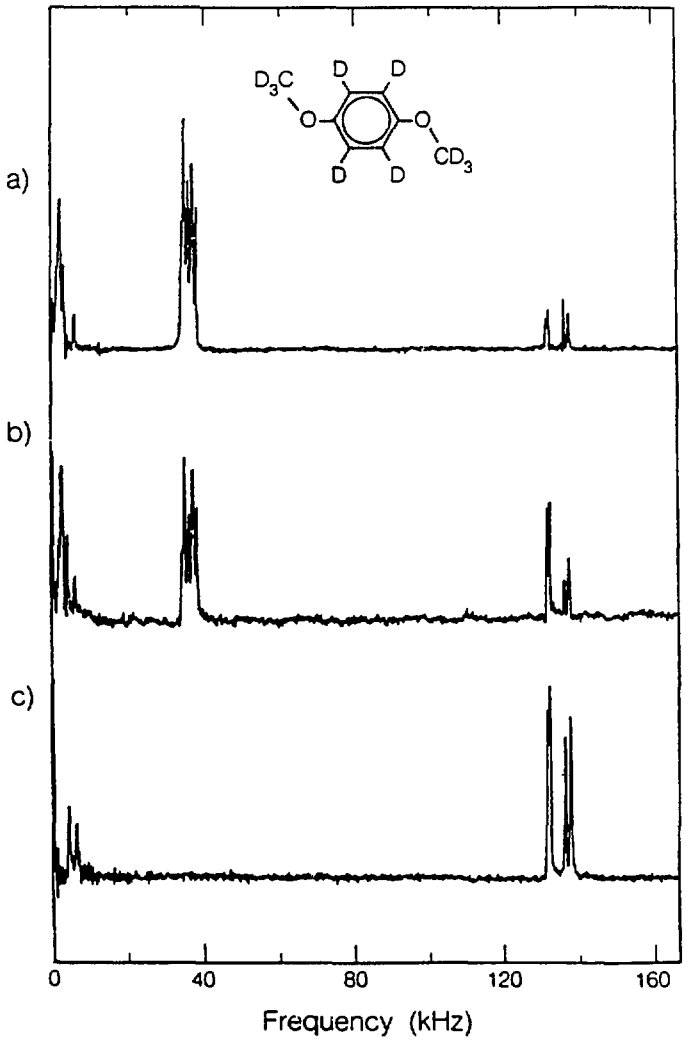

XBL 853-8831

IV. Indirect Detection with Selective Pulses

A). Introduction.

Above we have shown that dc pulses can initiate zero field evolution and equation (3.5) shows that this evolution can be made selective. All that is required for an indirect detection experiment is that the time evolution of the quadrupolar system be communicated to the protons.

We consider a spin system of deuterons and protons and the indirect detection by level crossing principles of Hahn et al.[2] During the demagnetization of the sample in the field cycle of Figure 3.3(b), sucessive crossings occur between proton and deuteron energy levels resulting in enhanced order in the deuteron system. After the evolution period and second pulse, remagnetization of the sample will bring about the same level crossings, though in reverse order. The high field magnetization of such protons is then modulated at the NQR frequencies of the deuterons thus contacted.

Using dc pulses that are multiples of 2π for the protons in the field cycle of Figure 3.3(b) (i.e. $\theta = \gamma_S B_{DC} \tau$ for the deuterons), we obtain the zero field spectrum of 60% - 70% deuterated 1,4-dimethoxybenzene-d4 ($CH_3OC_6D_4OCH_3$) shown in Figure 3.4(c). No signal is observed due to the protons, only the characteristic ν_+, ν_- and ν_o lines due to the crystallographically inequivalent aromatic deuterons.[1,13]

B). Results for Dimethoxybenzene - Comparison of zero field methods.

The experimental results for the dimethoxybenzene samples shown

in Figure 3.4 allow comparison of the signal-to-noise obtained in each of the different versions of the experiment. The length of each FID is roughly equal and the dwell time is equal for these three experiments. The pulsed direct detection (Figure 3.4b) and the sudden (Figure 3.4a) versions used 4 and 3 times as many signal averages, respectively, as the indirect detection version (Figure 3.4c). Thus the aromatic signal-to-noise obtained via the indirect method is at least twice as good as in the others. Our studies of partially deuterated diethylterephthalate and its perdeuterated analog provide further agreement with this result. Of course, the method requires that the dipolar coupling between deuterons and protons be sufficient to allow efficient spin diffusion during the field cycle, so protons spatially distant from a deuteron would be expected to provide less efficient polarization transfer.

C). Effects of Arbitrary dc Pulses

Arbitrary pulse lengths will produce proton signal in heteronuclear systems which can obscure low frequency (<50 kHz) deuterium lines. Figure 3.5 demonstrates this point in a series of indirectly detected zero field NQR spectra of diethylterephthalate-d4 ($CH_3CD_2CO_2C_6H_4CO_2CD_2CH_3$) obtained by the method described above. Proton signal is clearly visible in those spectra where the n x 2π condition is not met for the protons, but is eliminated with two n x 2π dc pulses. A further advantage of the initial selective 2π pulse on the protons is that the density operator ρ_I undergoes no t_1 dependent evolution; therefore, the dynamics of the level crossing

Figure 3.5 Indirect detection zero field NQR spectra of diethyl-terephthalate-d4 ($CH_3CD_2CO_2C_6H_4CO_2CD_2CH_3$). (a) Dc pulses used which do not satisfy the n x 2π criterion for the protons, thus signal due to both proton and deuteron evolution is observed. The proton signal appears as a broad hump below 50 kHz. (b). Same as (a) except that dc pulses now used cause the proton signal to appear inverted relative to the deuteron signal. (c). Dc pulses equal to n x 2π allow for selective detection of only the deuterium NQR spectrum. Low frequency lines can be clearly resolved with no interfering signal from proton evolution or absorption. Three lines may be assigned to each of two crystallographically inequivalent methylene deuterons. Calculated values of $(e^2qQ)/h$ and η from the observed frequencies are A: (e^2qQ/h) = 153.1 kHz, η = 0.051; B: (e^2qQ/h) = 149.8 kHz, η = 0.039.

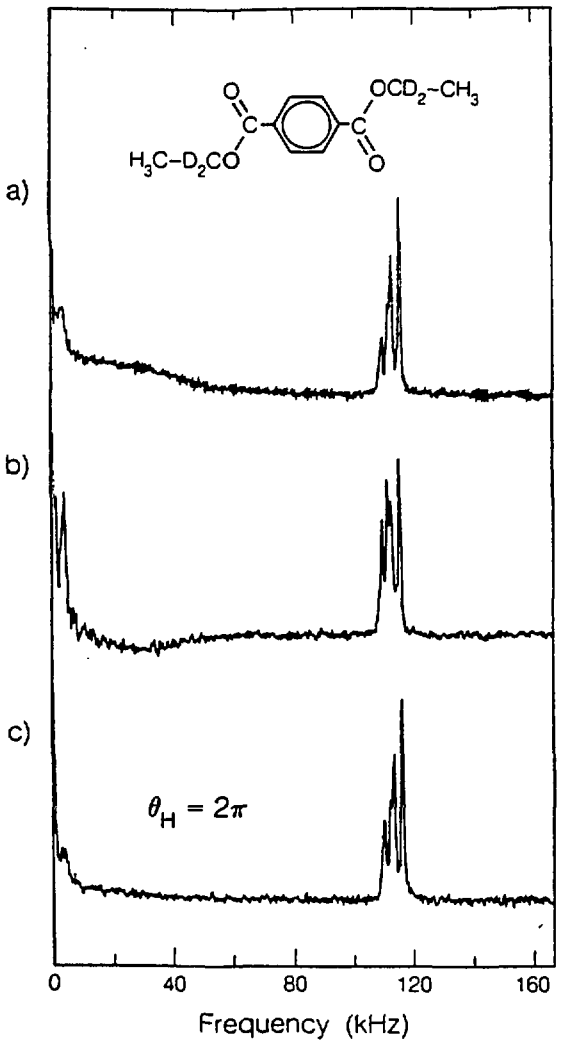

XBL 853-8829

should be sensitive only to deuterium evolution. Diethylterephthalate contains two crystallographically inequivalent methylene deuterons since the methyl-methylene bond is tilted out of the plane of the $-CO_2C_6H_4CO_2-$ moiety[14] thus producing the six line spectrum for two uncoupled quadrupolar nuclei with nonzero η. The magnitude of the observed signal depends upon the pulse lengths used, therefore the relative peak intensities are scaled differently in the spectra of Figure 3.5.

D). Application of Zero Field Indirect Detection to ^{14}N

Although the use of selective pulses and indirect detection has thus far been presented as a method of obtaining deuterium NQR spectra, the principles are entirely general and can be applied to any system in which there is sufficient contact between the observed and detected nuclei. As an example, we present a preliminary ^{14}N zero field NQR spectrum obtained from a sample of polycrystalline ammonium sulfate shown in Figure 3.6, obtained by the sequence in Figure 3.3(b) with indirect detection by protons. All six lines are resolved for the ν_+, ν_- and ν_o transitions of the two inequivalent ^{14}N sites and yield values of e^2qQ/h and η in agreement with single crystal results[15] and other field cycling experiments in which the ν_o lines do not appear.[16] Under other conditions the proton signal would obscure the low frequency lines but here the use of selective 2π pulses for the protons greatly reduces their contribution to the signal. Compensation for the inhomogeneity of the dc pulsed fields should provide increased discrimination against the proton signal.

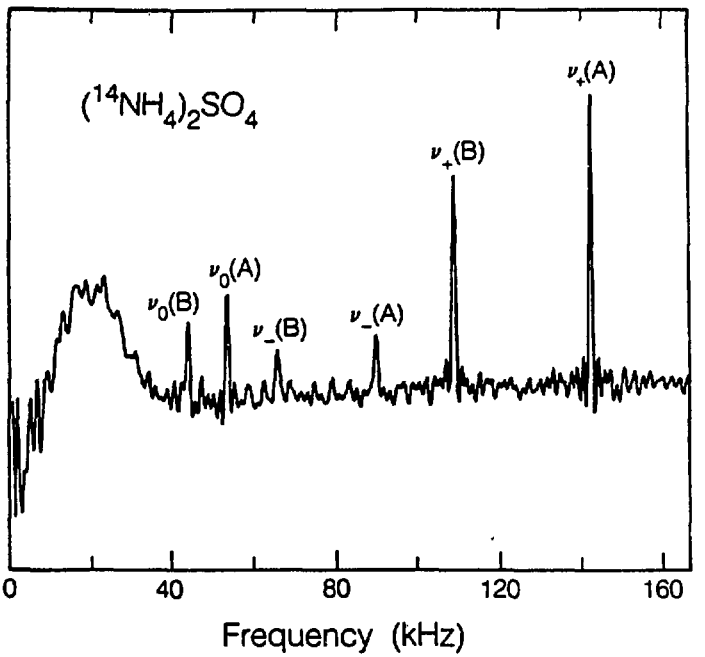

Figure 3.6. Indirectly detected pulsed zero field ^{14}N NQR spectrum of $(NH_4)_2SO_4$ with selective 2π pulses for the protons. Peaks corresponding to two inequivalent sites are labeled A and B. Residual proton signal appears below 40 kHz but has been reduced enough to allow for resolution of the ^{14}N NQR lines. From the frequencies observed at room temperature, (e^2qQ/h) and η can be calculated. Site A: $(e^2qQ/h) = 154.5$ kHz, $\eta = 0.688$, Site B: $(e2qQ/h) = 114.9$ kHz, $\eta = 0.747$. (At 296.1 K, Batchelder and Ragle (Ref. 16) give values of I: $(e^2qQ/h) = 154.53$ kHz, $\eta = 0.684$; II: $(e^2qQ/h) = 115.71$ kHz, $\eta = 0.749$.)

V. Summary

We have demonstrated two variations of the time domain zero field experiment which are performed by simply pulsing a sample demagnetized to zero field and that selective NQR spectra may be obtained which have the sensitivity advantage of indirect detection. The initial density operator need not be proportional to I_z in the variations presented here, so spin systems can be probed under a wider variety of conditions. Perhaps most important is that this work can be extended in experiments where one manipulates the spin system with pulse sequences analagous to those used in high field.. Composite pulses[17] shoud be applicable to the problem of inhomogeneity of the pulsed dc field, as well as to multiple pulse experiments and spin decoupling in zero field.

In addition, we note that the indirect detection experiment depends more on the relaxation times of the protons than those of the deuterons. This can be of utility when the deuteron T_1 is inconveniently long, or when T_{1Q} is inconveniently short. As long as the ^2H T_{1Q} is on the same order as the zero field time period, one can conceivably obtain the deuterium spectrum via the protons.

The dc pulsed variation of the zero field experiment allows for detection of NQR spectra without loss of information due to the proton background. This is in contrast with frequency domain techniques. Quadrupolar nuclei with small coupling constants are readily observed and resolution of ν_o lines for spin I = 1 systems permit spectral interpretation which is usually done with the help of double transition frequencies and a knowledge of the crystal structure.[18,19] The experiments were conducted on a homebuilt spectrometer[20] with

demagnetization times on the order of 100 ms and pulsed dc fields of 30 - 500 Gauss for times of 1 μs to a few hundred ms.

VI.A Appendix - Preliminary Low Temperature Zero Field Measurements

1). Pneumatic System

a). Layout and Operation

Preliminary low temperature zero field experiments have been conducted. A working low temperature pneumatic shuttling system designed to operate between liquid nitrogen temperature and room temperature was developed. The design had some drawbacks however and operation was not routine.

The system incorporated pneumatic shuttling of the sample using cooled ntirogen gas. A design using a vacuum to move the sample, as had been employed for the room temperature experiments, was not possible since cryogenic vacuum valves were not commercially available.

The entire setup along with the placement of the cryogenic solenoid valves is shown in Figure 3.7. Part numbers and manufacturers of the valves are given in Table 3.A1. In the Figure 3.7, nitrogen gas enters the apparatus at the right after being cooled in a copper heat-transfer coil immersed in liquid nitrogen. After entering the apparatus, the nitrogen shuttle gas's temperature was regulated by a thermocouple controlled temperature controller designed by the UCB Chemistry Department Electronics Shop (Drawing #485A1 and 683A1). The sample spent most of its time in high field so gas normally flowed from the tee through valve B and exited at valve C. Gas flowed from the tee up the sidearm exiting at valve E. This prevented heating of the sidearm. In previous designs, we did not

Figure 3.7. Schematic of the zero field low temperature apparatus (not to scale). Cryogenic valves (represented by the circles) are labeled A-E (an x means valve is closed in the resting state, i.e. when sample is in high field). Apparatus as shown in figure has sample in high field. After passing through the heat exchanger (not shown), the nitrogen shuttle gas enters apparatus at right and passes over heater. (Heater is controlled by a thermocouple-controlled termperature controller whose sensing thermocouple is located above the sample's resting place in high field and shown marked TC1. A second thermocouple is shown below the zero field region, both thermocouples allow for observation of temperature.) The gas splits into two paths; one through valve B, up the shuttle dewar pushing the sample into the high field region. Eventually this gas exits at valve C. In the second path, gas proceeds up the "sidearm" and exits at valve E. This cools the sidearm and prevents pressure variations upon shuttling to zero field. To move sample to zero field the state of all valves is reversed. In practice path from tee to valve B is roughly 2 feet, from tee to valve D is roughly 5 feet.

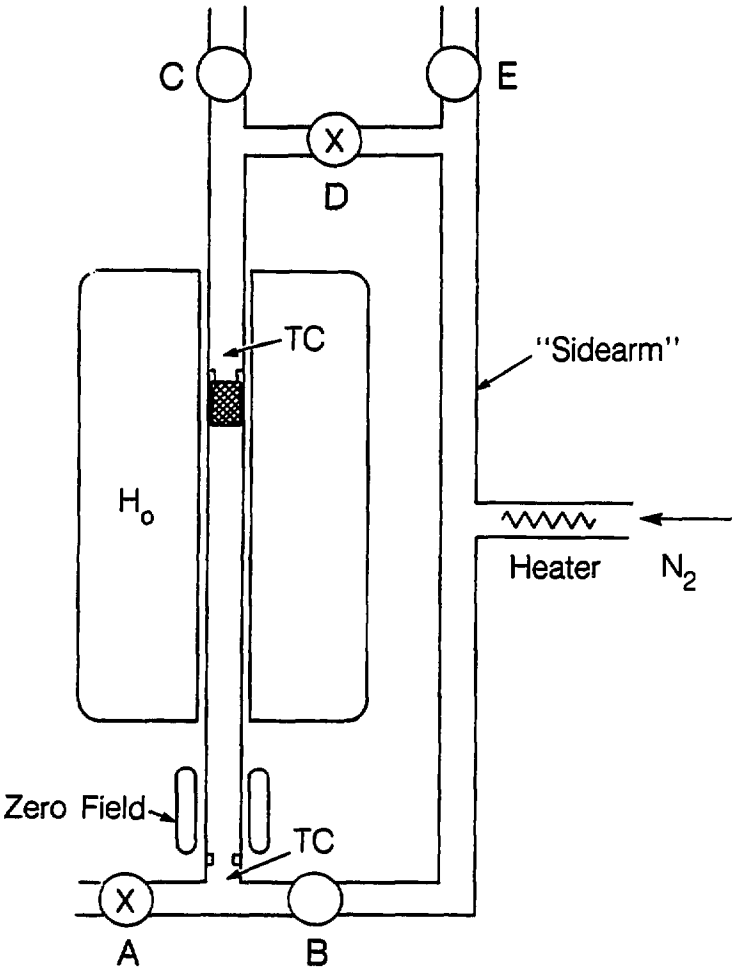

XBL 862– 10301

Table B1. Cryogenic Valves[a,b]

Valve[c]	Experimental System	Proposed Improvement
A	Asco 8263B 206[d]	Valcor SV93 C84D2B[e]
B	" "	Valcor C8407F[f]
C	" "	Valcor C8407F
D	AC Asco 2-Way	Valcor SV93 C84D2B
E	Valcor SV93 C84D2B	Valcor C8407F

[a]Asco valves made by Automatic Switch Company, Florham Park NJ 07932.

[b]Valcor valves made by Valcor Engineering Co., Springfield NJ 07081

[c]As in Figure B1.

[d]Stocked by Dept. of Chemistry Stockroom

[e]A 3-way dc controlled valve

[f]A 2-way dc controlled valve

perform this continuous cooling of the sidearm and so during the time that the sample spent in high field, the sidearm would warm up. Later when cold gas would hit this warm sidearm, it would expand and degrade shuttle performance. Temperature was monitored by thermocouples (TC1

and TC2) placed directly below the zero field region and directly above the probe head. These agreed within ±5 K.

The sample (6 mm od) traveled between high field and the zero field region in a glass dewar made in the Department Glass Shop. The glass dewar protruded nearly through the probe head where it joined a metal dewar which extended out the top of the magnet. The metal dewar was connected at the center of the probehead and extended along the center of the bore, eventually screwing into the top mounting stand. The dewar thus served as a conduit for the cold N_2 gas and also as the only means of support for the probehead and glass dewar. Even though the low temperature region of the apparatus was enclosed within the glass and metal dewars, we thought it prudent to use an independent thermocouple-controlled temperature control system to maintain the bore at room temperature. Nitrogen gas was used for the temperature control. The bore was sealed with plastic to prevent frosting of the dewar. The "sidearm" and connections between valves were constructed of plastic tubing surrounded by black foam rubber insulation. This is the same arrangement used for the liquid nitrogen lines in the lab which are used in filling the supercon magnets. Both the tubing and insulation are available at LBL.

During test experiments we recorded temperatures as low as 80 K and on one occasion one could observe liquid nitrogen traveling up the glass shuttle dewar. The thermocouple temperatures would drop ~10 K upon shuttling but would stabilize within several seconds, depending on duty cycle.

No systematic studies or striking results were obtained with the apparatus but a preliminary results of "Zilmite" (1,2,3,4-

tetrachloronapthalene bis(hexachlorocyclopentadiene) adduct) at 95 K is shown in Figure 3.8. The t_1 resolution is not adequate for any meaningful comparisons with the room temperature result,[20] but the spectrum does demonstrate the first signs of success.

b). Drawbacks

One drawback was that the rf coil for detection in high field was placed outside the glass shuttle dewar, reducing the filling factor. The dewar arced on occasion but returned to normal after evacuation. Dewars lasted ~one week between evacuations, we suspected gaseous helium from magnet fills was degrading the dewar's vacuum. Removing the dewar from the magnet before liquid helium fills of the superconducting magnet seemed to extend its life.

A second drawback was that the original design incorporated several solenoid valves which remained energized while the sample was in high field. Therefore when we operated the system at room temperature, considerable heat from the solenoids was produced and this heated the sample considerably (temperatures ~40° C were observed). We purchased more appropriate valves to remedy this problem, but they were never installed. The part numbers of the new and original systems are given in the table below.

A third drawback was that the gaseous nitrogen would sometimes liquefy as it passed through the heat transfer coil (which itself was immersed in liquid nitrogen). Reducing the pressure of the nitrogen gas reduced the problem but at the cost of limiting the attainable temperature range. After the experiments were halted, a report appeared by Yannoni et al.[26] which suggested pressurizing the liquid nitrogen dewar to ~2 atmospheres to reduce liquefaction.

Figure 3.8. ^{1}H Sudden transition low temperature zero field spectrum of "Zilmite". The spectrum is the Fourier transform of a 45 point t_1 fid collected with a zero field dwell time of 10 μs using a recycle delay of one minute.

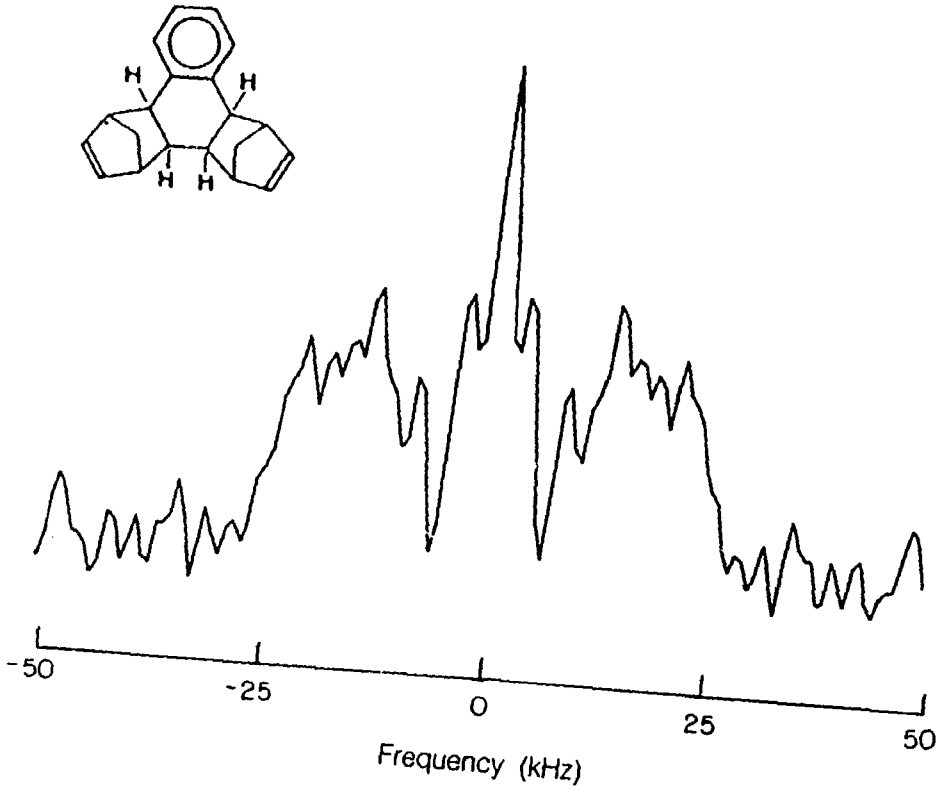
H
H
H
H
-50
-25
0
25
50
Frequency (kHz)

2). Mechanical Piston-based Low temperature system

A low temperature shuttling system based on a mechanical piston was under development during the course of our work. This seems to be the predominant method employed by workers performing low temperature field cycling NQR experiments.[27,28] The obvious advantage of piston systems is that the shuttling system and temperature regulation systems are completely independent. Temperature regulation is particularly easy since one must simply provide a stream of gas over the sample. Therefore, the system should work equally well at low temperatures as high temperatures. (This is in contrast with the pneumatic shuttling system whose cryogenic valves could not be expected to function much above room temperature.)

A preliminary low-temperature mechanical shuttle was constructed and tested. The piston housing was mounted directly above the superconducting magnet so that the entire piston housing, hoses, clamps, etc. were outside of the bore. Since the zero field region was directly below the supercon, this necessitated a piston rod of ~six feet. Vibrations in the rod caused by shuttling were transmitted to the rf coil (which was outside the glass shuttle dewar as in the earlier pneumatic system.) We believe this vibration caused arcing in the dewar which prevented data acquisition. The shuttling worked reasonably well (shuttle times ~.5 sec were obtained) but arcing prevented useful work.

3). Future Work

Work has stopped on the pneumatic system because of the great promise held by the piston. Therefore, the present comments will address the future plans for the piston system. A new dewar system was designed

that would fit outside a standard glass tube. This glass tube would then serve as the shuttle tube. Spacers would hold the glass tube inside the dewar and would be cut to allow circulation of the cold nitrogen gas through the inside and eventually around the outside of the glass shuttle tube. We felt this arrangement would eliminate stress of the dewar upon shuttling. Holes through the glass dewar would accommodate the leads of a thin foil rf coil which would be wrapped directly around the glass shuttle tube. This would improve filling factor, decrease rf power requirements and improve sensitivity. The intermediate field (IF) coil in the zero field region could also be wrapped directly around the shuttle tube offering similar advantages as with the rf coil. (The pneumatic shuttling system required placing the IF coil around the glass shuttle dewar, which reduces the attainable dc field.)

VI.B Appendix- Preliminary ^{14}N Experiments

We have examined the room temperature zero field indirect detection spectrum of a series of ^{14}N compounds. Sudden transition or pulsed zero field experiments were judged to be infeasible for typical nitrogen compounds since ^{14}N has a large quadrupole moment which results in values of e^2qQ/h routinely greater than 1 MHz. (A 1 MHz quadrupolar interaction corresponds to a field greater than 3 kGauss for ^{14}N.) Therefore we confined our attention to compounds where the nitrogen is present as NR_4^+ where R = H, CH_3, C_2H_5, etc, because there the quadrupole coupling constants are rather small (on the order of tens of kHz), arising from distortions of the bonding from a tetrahedral geometry. It soon became apparent that the T_1's of most of the compounds attempted were too short to conduct room temperature experiments and so we obtained the zero field spectra of only a few compounds. Hopefully, however, we have laid the groundwork for later low temperature experiments which will be able to circumvent the T_1 problem.

A). Experimental Method

High field T_1 measurements were carried out only on those samples which by rough measure had T_1's $\geq$ ~1 sec. Those samples meeting this criterion were measured by saturation recovery. Results of these measurements and the rough measurements are given in Table 3.B1

The sucessful zero field spectra were obtained by performing the indirect detection experiment. Generally we used a 350 Gauss pulsed field and pulse times were approximately 1.5 μsec corresponding to a ^{14}N pulse angle of 56°. The pulse time reflects not only the strength

Table 3.B1 T_1 Measurements

	T_1(sec)	PSL(points)	Comments
tetraethyl ammonium chloride	~1	50	-
tetrabutyl ammonium iodide	~1	50	-
ammonium tartrate	~1	17	no zf signal
$(NH_4)_2Al(SO_4)_2 \cdot 12H_2O$	~2	-	-
ammonium acid oxalate	≤1	-	no zf signal
ammonium acetate	≤1	-	no zf signal
NH_4V_2O	≤1.5	-	some zf signal
NH_4HCO_3	≤0.5	-	-
$(NH_4)_6Mo_7O_{24} \cdot 4H_2O$	-	-	no zf signal
$(NH_4)_2HPO_4$	-	-	some zf signal
$(NH_4)_2S_2O_8$	9-10	10	strong zf signal
$(NH_4)_2Cr_2O_7$	-	256	strong zf signal
NH_4BF_4	-	-	no zf signal
$N(CH_3)_4I$	-	-	no zf signal
$(NH_4)_2HC_6H_5O_7$	-	-	no zf signal
tetraethyl ammonium bromide	~1	-	no zf signal
NH_4ReO_2	-	-	some zf signal
NH_4HSO_4	21	-	strong zf signal

of the field but pulse shape imperfections, rise time and switching time of the electronics. The field was produced by the "TB" pulser with a solenoid and 6.6 Ω series resistance. The bucking coil was used with two inductors in series (20 mH of inductance each) to allow efficient level crossing between the ^{14}N and ^{1}H nuclei. Parameters for sucessful experiments are given in Table II.

The zero field spectra of two different samples of ammonium hydrogen sulfate, NH_4HSO_4, were obtained. One of the samples was dried at atmospheric pressure overnite at 132° C, the other under vacuum at ~140° C. Ammonium dichromate, $(NH_4)_2Cr_2O_7$, and ammonium persulfate, $(NH_4)_2S_2O_8$, were obtained directly from the bottle. The ammonium pyrosulfate, $(NH_4)_2S_2O_7$ was prepared by heating the persulfate at 180° C overnite according to the method of Traube et. al[21] as described in Gmelin.[22]

B). Results

The spectrum of ammonium sulfate was discussed in Chapter IV. It has no lines in common with those discussed below. The zero field spectra of four other nitrogen compounds were obtained, namely ammonium hydrogen sulfate, ammonium pyrosulfate, ammonium persulfate and ammonium dichromate. Experimental parameters and results are summarized in Tables 3.B2 and 3.B3, respectively, and spectra are reproduced in Figures 3.9 through 3.13. All samples gave intense features centered about zero frequency. Since these intensities reflect the proton signal and are also prone to artefacts we have not attempted to estimate their intensities in the Table.

The samples were not purified carefully enough for one to make

any definite statments about assignments. Results of X-ray crystal studies were found in the literature only for the persulfate[23,24] and the dichromate;[23,25] both were found to have only one crystallographically inequivalent nitrogen site per unit cell.

All samples except the dichromate gave lines at 37 kHz leading us to suspect a common impurity. One of the ammonium hydrogen sulfate samples has additional lines at 27.3, 58.9 and 85.6 kHz suggesting a single site with $e^2qQ/h = 96.3 \pm .5$ kHz and $\eta = 0.55 \pm .01$. It is impossible to say which of the two ammonium hydrogen sulfate samples is correct (if either) as the method of drying was rather crude. Further analysis of these systems must await experiments on samples of known purity.

Table 3.B2 Experimental Parameters for ^{14}N Zero Field Indirect Detection Experiments

	NFID(t_1)[a]	TI(μs)[b]	RA[c]	RDLY(sec)[d]	τ_{DC}(μs)[e]
NH_4SO_4(air dried)	443	5	2	30	1.5
NH_4HSO_4(vacuum dried)	332	3	2	30	1.5
$(NH_4)_2S_2O_8$	500	3	3	17	1.5
$(NH_4)_2S_2O_7$[f]	210	6	1	17	1.5
$(NH_4)_2Cr_2O_7$	460	3	1	15	2.1

[a] number of points in zero field t_1 fid.

[b] dwell time in zero field.

[c] number of phase-cycled fids collected.

[d] recycle delay between sucessive field cycles.

[e] dc pulse length used in zero field indirect detection experiment. 1.5 μs = 56° for ^{14}N, 2.1 μs value used smaller field and corresponds to only 28°.

[f] sample made by heating the persulfate.

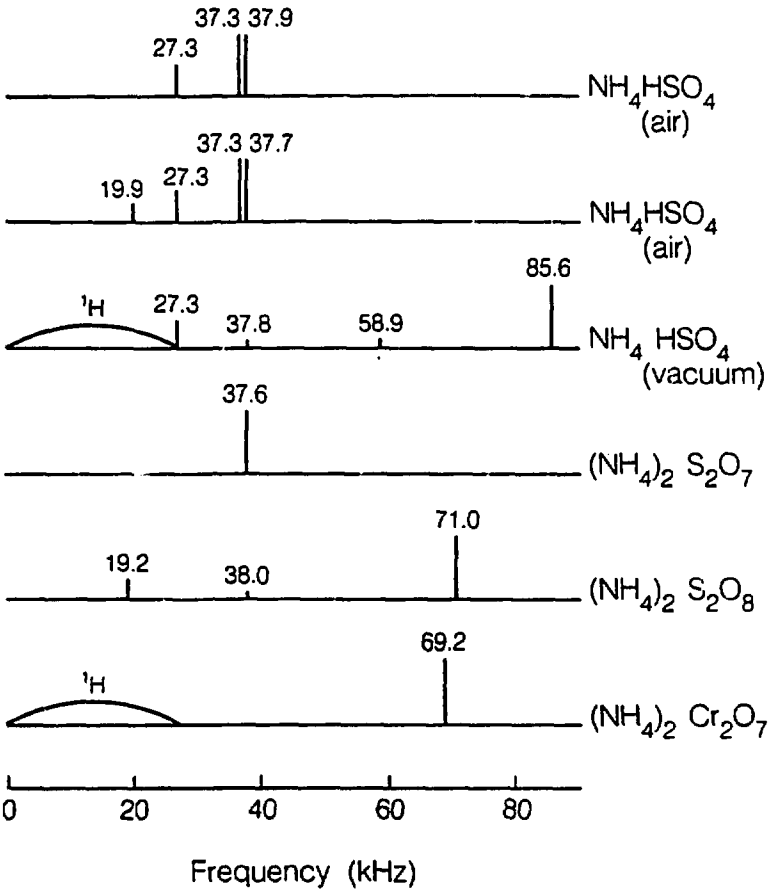

XBL 861-10589

Table 3.B3 Schematic of ^{14}N Zero Field Spectra

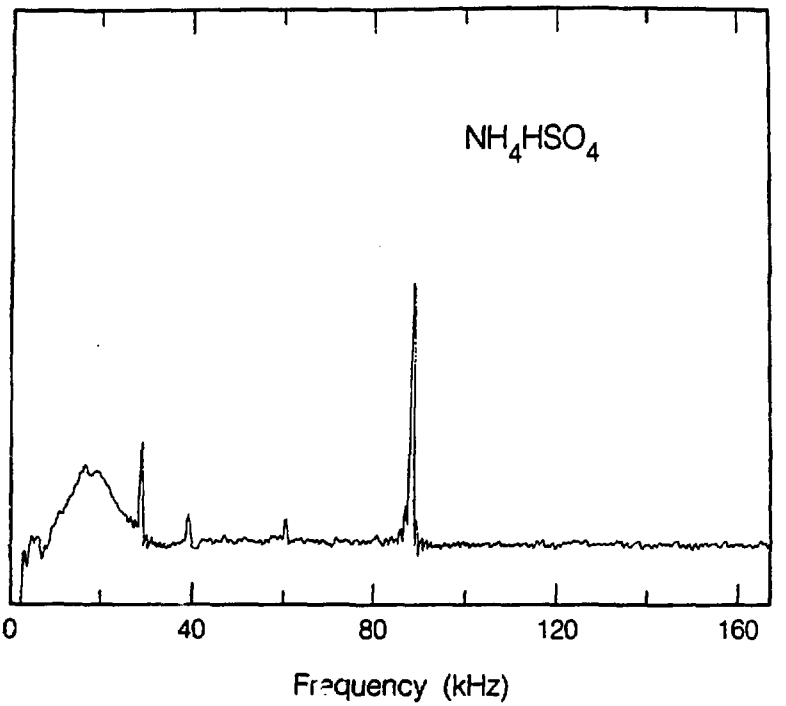

XBL 861-10586

Figure 3.9. ^{14}N Zero field indirect detection spectrum of a sample of NH_4HSO_4 dried at 140° C under vacuum overnite. The lines at 27.3, 58.9 and 85.6 kHz suggest a single site with $e^2qQ/h = 96.34 \pm .5$ kHz and $\eta = 0.55 \pm 0.01$. An additional line at 37.8 is similar to those found in the pyrosulfate, persulfate and the air-dried ammonium hydrogen sulfate. Proton signal is also seen below ~27 kHz.

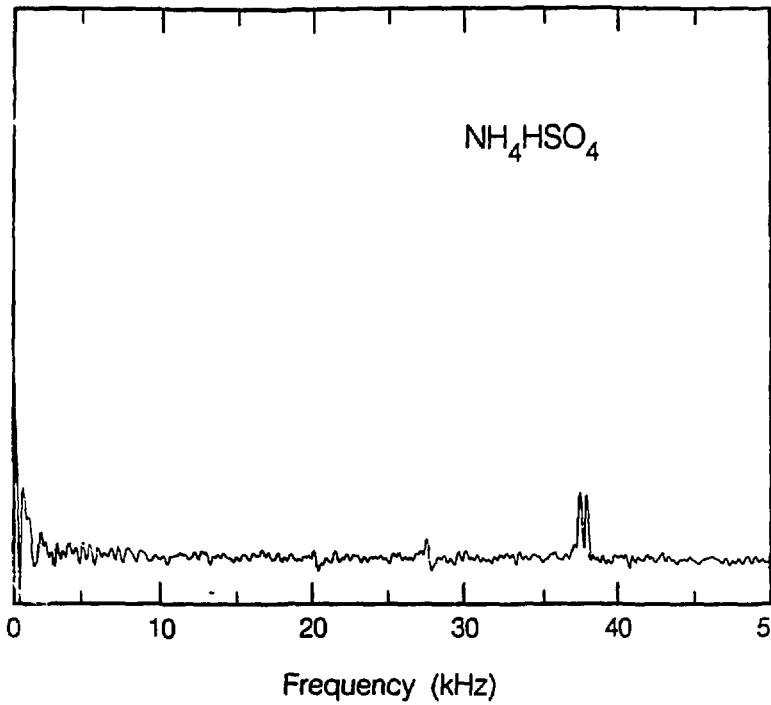

XBL 861-10585

Figure 3.10. ^{14}N Zero field indirect detection spectrum of a sample of NH_4HSO_4 dried overnite at -130° C at atmospheric pressure. This is referred to in the text as the air dried sample. Two well resolved lines centered at 37.6 and one additional line 27.3 kHz are the main features of the spectrum

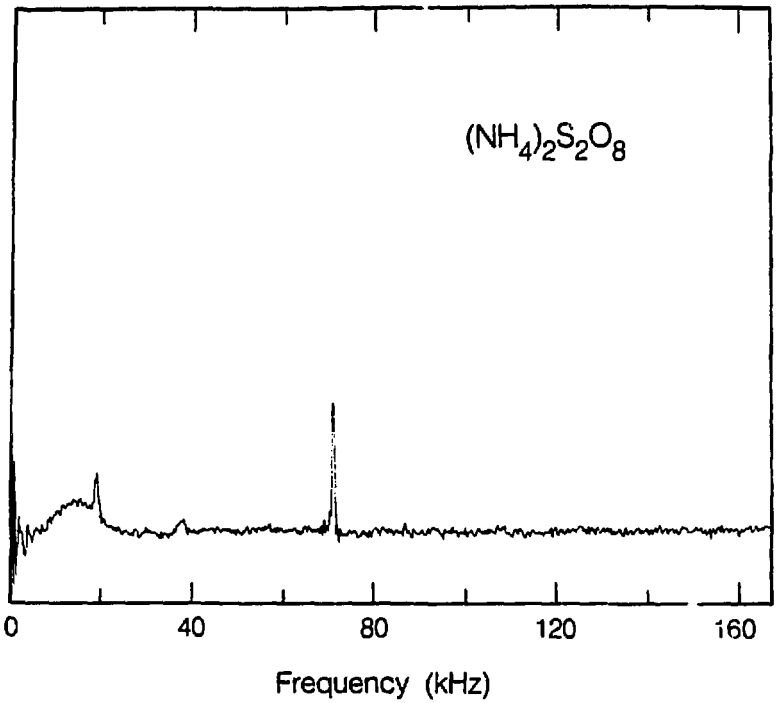

XBL 861-10587

Figure 3.11. ^{14}N Zero field indirect detection spectrum of ammonium persulfate. Three lines are observed, one each at 71.0, -38. and 19.2 kHz.

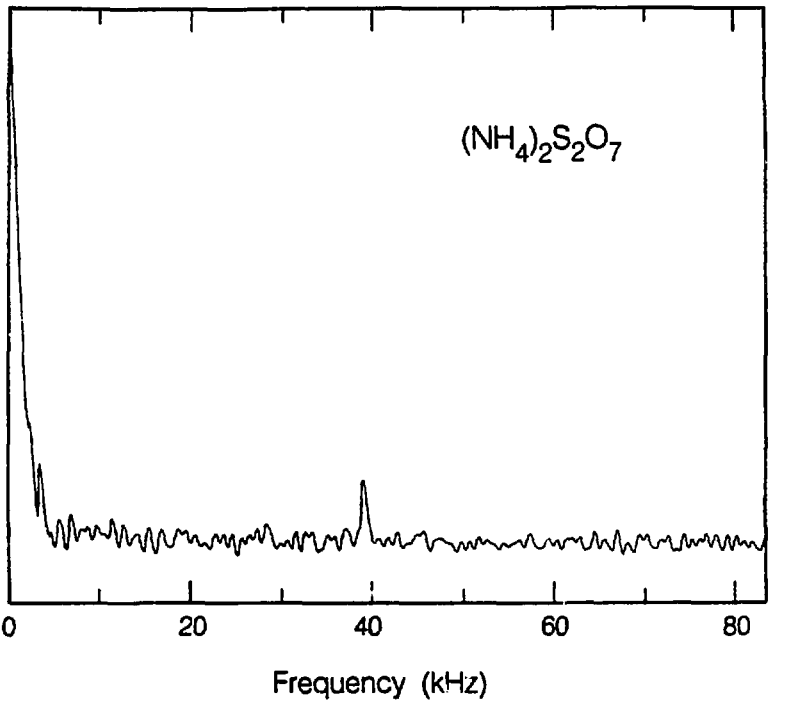

XBL 861-10584

Figure 3.12. ^{14}N Zero field indirect detection spectrum of a sample of ammonium persulfate heated overnite under vacuum at -180° presumably forming ammonium pyrosulfate.[21,22]

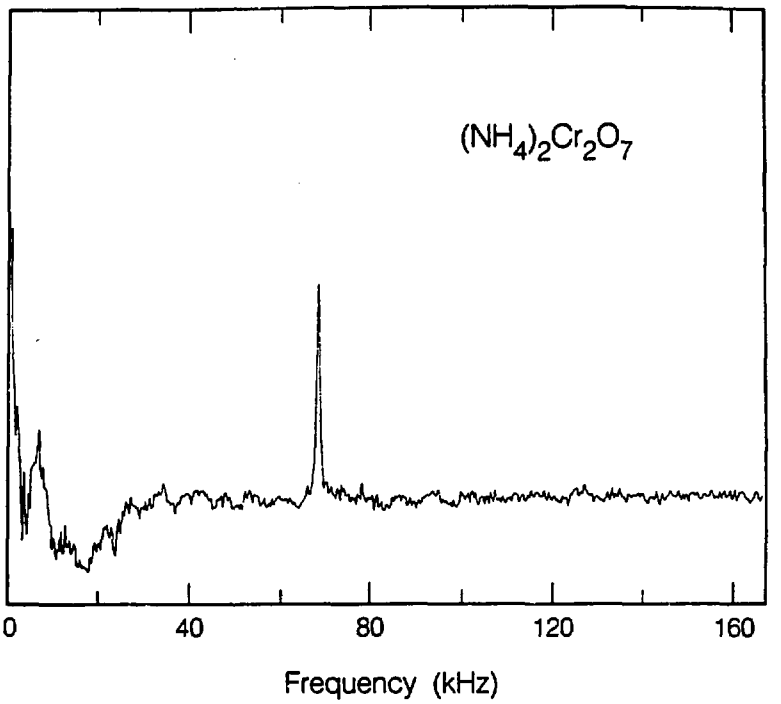

XBL 861-10588

Figure 3.13. ^{14}N Zero field indirect detection spectrum of a sample of ammonium dichromate.

VII. Chapter Three References

1. D.P. Weitekamp, A. Bielecki, D. Zax, K. Zilm and A. Pines, Phys Rev.Lett. 50, 1807(1983); A. Bielecki, J.B. Murdoch, D.P. Weitekamp, D.B. Zax, K.W. Zilm, H. Zimmermann and A. Pines, J. Chem.Phys. 80, 2232(1984).
2. J.C. Koo, Ph.D. Thesis, University of California, Berkeley, CA. (unpublished); J.C. Koo and Y.N. Hsieh, Chem.Phys.Lett. 9, 238(1971); R.L. Strombotne and E.L. Hahn, Phys.Rev. 133, A1616 (1964); R.E. Slusher and E.L. Hahn, Phys.Rev. 166, 332(1968).
3. D.T. Edmonds, Phys.Rep. 29, 233(1977); D.T. Edmonds, Int.Rev.Phys.Chem. 2, 103(1982).
4. A.G. Redfield, Phys.Rev. 130, 589(1963).
5. T.L. Brown, L.G. Butler, D.Y. Curtin, Y. Hiyama, I.C. Paul, R.B Wilson, J.Am.Chem.Soc. 104,1172(1982).
6. J.W. Clymer and J.L. Ragle, J.Chem.Phys. 77, 4366(1982).
7. W.P. Aue, E.Bartholdi and R.R. Ernst, J.Chem.Phys. 64 2229(1976).
8. E.D. Ostroff and J.S. Waugh, Phys.Rev.Lett. 16, 1097(1966); W.K. Rhim, D.P. Burum and D.D. Elleman, Phys.Rev.Lett. 37, 1764(1976); D. Suwelack and J.S. Waugh, Phys.Rev.B. 22, 6622(1982).
9. A.G. Anderson, Phys.Rev. 115, 863(1959); A.G. Anderson and S.R. Hartmann, Phys.Rev. 128, 2023(1962); V.S. Grechishkin, V.P. Anferov and N.J. Sinjavsky, Advan.Nucl.Quad.Reson. 5, 1(1983).
10. G.W. Leppelmeier and E.L. Hahn, Phys.Rev. 141, 724(1966); S. Vega, Adv.Magn.Reson. 6, 259(1973).
11. D.B. Zax, A. Bielecki, K.W. Zilm and A. Pines, Chem.Phys.Lett. 106, 550(1984).
12. J.M. Millar et al., to be published
13. T.H. Goodwin, M. Przybylska and J.M. Robertsen, Acta.Cryst. 3, 279(1950).
14. M. Bailey, Acta.Cryst. 2, 120(1949).
15. R. Blinc, M. Mali, R. Osrekar, A. Prelesnik, J. Seliger and I. Zupancic, Chem.Phys.Lett. 14, 49(1972).
16. L.D. Batchelder and J.L. Ragle, J.Magn.Reson. 37, 469(1980).
17. M.H. Levitt and R. Freeman, J.Magn.Reson. 43, 65(1981).

18. D.T. Edmonds and A.A.L. White, J.Magn.Reson. 31, 149(1978).
19. R.O. Day, N. Hadipour and J.L. Ragle, J.Magn.Reson. 57, 349(1984).
20. A. Bielecki, D.B. Zax, K.W. Zilm and A. Pines, to be published.
21. W. Traube, J. Hoerenz, and F. Wunderlich, Ber. 52, 1284(1919).
22. Gmelins Handbuch der Anorganischen Chemie, (Verlag, Berlin, 1936), Ammonium, Systemnummer 23, 299-301.
23. R.W.G. Wyckoff, Crystal Structures, (Interscience, New York, 1960) Second Edition, Volume 3.
24. W.H. Zachariasen and R.C.L. Mooney, Z.Krist. 88, 63(1934).
25. B. Gossner and F. Mussgnug, Z.Krist. 72, 476(1930).
26. R.D. Kendrick, S. Friedrich, B. Wehrle, H.H. Limbach and C.S. Yannoni, J.Magn.Reson. 65, 159(1985).
27. G.P. Jones, J.T. Daycock and T.T. Roberts, J.Sci.Instrum. (J.Phys.E.) 2, 630(1969) Series 2.
28. Y. Hsieh, P.S. Ireland and T.L. Brown, J.Magn.Reson. 21, 445(1976).

Chapter IV. Effect of Dipolar Coupling on Deuterium Zero Field NQR Spectra

Even though the dipolar coupling between deuterons is slight compared to that between protons, it can exert a profound influence on the ^2H NQR spectra. We will briefly examine this matter starting first with the unperturbed system.

I. Uncoupled System of Two deuterons.

The eigenstates of a single uncoupled deuteron in zero field are those of the familiar triplet manifold $|x\rangle$, $|y\rangle$, and $|z\rangle$ given by

$$\begin{aligned} |x\rangle &= 2^{-1/2}(\,|+1\rangle - |-1\rangle) & E_x &= K(1-\eta) \\ |y\rangle &= 2^{-1/2}(\,|+1\rangle + |+1\rangle) & E_y &= K(1+\eta) \\ |z\rangle &= |0\rangle & E_z &= -2K \end{aligned} \qquad (4.1)$$

where $K=e^2qQ/4h$ and the states $|+1\rangle$, $|-1\rangle$ and $|0\rangle$ are the eigenstates of I_z identified by their m quantum number, m = 1, 0, -1. The eigenstates of a system of two noncoupled deuterons consist of product states such as $|x_1x_2\rangle$, $|x_1y_2\rangle$, $|x_1z_2\rangle$ etc. The matrix elements of the operators $I_{1x}+I_{2x}$, $I_{1y}+I_{2y}$, and $I_{1z}+I_{2z}$ determine the time domain or frequency domain NQR spectra and are simply

$$\begin{aligned} \langle y_i|I_{ix}|z_i\rangle &= \langle z_i|I_{ix}|y_i\rangle = 1 \\ \langle z_i|I_{iy}|x_i\rangle &= -\langle x_i|I_{iy}|z_i\rangle = i \\ \langle x_i|I_{iz}|y_i\rangle &= \langle y_i|I_{iz}|x_i\rangle = 1 \end{aligned} \qquad (4.2)$$

where i=1,2. (We use the letter i as an index and also to represent

$(-1)^{1/2}$, but this distinction should be clear from the context. If we take $(e^2qQ/h)_1 \neq (e^2qQ/h)_2$ and $\eta_1 \neq \eta_2$, then only six nondegenerate transitions are allowed, i.e. the ν_+, ν_- and ν_o lines for each of the two deuterons, given by

$$\nu_{i,\pm} = \frac{3 \pm \eta_i}{4} \left[\frac{e^2qQ}{h}\right] \quad , \quad \nu_{i,o} = \nu_{i,+} - \nu_{i,-} \qquad (4.3)$$

and

$$\nu_{oi} = \nu_{i,+} - \nu_{i,-}$$

II. Dipolar Coupled System of Two Deuterons

A). The Zero Field Hamiltonian.

The zero field Hamiltonian for a pair of coupled deuterons can be written in the general form

$$H = H_{Q1} + H_{Q2} + H_D \qquad (4.4)$$

where H_{Qi} is the quadrupolar Hamiltonian of the i^{th} spin and H_D is the full dipolar Hamiltonian between the spins labeled here as one and two. Generally H_D is a small perturbation of the quadrupolar terms. For some purposes it is convenient to write H_{Q1} and H_{Q2} in the principal axis systems of their respective EFG tensors. One can then write H_D in a form where the operators $I_{i,u}$ (i=1,2, u=x,y,z) are written in their respective principal axis systems. We consider the case where the spherical polar coordinates θ,ϕ specify the position of deuteron two in a coordinate system whose axes are coincident with those of the EFG PAS of deuteron one, as shown in Figure 4.1. The relative orientation of the two tensors is specified by the rotation

Figure 4.1. A). Illustration of coordinate system used for EFG tensors. Assuming the DCD angle is 109.5^0 means the spherical polar coordinate θ of deuteron two in the PAS of deuteron one's EFG tensor is 35.25^0. Here $\phi = 0$.

B). Illustration of transformation of PAS_1 into PAS_2. Here the rotation operator $R(\alpha=0, \beta=-70.5^0, \gamma=180^0)$ when applied to PAS_1 makes it coincident with PAS_2.

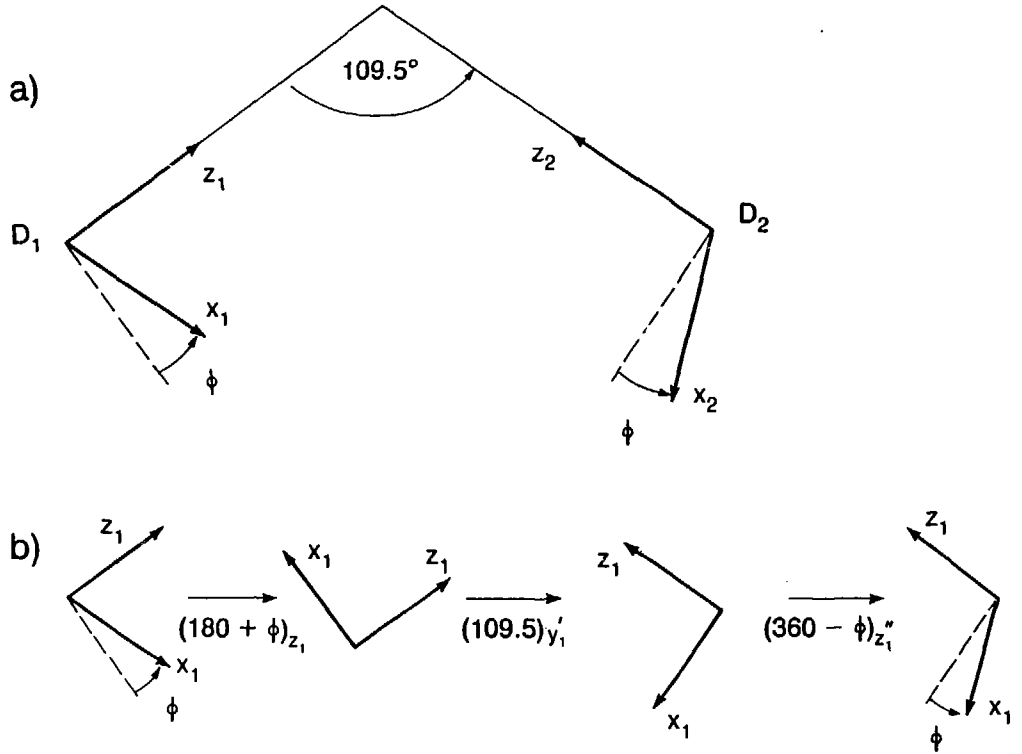
a)
109.5°
z_1
z_2
D_1
D_2
x_1
ϕ
x_2
ϕ
b)
z_1
x_1
ϕ
$(180 + \phi)_{z_1}$
x_1
z_1
$(109.5)_{y_1'}$
z_1
x_1
$(360 - \phi)_{z_1''}$
z_1
x_1
ϕ

XBL 861-6117

operator $R(\alpha\beta\gamma)$ which transforms the EFG tensor of deuteron one into that of deuteron two through the relation

$$\vec{r}_2 = R\vec{r}_1 \tag{4.5}$$

where r_1 is a vector in the PAS of EFG_1 and r_2 the corresponding vector expressed in EFG_2.

1). Explicit Expression

The explicit expression for H_D is given in reference (3) and can be written

$$H_D = I_1 \cdot D \cdot I_2 \tag{4.6}$$

$$\begin{aligned} = d\{ & [R_{xx}X' - 3R_{yx}XY - 3R_{zx}XZ]\, I_{1x}^{I}\, I_{2x}^{II} \\ & + [R_{yy}Y' - 3R_{xy}XY - 3R_{zy}YZ]\, I_{1y}^{I}\, I_{2y}^{II} \\ & + [R_{zz}Z' - 3R_{yz}YZ - 3R_{xz}XZ]\, I_{1z}^{I}\, I_{2z}^{II} \\ & + [R_{xy}X' - 3R_{yy}XY - 3R_{zy}XZ]\, I_{1x}^{I}\, I_{2y}^{II} \\ & + [R_{yx}Y' - 3R_{xx}XY - 3R_{zx}YZ]\, I_{1y}^{I}\, I_{2x}^{II} \\ & + [R_{yz}Y' - 3R_{zz}YZ - 3R_{xz}XY]\, I_{1y}^{I}\, I_{2z}^{II} \\ & + [R_{zy}Z' - 3R_{yy}YZ - 3R_{xy}XZ]\, I_{1z}^{I}\, I_{2y}^{II} \\ & + [R_{xz}X' - 3R_{zz}XZ - 3R_{yz}XY]\, I_{1x}^{I}\, I_{2z}^{II} \\ & + [R_{zx}Z' - 3R_{xx}XZ - 3R_{yx}YZ]\, I_{1z}^{I}\, I_{2x}^{II} \} \end{aligned}$$

where $d = \gamma^2h^2/(2\pi)^2r^3$, $X = \sin\theta\cos\phi$, $Y = \sin\theta\sin\phi$, $Z = \cos\theta$, $X' = X^2$, $Y' = Y^2$, and $Z' = Z^2$ and the operator I_{1u}^{I} is written in the coordinate system of EFG_I and I_{2u}^{I} is written in the coordinate system of EFG_{II}. The terms R_{ij} are the components of the rotation matrix $R(\alpha\beta\gamma)$ of equation (5) the elements of which are given in equation 1.19. Physically, equation (6) means that the dipolar interaction between

the two deuterons is a function of their distance and the relative orientation of their EFG tensors.

2). Effect of Exchange

One might wonder what happens upon substitution of EFG_1 into PAS_2 and vice versa, as illustrated in Figure 4.2. This substitution results in H_{ZF}' given in equation (7) below. This is simply an exchange of the EFG's themselves in a manner that the new 1 has the same relation to the new 2 as the old 1 had to the old 2. The dipolar Hamiltonian is unaffected by the transformation since the matrix R_{ij} and the angles θ and ϕ in equation (6) are identical in both cases. The switched and unswitched zero field Hamiltonians in this frame are then

$$\begin{aligned} H_{ZF} &= I_1 \cdot \Lambda_1 \cdot I_1 + I_2 \cdot \Lambda_2 \cdot I_2 \\ H_{ZF}' &= I_1 \cdot \Lambda_2 \cdot I_1 + I_2 \cdot \Lambda_1 \cdot I_2 \end{aligned} \tag{4.7}$$

Permutation of the spin labels 1 and 2 makes $H_{ZF} = H_{ZF}'$ and the two systems must produce identical zero field spectra.

B). Eigenstates of the Dipolar Coupled System.

In the presence of the dipolar coupling, the simple product states are no longer the eigenstates of the zero field Hamiltonian since from equations (2) and (6) one sees that H_D will "mix" the product states together. Using stationary perturbation theory[4] one finds the perturbed eigenfunctions $|i\rangle'$ (i = xx, xy, xz etc.) are given by

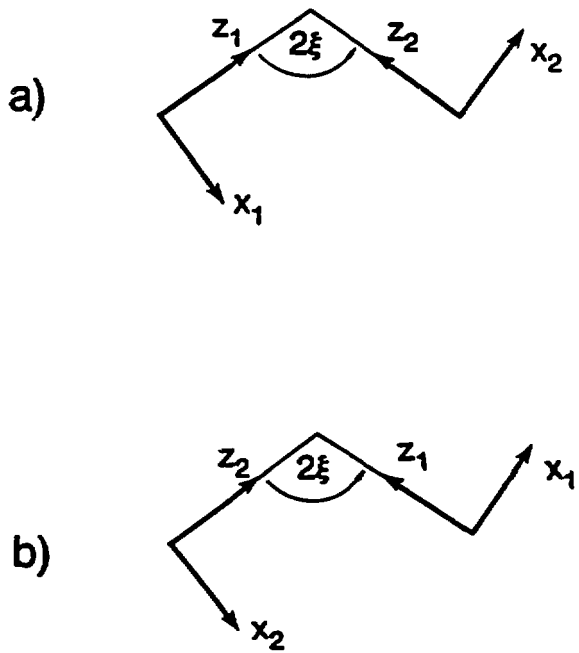

Figure 4.2 Illustration of exchange of EFG tensors.

$$|\,i\,\rangle' = |\,i\,\rangle + \sum_{j \neq i} \frac{\langle j|H_D|i\rangle}{E_i - E_j} \qquad (4.8)$$

where the summation is over the product states $|i\rangle$, assumed to be nondegenerate. If we examine the perturbed (and unnormalized) wavefunction $|xy\rangle'$ we find it has the form

$$|xy\rangle' = |xy\rangle + c_1|yz\rangle + c_2|yx\rangle + c_3|zx\rangle + c_4|zz\rangle \qquad (4.9)$$

where c_i are constants < 1. The admixture of additional components into the initial product states shifts the eigenvalues of the system as shown schematically in Figure 4.3. These admixed components of the coupled system eigenstates have the additional effect of producing many more allowed transitions in the NQR spectrum. This also is illustrated in Figure 4.3 along with the stick-plot obtained by computer simulation of one possible configuration of the methylene EFG tensors.

C. Simulations: Effect of Deuteron-Deuteron Dipolar coupling

As shown above the dipolar coupling transforms the NQR spectrum of coupled pairs of deuterons in a manner that depends upon the deuteron-deuteron internuclear distance, and the magnitude and relative orientation of their respective EFG tensors. Since the magnitude and orientation of the internuclear vector can be measured by neutron diffraction and the quadrupole coupling constants and asymetry parameters can be measured with fair accuracy from the spectrum, one expects to obtain the relative orientations of the two EFG tensors given a reasonably well resolved spectrum which features these dipolar splittings. In the following section we present a few simulations for typical two deuteron systems to show how dipolar

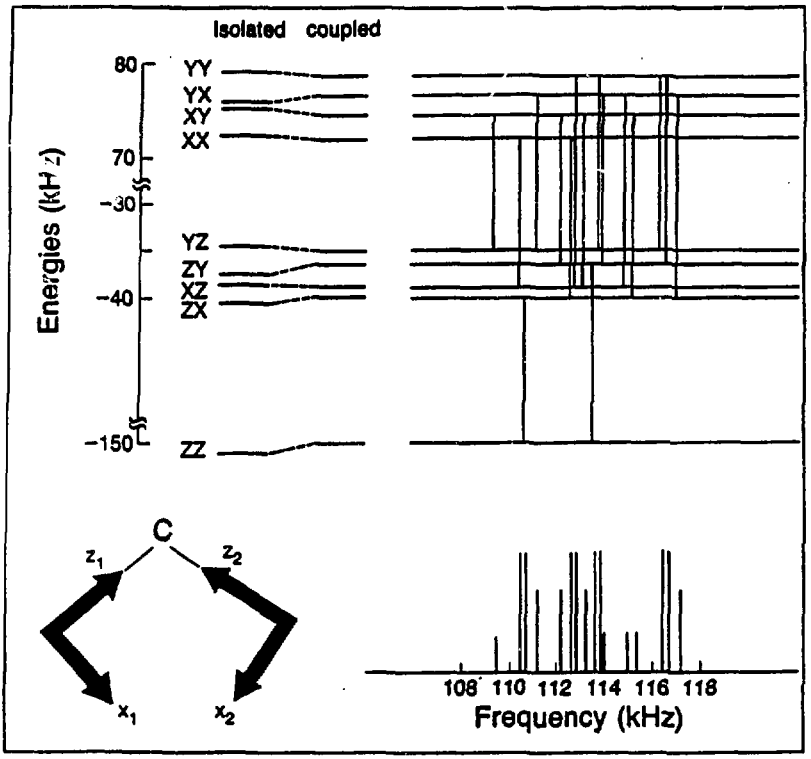

Figure 4.3. Top left: schematic of energy levels of eigenstates in the coupled and uncoupled case for two equivalent deuterons. Top right: illustation of allowed transitions in the ν_+/ν_- region between eigenstates of dipolar coupled deuterons in the zero field experiment. Bottom right: Resulting zero field spectrum for dipolar coupled deuterons. Frequencies and intensities were calculated by computer simulation for the CD_2 tensor orientations shown at bottom left and are to scale.

coupling may influence the experimental spectra. The simulations were performed using the program PJ:TOO, written by P. Jonsen and described in Appendix IV.A.

Our primary goal in undertaking the simulations is not to provide a comprehensive study but to get a qualitative idea of how the dipolar Hamiltonian perturbs the zero field NQR spectrum. For that reason we liberally use approximations to reduce the number of possible orientations for which one must calculate a zero field spectrum. Our second goal is to see how well we can fit the experimental zero field ^2H NQR spectrum of perdeuterated diethyl terephthalate. There, the methylene region shows dipolar splittings and is perhaps the best resolved spectrum to date. Therefore, the CD_2 simulations which follow will use parameters which match as closely as possible those of the diethyl terephthalate CD_2 case.

1). Methylene Groups

The simulations assumed the electric field gradient lay along the respective C-D bonds[5] and those of inequivalent CD_2's used quadrupolar parameters calculated directly from the sudden spectrum. We also assumed a geometry with r_{D-D} = 1.81 Å and a D-C-D bond angle of 109.5°. Two sets of simulations were performed; both assumed a high degree of symmetry in the molecule. The first assumed that the two quadrupolar tensors are related by a C_2 rotation about the D-C-D bisector and the second assumed that the tensors were related by a rotation of 109.5° about an axis passing through the carbon atom and perpendicular to the D-C-D plane. We refer to these informally as the flip and kick models, respectively. These seem like reasonable starting points for the simulations since single crystal measurements

have found similar situations in glycine[5] and malonic acid.[6] A similar approximation was used in the analysis of double resonance NQR studies by Edmonds et al.[7] A full set of simulations encompassing all possible orientations was beyond the scope of the present work.

a). Equivalent deuterons, $\eta \neq 0$

Both flip and kick models produced symmetric splittings about the unperturbed ν_+ and ν_- frequencies as can be seen in Figures 4.4 and 4.5; the splitting about the unperturbed ν_o frequency is reasonably symmetric but less so than in the ν_+ and ν_- cases. Both spectra have pronounced satellite lines, some of the kick orientations have satellite lines whose intensity approaches that of the major lines, so in that respect the kick spectra are more significantly perturbed. By calculating the quadrupole parameters directly from the major lines of these spectra one obtains values of the quadrupole coupling constants within ± 0.5% of the actual values and asymmetry parameters differing by -4% to +8% in the flip and < +6% in the kick.

b). Inequivalent deuterons, $\eta \neq 0$

Figures 4.5 and 4.6 show that both the flip and kick models produce spectra consisting of four major lines in the ν_+/ν_- region and two major lines in the ν_o region, in qualitative agreement with the spectrum expected from two inequivalent deuterons. Satellite lines and shoulders appear in both models, the flip spectra seem to be the more perturbed with more satellites of greater intensity. In both models, quadrupole coupling constants calculated from the four major peaks vary by ≤ ± 0.2% from the actual values input into the simulation. The asymmetry parameters calculated in this way varied from 0 to 7% in the flip spectra and by 0 to -6% in the kick. Even

Figure 4.4 Simulations for kick orientations of CD_2 group as a function of ϕ for equivalent deuterons. Simulations used $(e^2qQ/h) = 150.$ kHz and $\eta = .05$ with $r = 1.81$ Å.

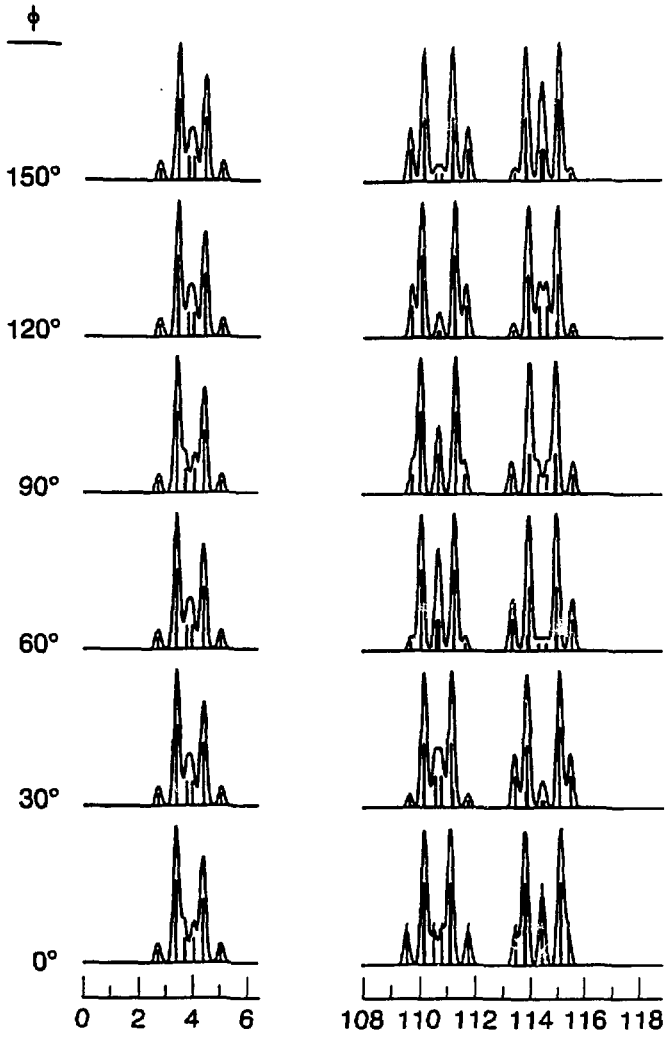

XBL 861-6109

Figure 4.5 Simulations for flip orientations of CD_2 group as a function of ϕ for equivalent deuterons. Simulations used $(e^2qQ/h) = 150.$ kHz and $\eta = .05$ with $r = 1.81$ Å.

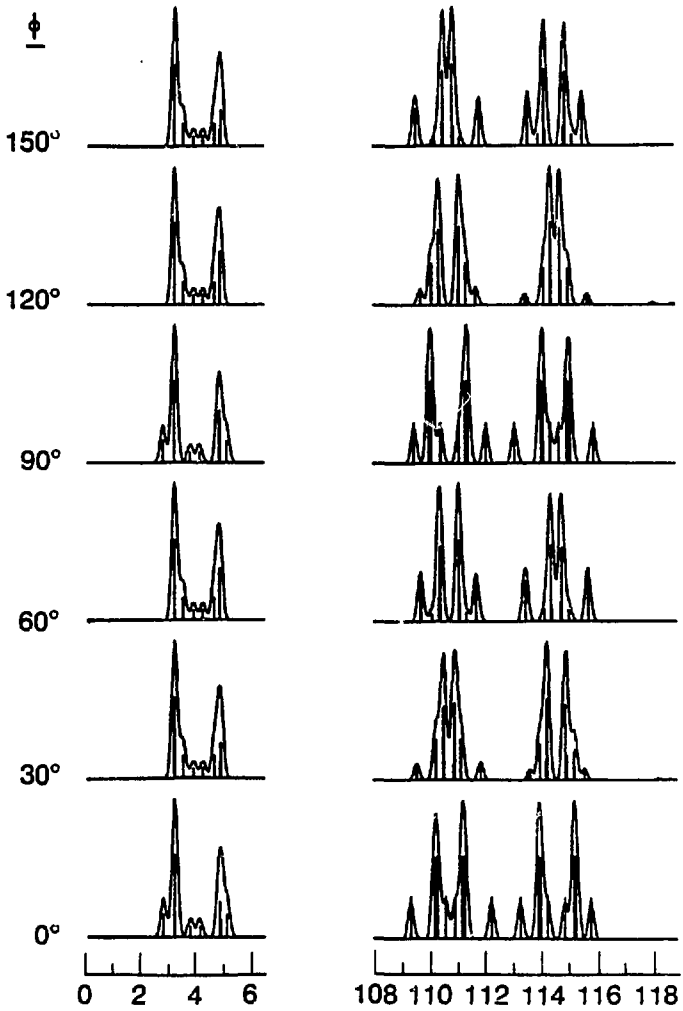

XBL 861-6105

Figure 4.6 Simulations for flip orientations as a function of ϕ for inequivalent deuterons. Simulations used parameters appropiate for diethyl terephthalate CD_2 case as discussed in text. Simulations used $(e^2qQ/h)_1$ = 152.67 kHz, η_1 = 0.049, $(e^2qQ/h)_2$ = 149.7 kHz, η_2 = .041 and r = 1.81 Å.

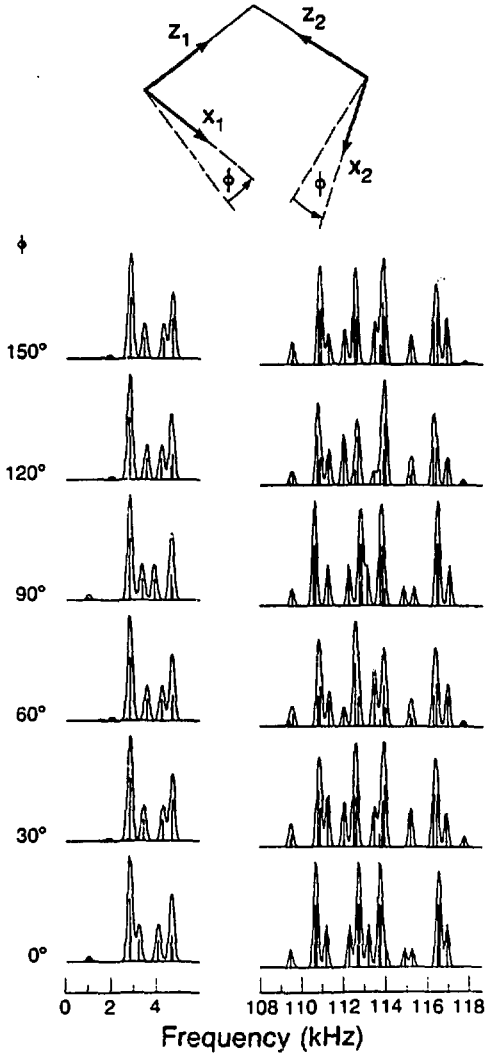
z_1
z_2
x_1
x_2
ϕ
ϕ
ϕ
150°
120°
90°
60°
30°
0°
0 2 4
108 110 112 114 116 118
Frequency (kHz)

XBL 861-9103

Figure 4.7 Simulations for kick orientations as a function of ϕ for inequivalent deuterons. Simulations used parameters appropiate for diethyl terephthalate CD_2 case as discussed in text. Simulations used $(e^2qQ/h)_1$ = 152.67 kHz, η_1 = .049, $(e^2qQ/h)_2$ = 149.7 kHz, η = .041 and r = 1.81 Å.

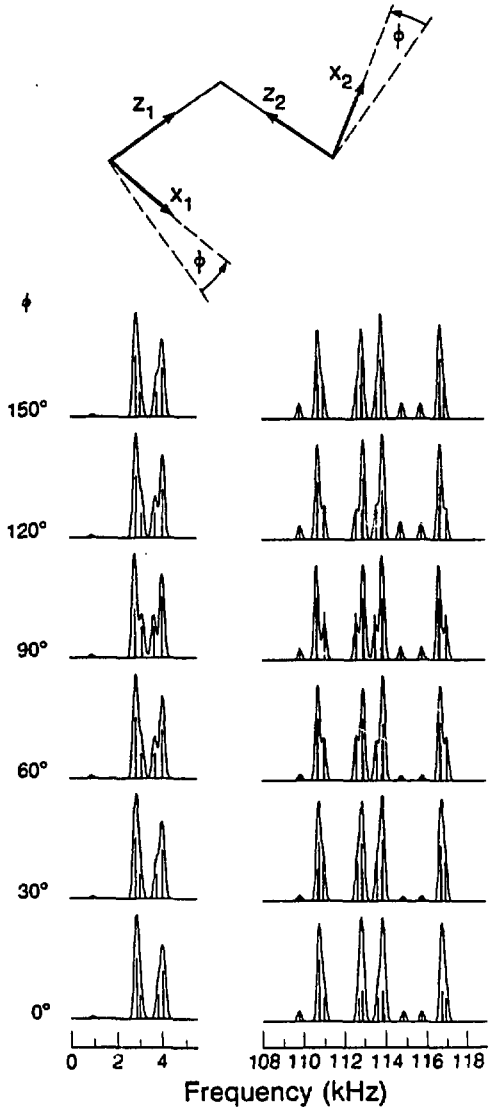
z_1
z_2
x_2
x_1
ϕ
ϕ
ϕ
150°
120°
90°
60°
30°
0°
0 2 4
108 110 112 114 116 118
Frequency (kHz)

XBL 861-9104

with the lines with 300 Hz linewidths seen in the methylene region of diethyl terephthalate, one calculates error limits of ~ ±0.1% in the quadrupole coupling constants and ±6% in the asymmetry parameters. These results mean that the dipolar coupling has virtually no effect on the qcc(quadrupole coupling constant). The effect of the dipolar coupling on the "apparent" asymmetry parameter is significant but still those calculated from the experimental spectrum should be close to within the experimental error of the real value. As linewidth increases, this becomes even more likely.

1.Simulation of Experimental Data -

Diethyl Terephthalate.

In the solid state diethyl terephthalate exists as a nearly planar molecule, shown in Figure 4.9. The terminal CH_2-CH_3 bonds are twisted ~9° out of the plane,[8] making the methylene deuterons crystallographically inequivalent. If the molecule was completely planar, and excluding any intermolecular effects, one would expect that the EFG tensors of the two deuterons composing a methylene group would be related by symmetry. As a first attempt at fitting the experimental spectrum we have performed simulations assuming that the two EFG tensors are configured in either the "flip" or "kick" geometries. We do not expect to be able to determine all of the 10 or so parameters which determine the experimental spectrum, but do expect that by making reasonable estimates we can get a good idea of the orientations of the tensors.

The experimental spectrum, obtained using the sudden zero field experiment is reproduced in Figure 4.8 and shows basically four major peaks which possess shoulders and splittings due to the dipolar

Figure 4.8 Results of simulations for CD_2 in diethyl terephthalate.

A) Tensor orientation producing best fit of experimental spectrum. Tensor 1 (left) is related to tensor 2 by a 180° flip about the C_2 axis. The x_1 axis lies -10° below the DCD plane and x_2 lies -10° above.

B) Reproduction of the ν_o and methylene ν_+/ν_- regions (note that the experimental ν_o region contains a split line at -1 kHz due to the aromatic deuterons.)

C) Best fit simulation of the CD_2 deuterons Parameters are given in the text and a Gaussian broadening function was applied to simulate the linewidth.

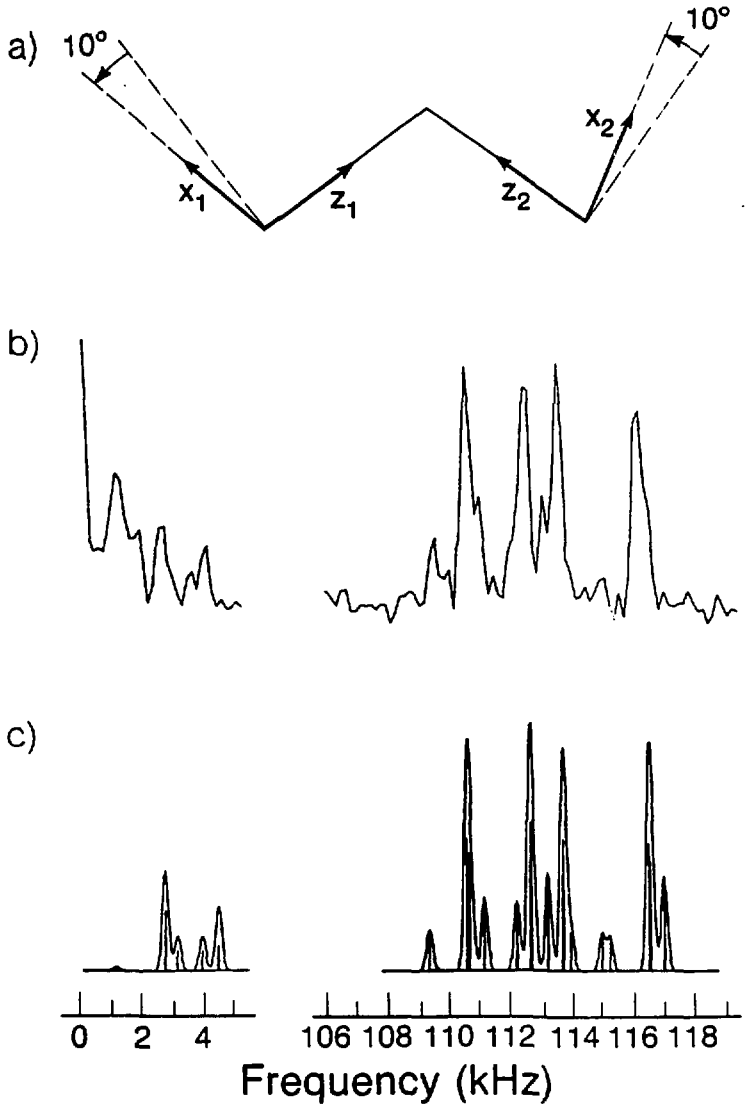
a)
10°
10°
x1
z1
z2
x2
b)
c)
0
2
4
106 108 110 112 114 116 118
Frequency (kHz)

XBL 861-6114

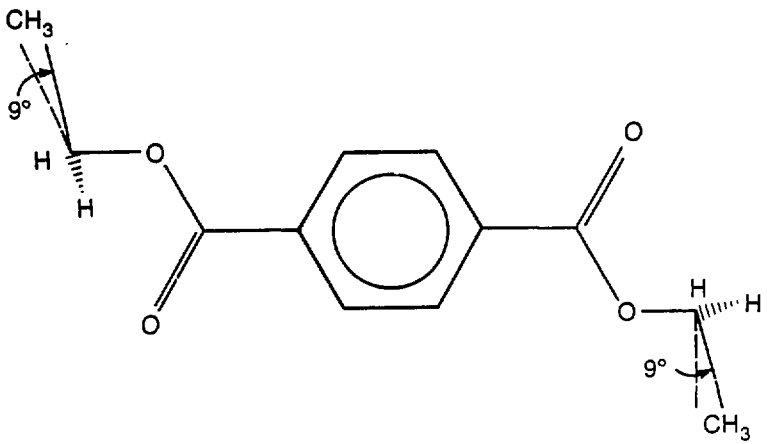

Diethyl terephthalate

XBL 861-6121

Figure 4.9 Schematic of solid state orientation of diethyl terephthalate. The bond angles and lengths are to scale and are taken from the x-ray data[8] (with the exception of the C-H bond lengths which are estimated). The molecule is centrosymmetric in the solid state and CH_2-CH_3 vector is oriented at ~9° from the plane defined by the aromatic ring.

coupling. A few smaller satellite lines are also evident. In general we note that the kick model spectra do not possess the shoulders or splittings evident in the major lines of the experimental version. In contrast, the flip spectra display both the shoulders and splittings. For these reasons we rule out the kick model. The best all around fit obtained, Figure 4.8, is then a flip spectrum corresponding to the case where the EFG y axes are tilted approximately 10^{o} out of the D_1CD_2 plane. The major peaks of the experimental spectrum are reproduced although there is slight disagreement in the frequencies of the satellite lines. Still the agreement is good.

2). Deuterons on Adjacent Aromatic Ring Sites

a). Equivalent Sites - $\eta = 0.05$

Figure 4.10 shows the stickplot simulation of the dipolar perturbed spectrum of two deuterons located on adjacent sites of an aromatic ring for two possible relative orientations of their EFG tensors. In both we have assumed the EFG y axes are perpendicular to the molecular plane, as was found in anthracene.[9] Also we have assumed that the electric field gradient of each of the two EFG tensors lies along the respective C-D bond and have taken $(e^2qQ/h)_1 = (e^2qQ/h)_2 = 180$ kHz, $\eta_1 = \eta_2 = 0.05$, typical values for static aromatic sites.[10,11] The distance r_{12} was taken to be 2.5 Å, calculated assuming 120^{o} bond angles in the ring and C-C and C-H distances equal to 1.4 and 1.1 Å, respectively.[8] The flip spectra feature ν_o and ν_- lines split by ~500 Hz and an unsplit ν_+ line. In both cases, the dipolar perturbation results in a spectrum which resembles that from two inequivalent uncoupled sites, especially since

Figure 4.10. Results for simulations of adjacent aromatic deuterons with equivalent EFG tensors.

A). Flip orientations with y axis of EFG_1 and EFG_2 perpendicular to the molecular plane.

B). Kick orientations with y axis of EFG_1 and EFG_2 perpendicular to the molecular plane.

Equivalent Sites

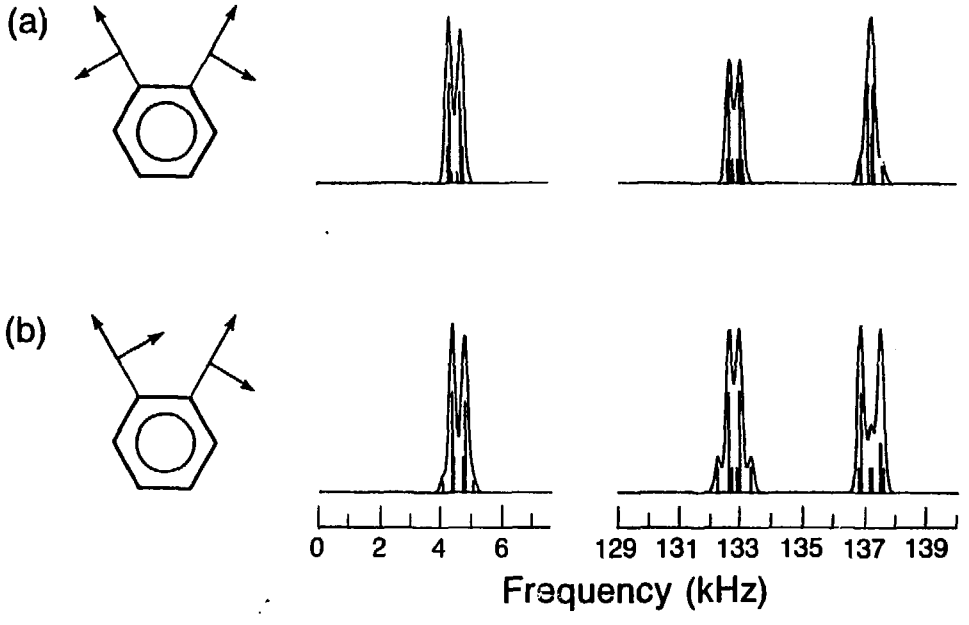

XBL 861-6113

the two apparent ν_0 lines coincide with the splittings observed in the ν_+/ν_- region. On this basis, one would calculate quadrupole coupling constants which differ by $\leq 0.2\%$ from the actual values and asymmetry parameters differing by $\leq 6\%$.

b). Equivalent sites - variable η

Additional simulations of the flip and kick orientations, Figures 4.11 and 4.12. show that there is very little change in the zero field spectrum once η is greater than zero. We have used the same broadening function in all these spectra (resulting in single lines of ~300 Hz in width-at-half-maximum).

c). Inequivalent sites with $\eta \neq 0$ - model for diethyl terephthalate

Simulations using the quadrupole coupling constant and η found experientally for the diethyl terephthalate aromatic sites are shown in Figure 4.13. Again the orientations featured in Figure 13 both have the EFG PAS y directions perpendicular to the molecular plane. One concludes from these simulations that the two orientations would not be distinguishable from a zero field experiment applied to this particular isomer.

D. Effect of Protons.

In this section we consider the effect that protons will have on the NQR spectra of nearby deuterons. By necessity all of the indirect spectra fall into this category.

1) Symmetry of the H-D Spectra.

The spectrum of a deuteron dipolar coupled to a single proton is easily calculated by writing the full dipolar Hamiltonian between them

in the principal axis system of the deuteron. One evaluates $H_D + H_Q$ in the eigenstates of the combined deuteron/proton system in a manner similar to that described for the deuteron/deuteron case. The resultant spectra show a great deal of symmetry in the relative orientations of the deuteron EFG and internuclear vector. The results of the simulations can be summarized

$$S(\theta,\phi) = S(180^\circ-\theta,\phi) = S(\theta,\phi+180^\circ) = S(\theta,-\phi) = S(\theta,180-\phi)$$

for all η. One can thus confine simulations to orientations of the internuclear vector confined to the first octant of a sphere centered about the EFG PAS system.

2). Simulations of CHD Methylene Groups

The CHD simulations assumed a DCH angle of 109.5°, therefore the angle between the EFG and H-D internuclear vector was taken to be 35.25°. The length of the H-D internuclear vector was taken to be 1.81 Å and we assumed e^2qQ/h = 152.7 kHz. (The value 152.7 is equal to that obtained experimentally from direct detection sudden experiments which will be described in the next chapter.)

a). CHD with η = 0 versus orientation

The unperturbed spectrum would consist of a 1:1:1 triplet at frequencies ± 114.5 and 0 kHz. In the simulations, one finds the dipolar coupling results in an almost symmetrical splitting of the high frequency lines as shown in Figure 4.14. The difference of the high frequency lines amounts to 5.41 kHz. This seems reasonable since $\gamma_H\gamma_D/2\pi r^3$ = 3.1 kHz and no quenching effect should exist since η = 0.[13] Calculation of the quadrupole parameters directly from this

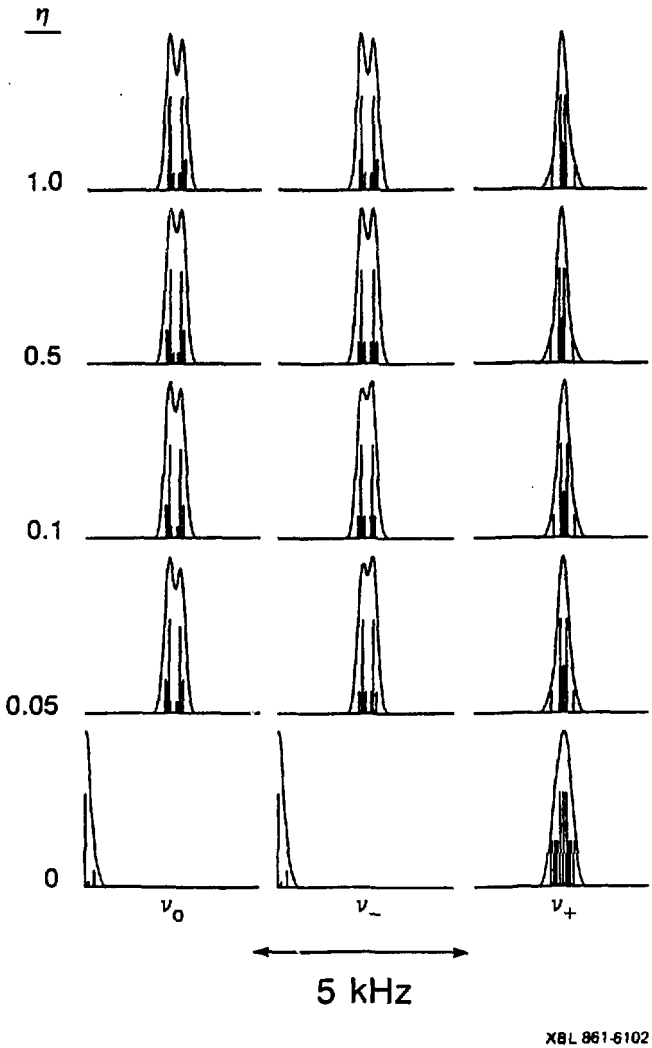

Figure 4.11 Flip orientations for adjacent aromatic deuterons with equivalent EFG tensors versus η.

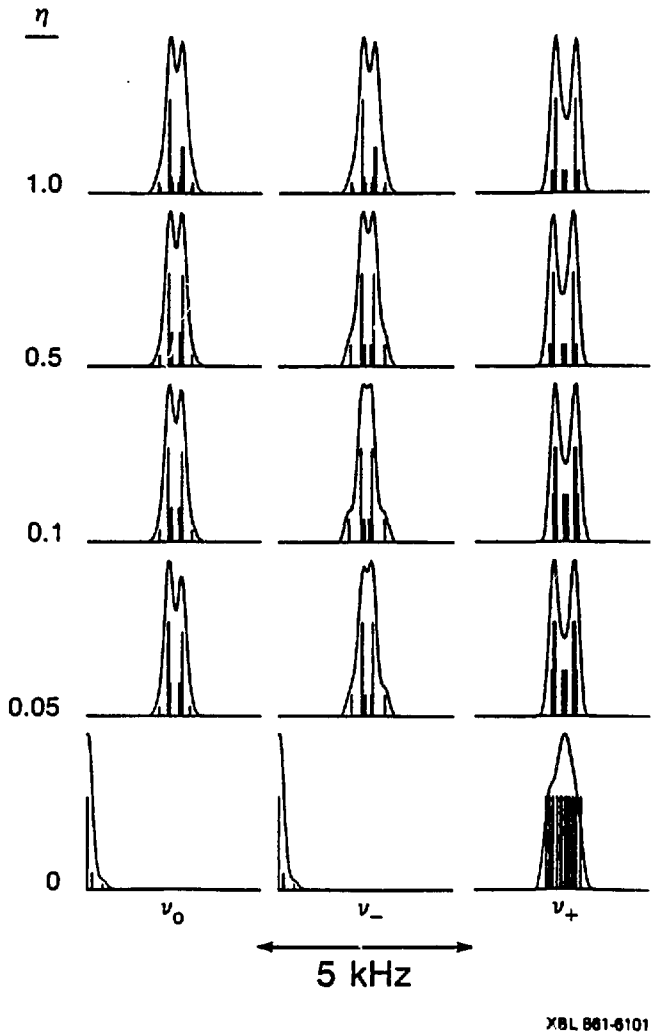

Figure 4.12 Kick orientations for adjacent aromatic deuterons with equivalent EFG tensors versus η.

Figure 4.13 Results for simulations of adjacent aromatic deuterons with inequivalent EFG tensors. This situation closely parallels that for diethyl terephthalate.

A). Flip orientations with y axes of EFG_1 and EFG_2 perpendicular to the molecular plane.

B). Kick orientations also with y axes of EFG_1 and EFG_2 perpendicular to the molecular plane.

Inequivalent Sites

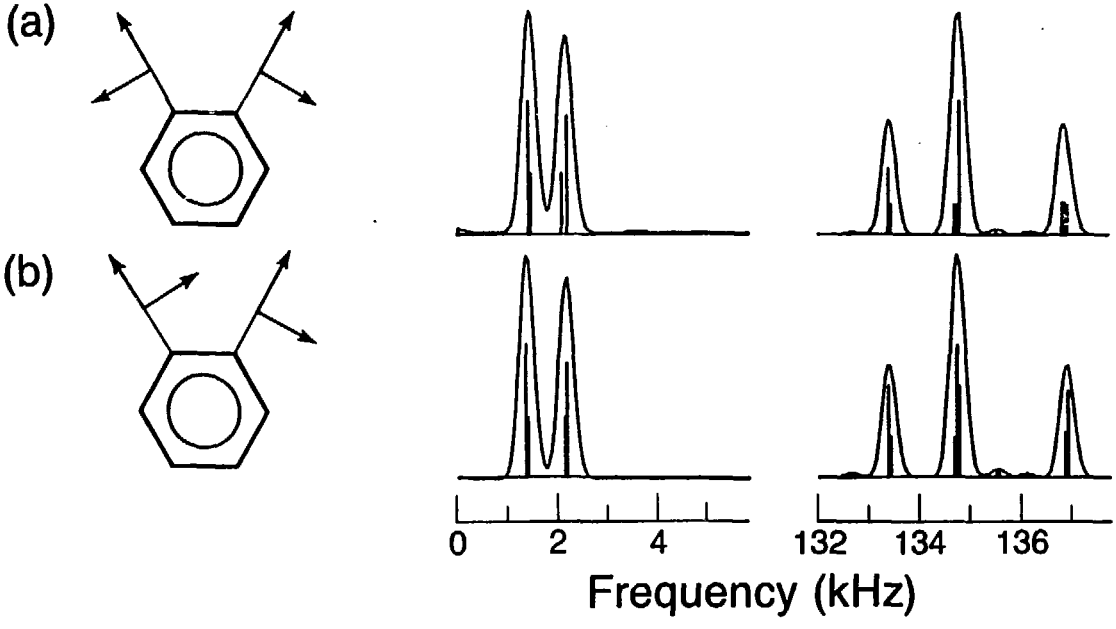

XBL 861-6112

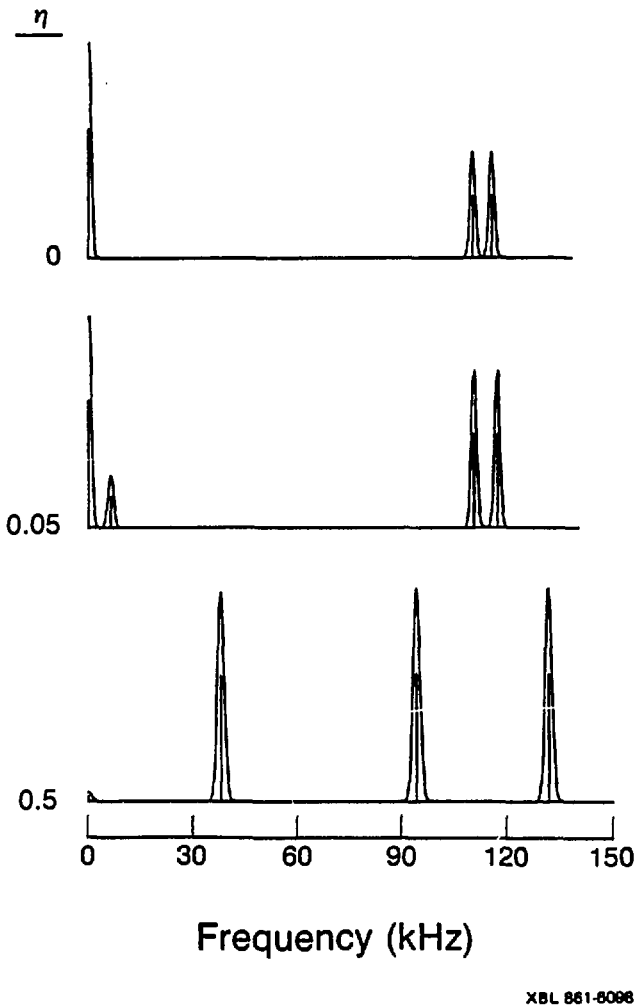

Figure 4.14 Simulations of CHD group versus η.

simulation results in a e^2qQ/h = 152.79 kHz and η = 0.071, a negligible error in the former but a substantial one in the latter.

b). CHD with η = 0.05 versus orientation - Comparison with experimental results.

The unperturbed spectrum should consist of equal intensity lines at 116.4, 112.6 and 3.81 kHz. The introduction of the slight asymmetry in the EFG tensor results in a spectrum only weakly dependent upon the relative orientation of the quadrupole and dipolar tensors, as shown in Table 4.1. There, ϕ is defined as the angle

Table 4.1. Zero field Spectra for CHD with η=.05 versus orientation[a]

ϕ[b]	Freq	Inten	Freq	Inten	Freq	Inten	Freq	Inten
0°	0.	.90	6.63	.22)	111.28	.67)	117.91	.67
30°	0..	.94	6.63	.22)	111.28	.67)	117.91	.67
60°	0.	.87	6.61	.22)	111.29	.67)	117.90	.67
90°	0.	.84	6.61	.22)	111.29	.67)	117.90	.67

[a]frequencies in kHz
[b]spherical polar coordinate of r_{HD} in deuteron PAS

between the proton-deuteron internuclear vector and the x axis of the deuteron EFG principal axis system. The frequencies of the various lines vary by no more that 10 Hz across the full range of orientations. The ν_+ and ν_- lines are shifted by -1.5 and -1.3 kHz respectively relative to the frequencies of the uncoupled case. Calculation of the quadrupole parameters from this spectrum yields e^2qQ/h = 152.79 kHz and η = 0.081, i.e. an error of < 0.1% for e^2qQ/h

and ~70% for η. We note that the relative difference between this apparent η and the real η is less than in section A above. The most striking feature of the simulation is the zero frequency line whose intensity comprises ~30% that of the total spectrum. Were this intensity equally divided by the lines at $\pm\nu$, the spectrum would exhibit the 1:1:1 ratio of $\nu_+:\nu_-:\nu_0$ expected for the unperturbed case. One expects some intensity to appear at zero since H_D has the effect of "mixing" together the eigenstates, thus allowing transitions between degenerate states.

This simulation closely parallels the physical situation of the CHD and CD_2 groups in diethyl terephthalate for which we can compare the experimental results of the sudden experiment (obtained with CD_2) and the indirect experiments (obtained with CHD), shown in Table 4.2

Table 4.2. Diethyl Terephthalate - Comparison of Results

	Sudden		Indirect	
	e^2qQ/h	η	e^2qQ/h	η
I	149.53±.14	0.042±.003	149.8±.4	0.039±.008
II	152.76±.14	0.049±.003	153.1±.4	0.051±.007

below. Error limits were estimated on the basis of the experimental linewidths of 300 Hz found in the sudden experiments and 800 Hz found in the indirect. These results agree with one another much more than the above simulations would predict and suggest either the simulations are in error or perhaps we are not taking into account some important aspect of the problem.

3). CHD with $\eta = 0.5$ versus orientation

The unperturbed spectrum consists of equal intensity lines at 133.59, 95.42 and 38.17 kHz. The calculated dipolar perturbed spectra were found to consist of essentially equal intensity lines (within 3%) at 38.56±.01, 95.31±.01 and 133.86±.01 kHz throughout the range ϕ=0° to ϕ=90°. Some intensity did occur at zero frequency, but this was <5% that of the other features. The increased asymmetry parameter reduces the perturbative effect of the dipolar coupling, in qualitative agreement with the predictions based on second moment calculations.[13] Calculation of the quadrupolar parameters from this spectrum yields e^2qQ/h = 152.78 and η = 0.505. errors of 0.1% and 1.%, respectively.

4). Simulations of Proton /Deuteron on Adjacent Ring Sites versus orientation

These simulations assumed HCC and DCC bond angles of 120°, therefore the angle between the deuteron efg and the proton-deuteron internuclear vector was taken as 120°. For this case one can estimate proton-deuteron internuclear distance of 2.5 Å. Simulations using e^2qQ/h=180 kHz η=0.22 show that the ν_+ and ν_- lines are shifted by -+.29 and -.25 kHz respectively , regardless of relative orientation of EFG and internuclear vector. A line at zero frequency is present at all orientations, its intensity ranges from 13%-16% that of the total spectrum. If one calculated the quadrupole coupling constants on the basis of the shifted lines, one would obtain e^2qQ/h=180.03 and η=0.028. The neglect of the dipolar interaction in this case results then in a negligible error in the quadrupole coupling constant. One obtains an error on the order of 30% for the asymmetry parameter.

E). Conclusions and Summary

The proton/deuteron simulations predict a rather large increase in the observed asymmetry parameter for both the methylene case and the proton and deuteron on adjacent ring sites case. Experimental observations to date of diethyl terephthalate do not substantiate this result. To our knowledge this is the only example for which both experiments have been performed. The deuteron/deuteron simulations predict that the quadrupole coupling constants measured directly from the spectra for dipolar coupled CD_2 systems and deuterons on adjacent ring sites will differ negligibly from the actual values; in both cases the aymmetry parameters predicted to differ by only $\leq +6\%$. Finally, we have attempted to fit the experimental zero field spectrum of the CD_2 groups in diethyl terephthalate by assuming that the the EFG tensors are related by a simple symmetry operation and have found that the best fit is produced by an orientation where the tensors are related by a C_2 flip about the D_jCD_2 bisector and each efg is oriented at a 10^0 angle with respect to the DCD plane.

Appendix IV.A The Program PJ:TOO.

The program PJTOO (written by Paul Jonsen) was used to simulate the sudden zero field spectra of two coupled deuterons. The program calculates the spectrum expected from a "sudden" version of the experiment where I_z of deuteron is detected in high field. We describe here the theory and operation of the program. First, the signal function for a single orientation of the spin system with respect to the laboratory frame is given by

$$S(t_1) = \mathrm{Tr}\{ I_{z,lab} \cdot U(t_1) \cdot I_{z,lab} \cdot U(t_1)^{-1} \} \qquad (4.12)$$

where $U(t_1) = \exp\{-i[H_D+H_Q]t_1\}$. The trace is evaluated in the eigenbasis of $H_Q + H_D$, thus $S(t_1)$ becomes

$$S(t_1) = \sum_{i,j,k,l} \langle i|I_{z,lab}|j\rangle\langle j|U(t_1)|k\rangle\langle k|I_{z,lab}|l\rangle\langle l|U(t_1)^{-1}|i\rangle$$

$$= \sum_{i,k} |\langle i|I_{z,lab}|j\rangle|^2 \cdot e^{i(\omega_i-\omega_j)t_1} \qquad (4.13)$$

where $h\omega_i/2\pi$ is the energy of eigenstate i. A powder distribution of crystallite orientations requires integration to obtain

$$S(t_1)_{powder} = \int S(t_1)\, d\Omega$$

$$= \sum \left[|\langle i|I_x|j\rangle|^2 + |\langle i|I_y|j\rangle|^2 + |\langle i|I_z|j\rangle|^2 \right] \times \exp\{i(\omega_i - \omega_j)t_1\} \qquad (4.14)$$

The program starts with the matrices $H_Q + H_D$ and I_i, i=x,y,z, all expressed in a convenient basis set (usually that of H_Q). The

program diagonalizes $H_Q + H_D$ and calculates the matrix R which transforms the original basis set into the $H_D + H_Q$ eigenbasis. Using R and its inverse, the matrices I_i are transformed into the zero field eigenbasis. From above one sees that the signal intensity at $\omega_{ij}=\omega_i-\omega_j$ contributed by states i and j is just the term in brackets above, so the program just calculates this sum for each ij pair and sums the intensities accordingly.

Appendix IV.B High Field NMR single crystal studies of Deuterium EFG tensor orientations

1). Basic Theory of the Experiments

Experimental details[5,6,9,20] and accounts of data manipulation[21] can be found elsewhere. In high field the NMR spectrum of each magnetically inequivalent deuteron of a particular orientation of a molecule consists of a two line spectrum (assuming no dipolar coupling). One generally studies these two line spectra as a function of the orientation of the crystal with respect to the magnetic field by mounting the crystal in such a way that one can rotate it about an axis parallel to or related to one of the three crystallographic axes. The field B_o is applied perpendicular to this rotation angle and one usally records the spectrum in regular intervals about these axes. The procedure is usually performed for a total of three perpendicular axes and then a least squares fitting routine is used.[21] These studies provide an accurate measurement of e^2qQ/h and η but we shall show that they cannot completely define the relative orientations of two coupled tensors.

We begin by examining the high field Hamiltonian for two coupled deuterons which is given by

$$H = H_{Q1} + H_{Q2} + H_D \qquad (4.15)$$

with

$$H_D = \frac{\gamma^2 h^2}{(2\pi)^2 r_{12}^3} [\, 1 - 3\cos^2\theta_{12}][I_{1-}I_{2+} + I_{1+}I_{2-}]$$

where θ_{12} is the angle between the deuteron-deuteron internuclear

vector, r_{12} and the applied field. The quadrupolar terms are given by

$$H_{Qi} = A_i(3I_{zi}^2 - \hat{I}_i^2)$$

where

$$A_i = \frac{e^2 q\, Q_i}{8}(3\cos^2\theta_i - \eta_i \sin^2\theta_i \cos 2\phi_i)$$

and θ_i and ϕ_i are the spherical polar coordinates describing the orientation of the field B_o in the PAS of the EFG of spin i(Figure 4.1). Clearly

$$H_{Qi}(\theta_i,\phi_i) = H_{Qi}(180\text{-}\theta_i,\phi_i) \tag{4.16}$$

and also

$$H(\theta_i,\phi_i) = H(\theta_i,-\phi_i) \tag{4.17}$$

Since H_D is unaffected by transformation concerning the orientations of the EFG tensors we have that $H_{ZF}(\theta,\phi) = H_{ZF}(\theta,\pm\phi) = H_{ZF}(180\text{-}\theta,\pm\phi)$. Now consider B_o oriented in the EFG PAS of deuteron i, described by the spherical polar coordinates θ_i and ϕ_i. Now further consider a rotation of the coordinate system by 180° about its x axis while keeping the orientation of B_o constant. The spherical polar coordinates θ', ϕ' of B_o in this rotated coordinate system are related to the original coordinates by the relations $\theta' = 180\text{-}\theta$, and $\phi' = -\phi'$. Clearly

$$\begin{aligned} H_{ZF}(\theta_1,\phi_1,\theta_2,\phi_2) &= H_{ZF}(\theta_1',\phi_1',\theta_2\phi_2) \\ &= H_{ZF}(\theta_1,\phi_1,\theta_2',\phi_2') \\ &= H_{ZF}(\theta_1',\phi_1',\theta_2',\phi_2') \end{aligned} \tag{4.18}$$

This means no single crystal high field measurement of this type can

distinguish the EFG PAS z from -z, or y or -y directions, and an EFG PAS system determined as x,y,z could equally be x,-y, -z. In summary the PAS of any EFG tensor has two orientations which are equivalent as far as the high field measurements are concerned, and they are related to one another by a π rotation about the x axis of that PAS.

2. Deuterium single crystal results.

In this section we report on high field ^2H single crystal studies by others on compounds similar to those we have studied with the zero field technique. Compilations of quadrupolar data obtained by a variety of methods(single crystal, liquid crystals and polycrystalline) can be found elsewhere.[22] It appears that there are only a few examples in the literature where the EFG tensors of the deuterons in a CD_2 group have been determined separately[5,6,23] and to our knowledge there has been only one determination of the tensors of the aromatic sites in a ring compound.[9] We will discuss these cases, namely α-glycine, malonic acid and anthracene below.

a). Malonic acid

The first CD_2 single crystal determination was done by Derbyshire et al.[23] in 1969 on a room temperature perdeuterated sample of malonic acid using an 8 MHz wideline spectrometer. X-ray results[24] show that the material is triclinic $P\bar{1}$ with two molecules in the unit cell related by a center of symmetry; thus there are four crystallographically inequivalent sites.[d] The wideline measurements were able to make a determination of the quadrupole coupling constants and the orientations of the EFG tensors of all four of these sites.[1] Later pulsed measurements by Haeberlen[6] at 55 MHz were able to resolve

fine structure in the single crystal spectra due to dipolar couplings between the CD_2 deuterons. They also determined the room temperature quadrupole coupling constants and the orientations of the EFG tensors. Their results, presumably more accurate, differ somewhat from the earlier measurements, but are in qualitative agreement. By manipulation of the sign of the CD_2 dipolar coupling these authors could infer from fine structure line shape simulations of their experimental data that $eq > 0$ for the CD_2 sites. The orientation of the tensors with respect to the molecular frame as determined by Haeberlen et al. are shown in Figure 4.15. One can observe that the relative orientation of the two tensors is very close to the "kick" model in which the tensors are related by a -109.5° rotation about the fixed frame y axis. The details of the analysis of Haeberlen's data are discussed in Appendix IV.C .

b). α-Glycine($ND_3^+CD_2COO^-$)

In the solid phase α-glycine exists with two molecules/unit cell,[16] the EFG tensors of which are related by a plane, thus yielding five inequivalent sites in all. Room temperature single crystals were studied in high field and the EFG tensor orientations and quadrupole coupling parameters were determined for the static CD_2 and the motionally averaged ND_3 group.[5] Typical linewidths can be inferred to be about 1.5 kHz width at half maximum. Comparison of the CD_2 orientations with the C-H bond directions obtained from neutron diffraction studies[16] showed that the two were within $< 1^{\circ}$ of one another. The orientation of the methylene tensors with respect to the molecular frame are shown in Figure 4.16 along with the orientations obtained by a π_x rotation applied to EFG_2. In the latter case we note

that the two tensors are approximately related by a C_2 rotation about the fixed frame y' axis.

c). Anthracene.

In the solid state anthracene exists in a monoclinic form with 2 molecules per unit cell.[25] Wide line NMR at 7.8 MHz was performed.[9] The quadrupole coupling constants and EFG tensor orientations determined for the six magnetically inequivalent sites all fell within the range 181 ± 3 kHz and η = 0.064 ± .013. The error limits of the quadrupole coupling constants were given as ± 3.3 kHz. In all cases the y axes of the EFG tensors were determined to be perpendicular to the molecular plane.

Appendix IV.C Analysis of the Deuteron Single Crystal Data (a worked example in classical mechanics)

1). General

Given two tensors T_1 and T_2 which generally possess different PASs and different eigenvalues, we want to find the rotation operator $R(\alpha\beta\gamma)$ which rotates the PAS of T_1 into the PAS of T_2. Our primary motivation is that the computer program which simulates the dipolar coupled NQR spectrum of two deuterons (PJ:Too) requires this information. The reason why this is a problem is that the eigenvectors of T_1 and T_2 (which correspond to their PAS directions) are generally specified in the literature in an arbitrary frame, and so the Euler angles α,β,γ are not obvious from a simple examination.

One method to find the Euler angles relies on the following strategy. In the PAS of the EFG of deuteron 1 (PAS_1 hereafter), the eigenvectors of deuteron 1 have a simple form when written in a Cartesian basis, namely

$$u^*_{x1} = \begin{bmatrix}1\\0\\1\end{bmatrix} \quad , \quad u^*_{y1} = \begin{bmatrix}0\\1\\0\end{bmatrix} \quad , \quad \text{and } u^*_{z1} = \begin{bmatrix}0\\0\\1\end{bmatrix} \tag{4.19}$$

where we use the star to indicate the PAS of T_1. Using simple classical mechanics, we can transform the eigenvectors of deuteron 2 to PAS_1. Now α and β will be specified by the spherical polar coordinates of u_{z2} in PAS_1.[15] Finally we can solve for γ using the relation (given in equation 4.22 below) between the eigenvectors of T_2 written in PAS_2 and PAS_1. We work this out in detail below.

Consider a tensor T_1 written in its PAS and the related tensor T_1' specified by[2]

$$T_1' = MT_1M^{-1} \tag{4.20}$$

where $M = M(\alpha\beta\gamma)$ as defined here as the rotation operator which rotates PAS_1 into the PAS of a second tensor, PAS_2. The eigenvectors of T_1 in PAS_1 are simply those of equation (19). With M as we have defined it, transformations of a vector r from PAS_1 to PAS_2 is accomplished by[2]

$$r' = Mr \quad . \tag{4.21}$$

Similarly, tranformation of a vector p written in the PAS to that of T_1 is accomplished by

$$p' = M^{-1}p \quad . \tag{4.22}$$

Thus we can write the eigenvectors of T_2 in the PAS_1 frame by

$$u'_{j2} = M^{-1}u_{j2} \quad , \quad j = x, y, z. \tag{4.23}$$

As we have defined things, $M(\alpha\beta\gamma)$ is the rotation operator that when applied to the coordinate system PAS_1 will transform it in such a way that it will then be superimposable on PAS_2.

2). Glycine.

For the particular case of the glycine methylene deuteron EFG tensors, Haeberlen[5] reports the eigenvectors u_x, u_y and u_z in the "standard orthogonal" (SO) frame, which is simply the Cartesian frame defined by taking the x axis parallel to the crystalline a axis, the z axis parallel to the reciprocal lattice vector c^*, and y perpendicular to x and z. The spherical polar coordinates of the eigenvectors for the methylene deuterons reported by Haeberlen are reproduced in Table 4.A1. From these we can calculate the Cartesian coordinates of the

eigenvectors. The first step is to transform the eigenvectors of the Table to PAS_4. The eigenvectors of D_4 in this frame will of course be

Table 4.A1. Glycine CD_2 EFG Eigenvectors[5]

		θ	ϕ			θ	ϕ
D4	u_{x4}	8.5°	105.7°	D5	u_{x5}	131.1°	66.4°
	u_{y4}	86.9	354.3		u_{y5}	69.3	137.2
	u_{z4}	97.9	83.8		u_{z5}	48.3	27.5

identical to those given in equation 19. The remaining transformations are carried out[14]

$$u^*_{x5} = (u_{x5}\cdot u_{x4})u^*_{x4} + (u_{x5}\cdot u_{y4})u^*_{y4} + (u_{x5}\cdot u_{z4})u^*_{z4} \qquad (4.24)$$

and similarly for the other eigenvectors. The star is meant to indicate PAS_4, therefore the u^*_{x5} indicates the eigenvector u_{x5} expressed in the PAS_4 coordinate system. The dot product is invariant to coordinate transformation, thus it can be evaluated with the eigenvectors obtained from the literature, which are expressed in the SO frame. This process yields

$$u^*_{x5} = \begin{bmatrix} -.565 \\ .196 \\ .803 \end{bmatrix}, \quad u^*_{y5} = \begin{bmatrix} .466 \\ -.726 \\ .505 \end{bmatrix}, \quad u^*_{z5} = \begin{bmatrix} .680 \\ .660 \\ .320 \end{bmatrix} \quad . \qquad (4.25)$$

One recalls that when transforming from coordinate system x,y,z to x', y', z', the Euler angles α and β are simply the spherical polar coordinates of z' in the x,y,z, frame.[15] In this case we can see

$$u^*_{z4} \cdot u^*_{z5} = .68 = \cos\beta = \cos\beta \tag{4.26}$$

We can find the spherical polar coordinate $\phi = \alpha$ by finding the angle between the x^*_4 axis and the projection of z^*_5 on the $x^*_4y^*_4$ plane. This is done by writing

$$e^*_{x4} \cdot P_x(u^*_{z5}) = (1\ 0\ 0) \cdot \begin{bmatrix} 0.680 \\ 0.660 \\ 0.0 \end{bmatrix} \tag{4.27}$$

$$= |P_x| \cos\phi = |P_x| \cos\alpha$$

where e^*_{x4} is the unit vector in the direction of U^*_{x4}. Solution of the above equations yields $\alpha = 44.14^\circ$ and $\beta = 71.33^\circ$. From equation 23 the eigenvectors of D_5 written in PAS_4, designated as u^*_{i5}, will be

$$u^*_{x5} = M^{-1} \begin{bmatrix} 1 \\ 0 \\ 0 \end{bmatrix} \quad , \quad u^*_{y5} = M^{-1} \begin{bmatrix} 0 \\ 1 \\ 0 \end{bmatrix} \tag{4.28}$$

etc. Since $M^{-1} = M^T$, using equation 1.19 yields

$$M^T \begin{bmatrix} 0 \\ 1 \\ 0 \end{bmatrix} = \begin{bmatrix} -\cos\alpha \cdot \cos\beta \cdot \sin\gamma - \sin\gamma \cdot \cos\gamma \\ -\sin\alpha \cdot \cos\beta \cdot \sin\gamma + \cos\alpha \cdot \cos\gamma \\ \sin\beta \cdot \sin\gamma \end{bmatrix} = \begin{bmatrix} .466 \\ -.726 \\ .505 \end{bmatrix} \tag{4.29}$$

and similarly

$$M^T \begin{bmatrix} 1 \\ 0 \\ 0 \end{bmatrix} = \begin{bmatrix} \cos\alpha \cdot \sin\beta \cdot \cos\gamma - \sin\alpha \cdot \sin\gamma \\ \sin\alpha \cdot \cos\beta \cdot \cos\gamma + \cos\alpha \cdot \sin\gamma \\ -\sin\beta \cdot \cos\gamma \end{bmatrix} = \begin{bmatrix} -.565 \\ .196 \\ .803 \end{bmatrix} \tag{4.30}$$

which leads to $\gamma = 147.95^\circ$.

With the angles α, β, γ one can describe the relative orientations

of the two tensors but still needs to know their relationship with the molecular frame. This is accomplished by finding the coordinates of the deuteron-deuteron internuclear vector, r, in the PAS of EFG_4. For glycine one has two options

1) use the neutron diffraction data[16] and find r by transformation of the crystal frame coordinates of H4 and H5 to the SO frame, or;

2) assume the C-H vector extending from the methylene carbon atom to H_i is colinear with the z axis of the EFG PAS of deuteron i. From the neutron data one can verify that

$$\vec{CH}_4 \;//\; \vec{z}_4 \qquad \text{and} \qquad \vec{H}_5C \;//\; \vec{z}_5$$

(the symbol // means parallel to) where CH_4 is the bond vector between the methylene carbon and H_4 and whose origin is on the carbon and H_5C is the similar vector between H_5 and the carbon but whose origin is defined on H_5. Therefore

$$\vec{r}_{45} = -\left(\vec{z}_4 + \vec{z}_5\right) \quad .$$

Writing the coordinates of r in PAS_4 leads eventually to $\theta_r = 144.29^0$ and $\phi = 224.1^0$.

3). Malonic acid

Finally, we shall discuss the malonic acid data[6] which is reproduced in Table 4.A2 below. From a rough sketch, one can see that the PAS of D_3 is right-handed and that of D_4 is left-handed. To correct this problem we define a new coordinate system D_4' specified by u_{x4}, u_{y4} and $-u_{z4}$. In a manner similar to that used in section 2) above we find $\alpha,\beta,\gamma = 204.4^0$, 108.3^0, and 149.3^0, respectively. The

Table 4.A2. Malonic acid CD_2 EFG Eigenvectors

		θ	ϕ			θ	ϕ
D3	u_{x3}	85.8^0	55.9^0	D4	u_{x4}	90.1^0	324.0^0
	u_{y3}	35.5^0	151.8^0		u_{y4}	34.3^0	234.1^0
	u_{z3}	54.8^0	323.0^0		u_{z4}	55.7^0	53.9^0

coordinates of r assuming that both efg's point "out" from C to H leads to $\theta_r = 144.0^0$ and $\phi_r = 204.5^0$.

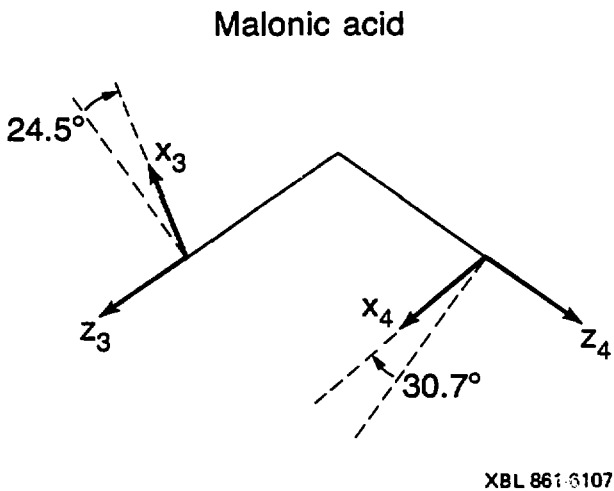

Figure 4.15 Tensor orientation of malonic acid's CD_2 group from data of Haeberlen et. al.[5]

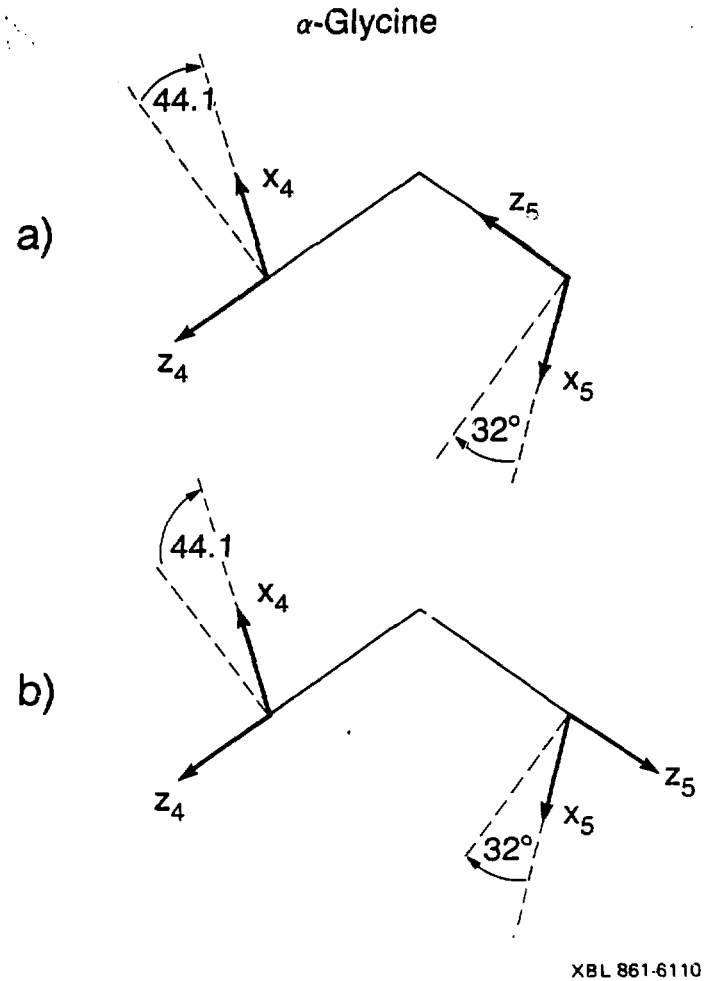

Figure 4.16 Tensor orientations of α-glycine CD_2 group as found by Haeberlen et. al[6];

A) Orientation as reported

B) Equivalent orientation formed by 180° rotation of EFG_2 about fixed frame y axis.

Appendix IV.D Consideration of EFG Tensor Orientations

In this section we concern ourselves with the symmetry of systems of coupled deuterons in zero field. Our goal is to get a physical feeling of what relative orientations of deuteron EFG tensors will produce identical zero field spectra. This will reduce the number of simulations required for a given system and allow us to make comparisons with the literature.

We recall the quadrupolar Hamiltonian is composed of spin and spatial variables. Rotation of these spin and spatial variables by an identical amount about a common axis leaves the total system invariant, since this amounts to a simple redefinition of the spin and spatial coordinate systems. In what follows we are interested in different relative orientations of the EFG tensors and so we shall employ a fixed spin coordinate system and perform rotations of the spatial variables alone.

1. Isolated Deuteron.

Consider a system composed of a single isolated deuteron. A 180° rotation of the spatial variables about any of the EFG tensor's principal axes leaves the quadrupolar Hamiltonian invariant. This is shown schematically in Figure 4.17. If we start with the quadrupolar Hamiltonian in its PAS system, for example, then H_{Q1} is given by[2]

$$H_{Q1} = I_1 \cdot \Lambda_1 \cdot I_2 \qquad (4.31)$$

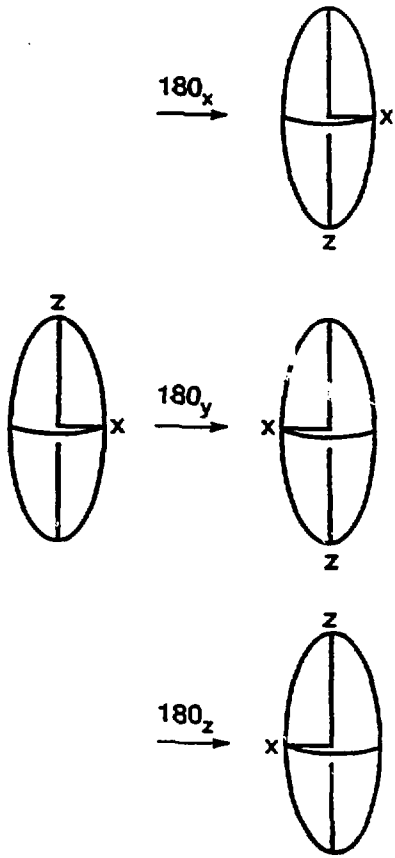

Figure 4.17. "Aestheticized" depiction of equivalent EFG tensor orientations for uncoupled deuterons. A 180° rotation about any of the principal axes results in an equivalent orientation.

$$= I_i \cdot \begin{bmatrix} A^i_{xx} & 0 & 0 \\ 0 & A^i_{yy} & 0 \\ 0 & 0 & A^i_{zz} \end{bmatrix} \cdot I_i \quad ,$$

and rotation of the spatial variables about the EFG PAS x axis is described by

$$H_Q' = R_x(180)\, H_Q\, R_x(180) \qquad (4.32)$$

$$= I_i \cdot \begin{bmatrix} 1 & 0 & 0 \\ 0 & -1 & 0 \\ 0 & 0 & -1 \end{bmatrix} \cdot A_i \cdot \begin{bmatrix} 1 & 0 & 0 \\ 0 & -1 & 0 \\ 0 & 0 & -1 \end{bmatrix}$$

$$= H_Q$$

and similarly for rotations of 180_y and 180_z. For the isolated spin, the total zero field Hamiltonian is just H_Q and since it is invariant to these 180° rotations, the zero field spectra will be also.

2). Coupled System of Two Deuterons.

We consider a system of two coupled deuterons whose zero field Hamiltonian can be written

$$H = H_{Q1} + H_{Q2} + H_D \quad . \qquad (4.33)$$

As shown in section II.A the Hamiltonian will be a function of the relative orientation of the two EFG tensors. The dipolar coupling reduces the symmetry found in the isolated case because the symmetry operations of the Hamiltonians H_{Q1}, H_{Q2} and H_D will not generally coincide. No longer will a 180° rotation of an EFG tensor about one of its principal axes leave the total zero field Hamiltonian (hence the zero field spectrum) invariant. Orientations of the type shown in Figure 4.18 will no longer be equivalent.

We shall consider a few concrete examples of tensor orientations

Figure 4.18. Series of inequivalent tensor orientations for coupled deuterons of methylene group. Rotation of EFG_2 by 180^0 about z_2' produces orientation labeled "II" which is inequivalent to "I". Similarly, rotatin of EFG_2 about x_2' (producing "III") does not produce an orientation equivalent to I. Note we use right handed coordinate systems throughout.

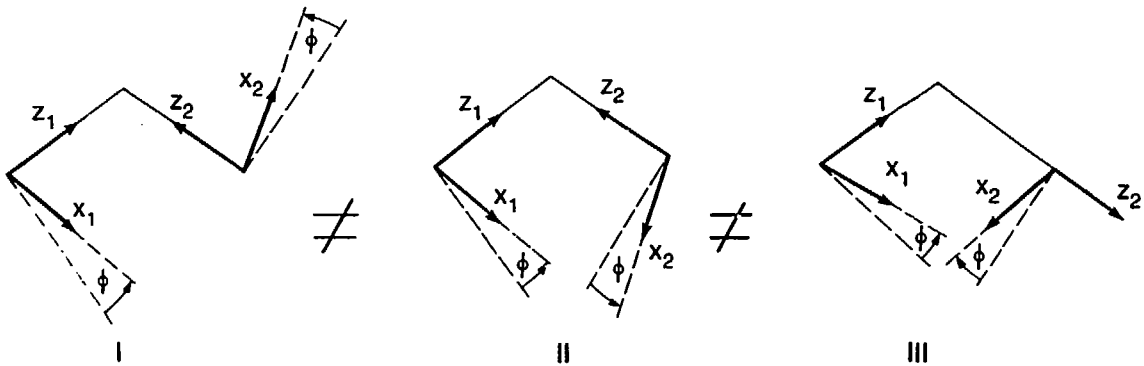

XBL 861-6118

and demonstrate one method of determining whether their zero field Hamiltonians are equivalent. We shall employ a coordinate system whose x axis is colinear with the internuclear vector between deuterons 1 and 2. This constitutes a principal axis system for the dipolar Hamiltonian. The dipolar Hamiltonian's effect in mixing the product eigenstates will depend upon the relative orientations of the quadrupolar Hamiltonians and the internuclear vector, but in this reference frame the form of H_D will remain constant. Our prime motivation is the understanding of CD_2 groups but this treatement is entirely general.

a). Two tensors related by $R_y(2\zeta)$ Figure 4.19 shows 2 possible relative orientation of the two EFG tensors. We wish to express the zero field Hamiltonian in the fixed frame xyz, therefore we must transform the PAS EFG tensors Λ_I into the fixed frame. We shall refer to the system of Figure 4.19a as the unprimed system and of 4.19b as the primed system. We can write the unprimed fixed frame Hamiltonian as

$$H_{ZF,f} = I_1 \cdot R_1 \Lambda R_1^{-1} \cdot I_1 + I_2 \cdot R_2 \Lambda R_2^{-1} \cdot I_2 + H_D \qquad (4.34)$$

where

$$R_1 = R_1(\alpha\beta\gamma) = R_1(0,-\xi,0) = R_y(-\xi)$$
$$R_2 = R_2(\alpha\beta\gamma) = R_2(0,\xi,0) = R_y(\xi)$$

and we note that the rotation operator $R_y(\pm\xi)$ refers to rotation about the fixed axis y. Similarly, the primed system's fixed frame Hamiltonian is given by

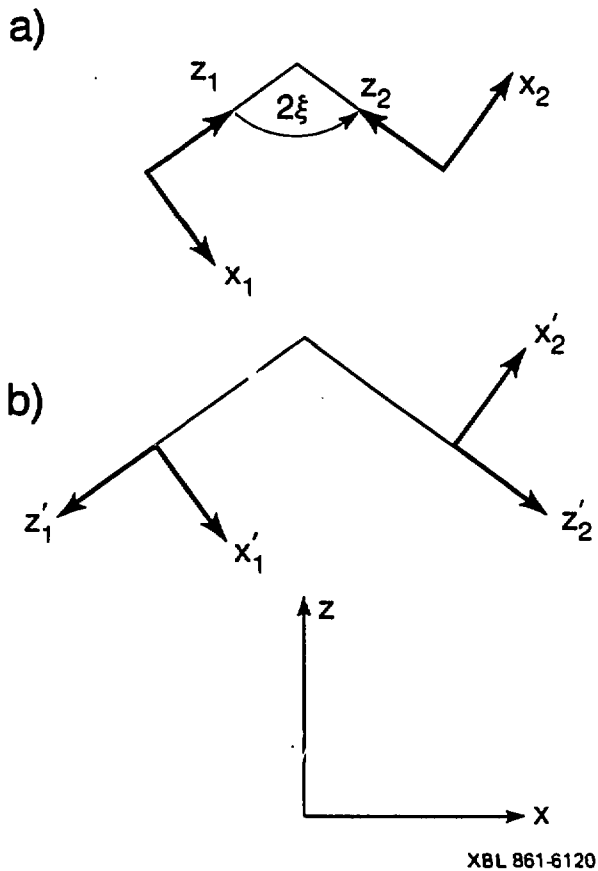

Figure 4.19. A). EFG_1 is rotated into the fixed frame coordinate system (shown at bottom) by the operator $R(0,-\xi,0)$ and EFG_2 by the operator $R(\xi)$.

B). The primed coordinate system PAS_1' is related to the fixed frame by $R(p,\xi+180^\circ,0)$, PAS_2' by $R(0,180^\circ-\xi,180^\circ)$.

$$H'_{ZF,f} = I_1 \cdot R'_1 \Lambda_1 R'^{-1}_1 \cdot I_1 + I_2 \cdot R'_2 \Lambda_2 R'^{-1}_2 \cdot I_2 + H_D \qquad (4.35)$$

where

$$R'_1 = R_z(180)R_y(\xi+180) = R_z(180)R_y(180) \cdot R_2$$
$$R'_2 = R_z(180)R_y(180-\xi) = R_z(180)R_y(180) \cdot R_1 \quad .$$

One can thus write

$$H'_{ZF,f} = R_z(180)R_y(180) \cdot (I_1 \cdot R_2 \Lambda_1 \cdot R_2^{-1} \cdot I_1 + I_2 \cdot R_1 \Lambda_2 R_1^{-1} \cdot I_2 + H_D) \cdot R_y(180)R_z(180) \qquad (4.36)$$

since H_D is invariant to the 180_y and 180_z rotations. The term H" will possess the same set of eigenvalues and eigenfunctions as $H_{ZF,f}$ as can be seen from simulations or extensions of arguments given for equation (7). Given this fact, we can show that $H'_{ZF,f}$ will produce the same spectrum as $H_{ZF,f}$ itself. Using H' as the relevant zero field Hamiltonian the signal function for the sudden experiment is given by[19]

$$S(t_1) = TR \left[I_{z,lab} U'(t_1) I_{z,lab} U'(t_1)^{-1} \right] \qquad (37)$$

where

$$U'(t_1) = \exp(-iH'_{ZF,f} t_1) \quad .$$

Using the expression above for $H'_{ZF,f}$ and expanding $I_{z,lab}$ in terms of its spherical polar coordinates in the fixed frame one has

$$S(t_1) = TR \left[R_x R_z [I_x \sin\theta\cos\phi + I_y \sin\theta\sin\phi + I_z \cos\theta] R_z^{-1} R_x^{-1} \cdot U(t_1) \cdot R_x R_z [I_x \sin\theta\cos\phi + I_y \sin\theta\sin\phi + I_z \cos\theta] \tilde{R}_z^1 \tilde{R}_x^1 \cdot U(t_1)^{-1} \right]$$

$$= TR \left[[-I_x \sin\theta\cos\phi + I_y \sin\theta\sin\phi - I_z \cos\theta] \cdot U''(t_1) \right.$$

$$\left. [-I_x \sin\theta\cos\phi + I_y \sin\theta\sin\phi - I_z \cos\theta] \cdot U''(t_1)^{-1} \right] \quad (4.38)$$

where $U''(t_1) = \exp(-iH''t_1)$. If we evaluate this trace in the zero field eigenbasis, we obtain

$$S(t_1) = \sum \left[\langle i|-I_x \sin\theta\cos\phi - I_y \sin\theta\sin\phi - I_z \cos\theta|j\rangle\langle j|U''(t_1)|k\rangle \times \right.$$

$$\left. \langle k|-I_x \sin\theta\cos\phi - I_y \sin\theta\sin\phi - I_z \cos\theta|l\rangle\langle l|U''(t_1)^{-1}|i\rangle \right]$$

$$= \sum_{i,k} |\langle i|-I_x \sin\theta\cos\phi + I_y \sin\theta\sin\phi - I_z \cos\theta|k\rangle|^2 \exp(it_1\omega_{ik}) \quad (4.39)$$

where $\omega_{ik} = \omega_i - \omega_k$. This is the signal due to only one orientation of the molecular fixed coordinate system with respect to the laboratory system. To obtain the signal from a powder distribution one integrates to find

$$S(t_1)_p = \sum (|\langle i|I_x|k\rangle|^2 + |\langle i|I_y|k\rangle|^2 + |\langle i|I_z|k\rangle|^2) \exp(-it\omega_{ik}) \quad (4.40)$$

which is identical to the expression one would obtain starting with H_{ZF} as the zero field Hamiltonian rather than H'_{ZF}. Therefore the two orientations yield identical zero field spectra. This prediction is born out by simulations of the type described earlier in the Chapter.

b). Two planar tensors related by an $R_z(\pi)$ rotation.

We describe the situation where the EFG tensors are related by a

180^{o} rotation about the fixed frame z axis, as shown in Figure 4.20. The operator R_1 which rotates the EFG_1 PAS into the fixed coordinate system is simply

$$R = \bar{R}_1^{-1} \tag{4.41}$$
$$R_1 = R_y(-180+\xi)R_z(180) \quad .$$

Similarly, one can write

$$R_2 = R_y(\xi-180) \tag{4.42}$$

and the corresponding operators for the primed system are

$$R_1' = R_z(180)R_y(\xi-180)R_z(180) \tag{4.43}$$
$$R_2' = R_z(180)R_y(\xi-180)$$

Now one can write

$$H = I_1 \cdot R_1 \Lambda_1 R_1^{-1} \cdot I_1 + I_2 \cdot R_2 \Lambda_2 R_2^{-1} \cdot I_2 + H_D \tag{4.44}$$
$$H' = R_z(180) \cdot H \cdot R_z(180)^{-1} \tag{4.45}$$
$$= H$$

by the same arguments as used in the previous case.

c). Two nonplanar tensors related by Ry(2ξ) rotation. By examination of this case, Figure 4.21, one can write

$$H_{Qi}' = R_y(180)H_{Qi}R_y(180)^{-1} \tag{4.46}$$

and then as in cases a and b we have that $H' = H$. In this case conversion between the unprimed and primed systems takes place via a 180^{o} rotation that is not a symmetry operation of the quadrupolar tensors, in contrast to cases a and b. In those cases, since the transformation was accomplished by a symmetry operation of the quadrupolar and dipolar parts of the zero field Hamiltonian, then no

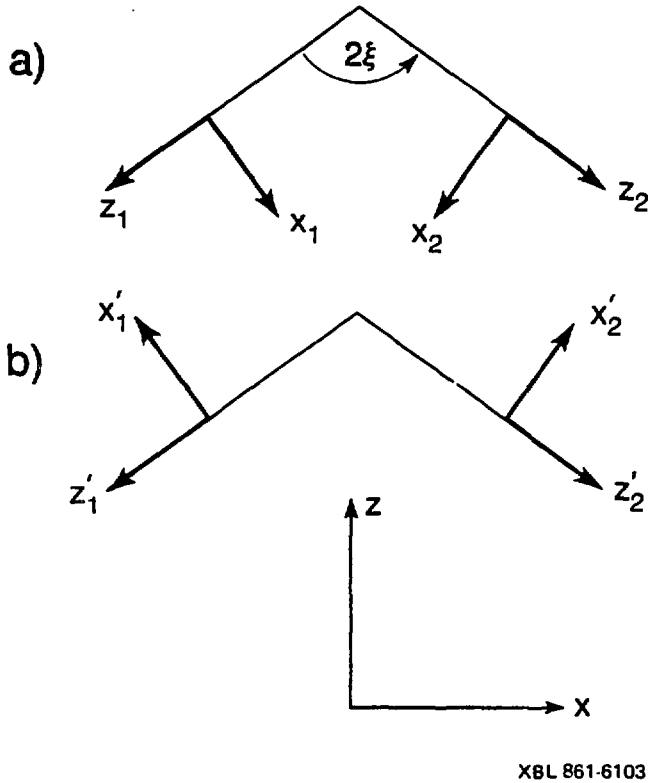

Figure 4.20 R(180,ξ-180°,0) takes PAS_1 into the fixed frame and R(ξ-180°,0,0) takes PAS_2 into the fixed frame.

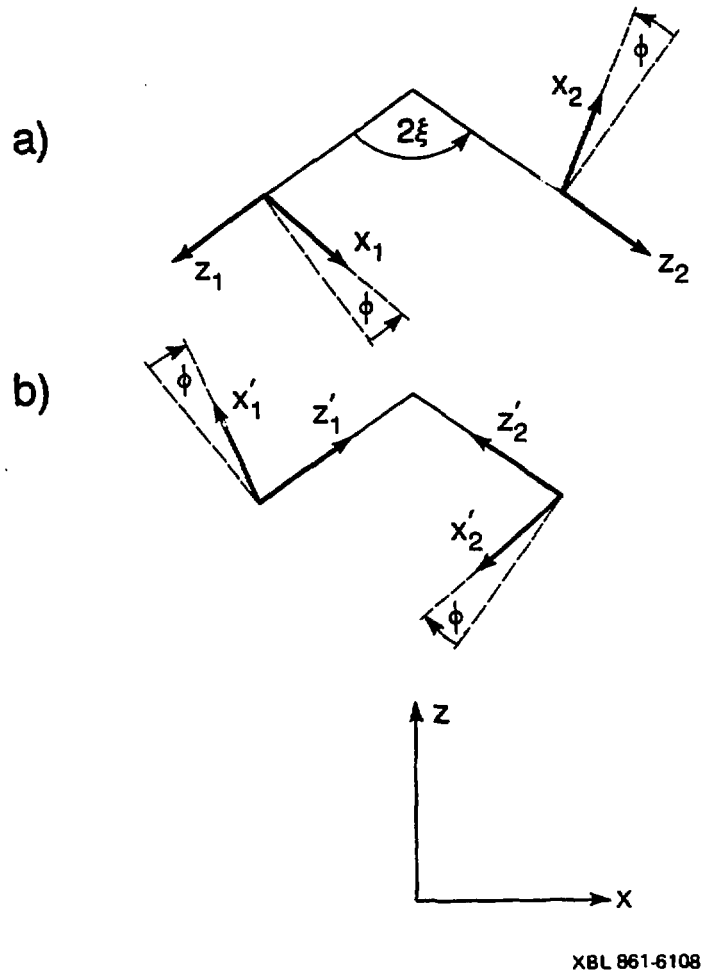

Figure 4.21. Two equivalent orientations for the EFG tensors of a methylene group.

change would be seen in the zero field spectrum if the system were to rapidly jump between the orientation of the primed and unprimed systems. No motional averaging of the spectrum would occur. This is not true for case c, rapid jumping between the two systems will motionally average the quadrupolar parts of the Hamiltonian and can therefore produce significant changes in the zero field spectrum.

d). A different version of two tensors related by $R_y(-2\xi)$. We consider this case because we have already seen that given a system where both z axes of the EFG tensors point "in", we can find an equivalent orientation where both point "out". We then ask, given a system where one points "in" and one points "out", can we find an equivalent orientation where both point in or out. We start with the planar case, Figure 4.22 , from which we will be able to draw conclusions regarding the more general nonplanar case. As before we can write

$$\begin{aligned} R_1 &= R_y(-\xi) & R_1' &= R_y(\xi) \\ R_2 &= R_y(\xi) & R_2' &= R_y(\xi-180) \end{aligned} \quad . \tag{4.47}$$

Now the corresponding unprimed and primed system Hamiltonians are

$$\begin{aligned} H &= I_1 \cdot R_y(-\xi) A_1 R_y(-\xi)^{-1} \cdot I_1 + I_2 \cdot R_y(\xi) A_2 R_y(\xi)^{-1} \cdot I_2 + H_D \\ H' &= I_1 \cdot R_y(-\xi) A_1 R_y(-\xi)^{-1} \cdot I_1 + I_2 \cdot R_y(\xi-180) A_2 R_y(\xi-180)^{-1} \cdot I_2 + H_D \end{aligned} \tag{4.48}$$

We note that

$$\begin{aligned} R_y(\xi-180) A_2 R_y(\xi-180)^{-1} &= R_y(\xi) R_y(-180) A_2 R_y(-180)^{-1} R_y(\xi)^{-1} \\ &= R_y(\xi) A_2 R_y(\xi)^{-1} \end{aligned} \quad .$$

since for this orientation the y axis of the PAS of EFG_2 is colinear

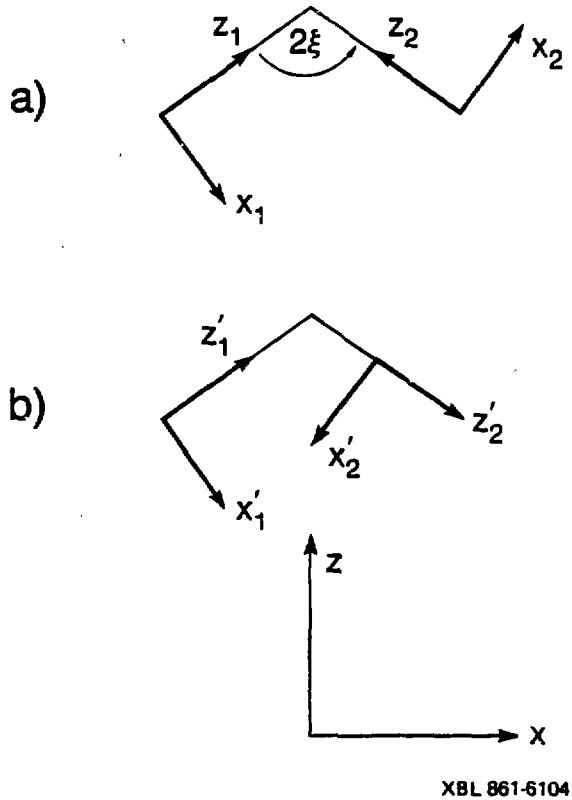

Figure 4.22. Two equivalent orientations of the EFG tensors. This is a special case, however, since the equivalence requires colinearity of the fixed frame y axis and one of the principal axes of deuteron two's EFG tensor.

with the fixed frame y axis. Therefore H_Q produces the same zero field spectrum as H_Q'. Clearly this equivalence comes about only because of the colinearity of the y fixed axis and one of the axes of deuteron two's PAS. In the general case, i.e. nonplanar, one would not have this situation and in that case the zero field spectra would differ. Examples of these general cases were shown earlier in Figure 4.18.

Appendix IV.E Transformations between Crystalline Frames and the Standard Orthogonal Frame

From time to time one wishes to make computations with atomic coordinates given in the x-ray or neutron diffraction literature. Typically the position of an atom is expressed in a crystalline frame in terms of its fractional coordinates x,y,z along the crystalline axes a, b, and c respectively. The x,y, and z defined here are generally different from the Cartesian coordinates. In this manner the position vector of an atom i is given

$$\mathbf{r} = x_i\vec{a} + y_i\vec{b} + z_i\vec{c} \tag{4.50}$$

where

$$|\vec{a}| = a\ ,\ |\vec{b}| = b\ ,\ |\vec{c}| = c$$

and

$$\angle(\vec{a},\vec{b}) = \gamma,\quad \angle(\vec{a},\vec{c}) = \beta \quad \text{and} \quad \angle(\vec{b},\vec{c}) = \alpha\ .$$

In general $\alpha,b,\gamma \neq 0$. We describe transformation to a Cartesian frame known as the standard orthogonal frame defined such that

$$x_{SO} \,//\, \vec{a}\ ,\quad y_{SO} \,//\, \vec{c}^{*}\ ,$$

and y_{SO} is in the ab plane. The vector c* is the reciprocal lattice vector defined by the vector cross-product[17]

$$\vec{c}^{*} = \frac{\vec{a} \times \vec{b}}{\vec{a}\cdot\vec{b} \times \vec{c}} \cdot 2\pi \tag{4.51}$$

Transformation from the crystal frame to the SO frame is defined by

$$U = Mu \tag{4.52}$$

where u represents the crystalline coordinates and U the SO coordinates. The matrix M is defined by[18]

$$M = \begin{bmatrix} a & b\cos\gamma & c\cos\beta \\ 0 & b\sin\gamma & Q \\ 0 & 0 & V/(ab\sin\gamma) \end{bmatrix} \tag{4.53}$$

where

$$Q = c[\cos\alpha - \cos\beta\cos\gamma]/\sin\gamma \tag{4.54}$$

and

$$V = abc\sqrt{1 - \cos^2\alpha - \cos^2\beta - \cos^2\gamma + 2\cos\alpha\cos\beta\cos\gamma} \tag{4.55}$$

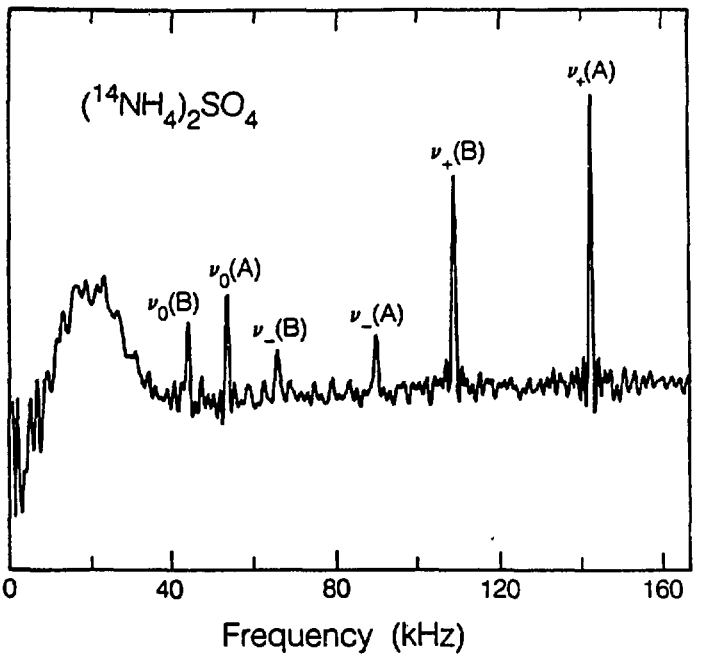

Figure 3.6. Indirectly detected pulsed zero field ^{14}N NQR spectrum of $(NH_4)_2SO_4$ with selective 2π pulses for the protons. Peaks corresponding to two inequivalent sites are labeled A and B. Residual proton signal appears below 40 kHz but has been reduced enough to allow for resolution of the ^{14}N NQR lines. From the frequencies observed at room temperature, (e^2qQ/h) and η can be calculated. Site A: $(e^2qQ/h) = 154.5$ kHz, $\eta = 0.688$, Site B: $(e2qQ/h) = 114.9$ kHz, $\eta = 0.747$. (At 296.1 K, Batchelder and Ragle (Ref. 16) give values of I: $(e^2qQ/h) = 154.53$ kHz, $\eta = 0.684$; II: $(e^2qQ/h) = 115.71$ kHz, $\eta = 0.749$.)

20. W. Derbyshire, T.C. Gorvin and D. Warner, Mol.Phys. 12, 299(1967).
21. G.M. Volkoff, H.E. Petch and D.W.K. Smellie, Can.J.Phys. 30, 279(1952).
22. F.S. Millet and B.P. Dailey, J.Chem.Phys. 56, 3249(1972); P.L. Olympia Jr., I.Y. Wei and B.M. Fung, J.Chem Phys. 51, 1610(1969); R.G. Barnes in Advances in NQR, J.A.S. Smith, editor, (Heyden, London, 1972), I, 335.
23. W. Derbyshire, T.C. Gorvin and D. Warner, Mol.Phys. 17, 401(1969).
24. J.A. Goedkoop and C.H. MacGillavry, ActaCryst, 10, 125(1957).
25. A.M. Mathieson, J.M. Robertson and V.C. Sinclair, Acta Cryst. 3, 245(1950); J.M. Robertson, Rev.Mod.Phys. 30, 155(1958).

Chapter V. Experimental Studies Using ^2H Zero Field NQR

The quadrupole parameters of a deuteron reflect the electronic environment at that site. As a result quadrupole coupling constants are a sensitive measure of motion, structure and bonding in solids. With the development of solid state high field NMR techniques, deuterium powder patterns have been studied extensively in an attempt to model systems of interest.[1] Obtaining these spectra is often difficult as a spectrometer with high power, rapid digitization and quick recovery capibilities is required to characterize the free induction decay of broad line spectra.[2-3] In addition, these broad lineshapes are not sensitive to subtle motions, small asymmetry parameters or slight differences in quadrupolar coupling constants. Double resonance NQR[4-5] also provides a means of determining values of the quadrupole parameters but is often limited by the absorption of the proton system at low frequencies. Single crystal studies[6-9] may also be conducted to determine quadrupolar information but are often tedious and time consuming procedures which require extensive data collection and manipulation. Furthermore not all cases of interest are accessible by such studies.

On the other hand, Zero field ^2H NQR[12-15] provides a sensitive means of obtaining high resolution quadrupolar spectra in polycrystalline solids since it removes the orientational anisotropy which produces the broad high field lineshapes. By using either the sudden transition[12] or the selective zero field indirect detection (ZFID)[13] experiments, small quadrupole coupling constants and

asymmetry parameters can be determined directly from the observed frequencies. In this chapter we present the results of zero field experiments on several deuterated polycrystalline organic solids and inorganic hydrates and compare the results obtained with these from high field powder patterns.

I. Deuterium Powder Patterns

A). Introduction

Theoretically the same type of information obtainable from a deuterium zero field NQR spectrum is also obtainable from a deuterium high field powder pattern. Although simple in theory, the experimental difficulties involved in obtaining such a powder pattern can be quite severe.[16-17] Due to the large linewidths(~hundreds of kilohertz), signal-to-noise can be a problem since the signal is spread over a large bandwidth. High rf powers are also generally required to excite the signal evenly over its this large bandwidth. Distortion in the powder pattern frequently results since the spectral density of the exciting rf radiation is generally uneven over the powder pattern. In addition, the large linewidth means the signal damps out in times ~100's of μsec and fast digital sampling is required.[16]

Methods do exist to help alleviate these problems. The problem of uneven spectral density can be dealt with by use of high power or composite pulses[18] which compensate for small B_1 fields. These pulses, discussed in detail elsewhere,[18] often provide spectral excitation as good or better than one would obtain using much larger B_1 fields. Minor distortions of the spectrum due to the uneven

spectral density of the exciting rf can also be treated by convolution of the frequency domain spectrum with an appropriate function.[17] A problem related to the fast-damping of the signal stems from the fact that NMR receivers always require a finite amount of "recovery time" after an rf pulse before they can come out of saturation and acquire useful data. Since these recovery times can be anywhere from 1 μsec to 10's of μsec (depending on the preamp, the Q of the probe and one's ingenuity), a large portion of the quadrupolar fid can be lost if one performs the simple 90°-acquire sequence. The solution, of course, is to use an echo. The experiments that follow utilize the quadrupolar echo sequence[19-20], 90_x-τ-90_y-acquire, and its composite pulse variation.[18]

Still one problem that is not so easily solved is the superposition in the spectrum of signals from all sites. Unless the sites can be "filtered" using some property such as their relaxation,[1] one must resort to selective deuteration to resolve different site. Techniques for selective deuteration are well known, but generally expensive and tedious.

B). Basic Theory of Powder Patterns.

Deuterium powder patterns are described in detail elsewhere.[1,21-23] The experimental lineshape is dictated not only by H_Q but the dipolar Hamiltonian as well and also the characteristic motions of the system. We will ignore the motion for now and will also ignore H_D except to say that it generally blurs out the sharp singularities predicted from H_Q alone. Typically the dipolar effect on quadrupolar powder patterns is simulated by convolution of the pure quadrupolar lineshape with an appropriate broadening function, e.g. a

Gaussian.

In general a static isolated deuteron produces a powder pattern with singularities appearing at[23] $\nu_1=\nu_o\pm(3e^2qQ/8h)(1-\eta)$ and steps or edges appearing at $\nu_3=\nu_o\pm(3e^2qQ/4h)$ where ν_o is the resonance frequency of the deuteron in the absence of the quadrupolar interaction. Shoulders can appear at $\nu_2=\nu_o\pm(3e^2qQ/h)(1+\eta)$. In most of the situations we shall encounter below $\eta\leq.05$ and the features at ν_1 and ν_2 are unresolved. In the case of larger η the ν_2 shoulders are often broadened out by the dipolar interaction.[24]

Figure 5.1 shows the well known spectrum predicted for the case of $\eta=0$. The splitting between the "horns" is given by $\Delta\nu_1=3e^2qQ/4h$ and the edges of the powder pattern pattern are separated by $\Delta\nu_3=3e^3qQ/2h$, thus for a theoretical powder pattern $\Delta\nu_2=2\Delta\nu_1$. Symmetric lineshapes similar to that of Figure 5.1 are expected for the majority of "static" sites since they will usually have $\eta\leq.05$.[1] Very often, as e^2qQ/h increases, the signal-to-noise will be such, however, that only the horns of a given site will be visible. Rotating methyl groups (for which e^2qQ/h are typically ~40kHz) will be a notable exception.

C). Experimental Details.

The quadrupolar echo spectra were obtained using the quadrupolar echo sequence with τ typically equal to 20 μsec. The quadrupolar echo spectra were obtained with ninety times of 3.0 μsec obtained using a Drake L7 tuned amplifier driven by an ENI 5100L(~1 kW final output). Spectra utilizing the composite sequence, given in equation (1) below, were obtained with ninety times of 6.4 μsec using the ENI alone. Pulse shapes and pulse droop encountered with the L7 produced poor

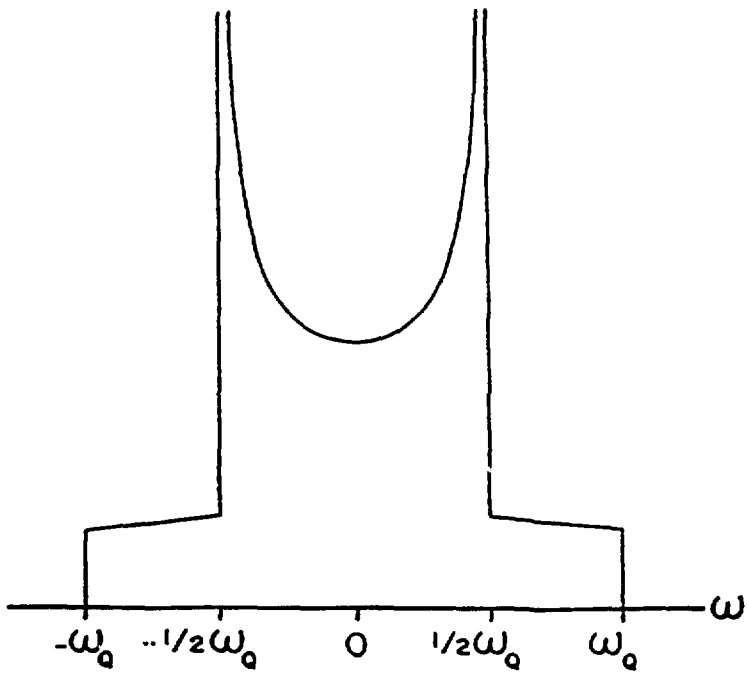

XBL 8111-12667

Figure 5.1). Theoretical powder pattern for isolated spin one in an axially symmetric EFG. Here $\omega_Q = 3e^2qQ/4h$ and θ is the angle between the electric field gradient and B_o, the applied field. (Figure courtesy of R. Eckman)

results and were therefore deemed unsuitable for the composite experiments. All high field spectra were obtained at room temperature on a spectrometer with a 55 Mhz ^2H resonance frequency.

The maximum sampling rate on the spectrometer was TI 4 (dwell time= 4 μsec); greater effective sampling rates were obtained by a simple three-step procedure: 1) acquisition of the fid with dwell time Δ to obtain signal $S(t_1)$ at $S(0)$, $S(\Delta)$, $S(2\Delta)\ldots$, $S((nfid-1)\Delta)$; 2) repetition of the experiment but delaying acquisition by $\Delta/2$ to obtain signal at $S(\Delta/2)$, $S(3\Delta/2)\ldots,S((nfid-1/2)\Delta)$; 3) feathering of the two signals together to obtain effective sampling rate of $1/2\Delta$. Clearly this method required twice an long as would the experiment done with a faster data acquisition system. Our effective times calculated below are defined as the time it would have been taken to do the experiment on a spectrometer equipped with the faster data acquisition system.

Effect of receiver drift and drift of the pulse break-through were countered by a phase-shifting scheme where noted. For the composite sequence[18] this amounted to acquisition of the signal under the two sequences a and b below followed by subtraction of one from another.

$$\begin{aligned} &\text{a} \quad 90_{\bar{x}}\text{-}180_{x}\text{-}90_{\bar{x}}\text{-}135_{x}\text{-}45_{\bar{x}} - t_1 - 90_{\bar{y}}\text{-}180_{y}\text{-}90_{\bar{y}}\text{-}135_{y}\text{-}45_{\bar{y}} \\ &\text{b} \quad 90_{x}\text{-}180_{\bar{x}}\text{-}90_{x}\text{-}135_{\bar{x}}\text{-}45_{x} - t_1 - 90_{y}\text{-}180_{\bar{y}}\text{-}90_{y}\text{-}135_{\bar{y}}\text{-}45_{y} \end{aligned} \qquad (5.1)$$

D). Results

Figure 5.2 shows the quadrupolar echo[19,20] spectrum of perdeuterated p-dimethoxybenzene. The methyl group produces a symmetric powder pattern similar to that seen in Figure 1. Small blips

There are still other peaks in Fig. 9 that need to be explained. In particular, the peaks at M = 77, 91, and 105 (with $\Delta M = 14$) have no counterparts in Fig. 7. Identifying them is easier than explaining their presence. Collectively, they represent aromatic ion species — e.g., note M = 91 in the toluene fragment of Fig. 5: $\phi\text{-}CH_2^+$. For M = 105 the side chain is simply one methylene unit larger, $\phi\text{-}CH_2CH_2^+$, while for M = 77 one expects ϕ^+.

However, the presence of these aromatic ions does not uniquely reveal their origin. The simplest explanation would be to point to the phthalates, which contain the aromatic ring. Figure 8 shows that dioctyl phthalate in the MS produces fragments at M = 77, 91, and 105 in significant amount, but still vastly less than the M = 149 fragment (which does not agree with the relative abundances seen in Fig. 9, even assuming plausible superposition of these peaks on those of linear species at the same M).

An alternative explanation, also involving the phthalates, would suggest complex gas-phase chemistry in the original plasma which entirely stripped all chains from the aromatic ring and then built new molecules by adding hydrocarbon chains to it. While this might seem to be rather severe, it is indeed believed to be the origin of the fragment ions in the MS at those M for dioctyl phthalate (Fig. 8). But if this had occurred in the original plasma, these species (M = 77, 91, 105) would ultimately have been drawn to the cathode and would have appeared in the field wire MS -- but they do not appear in Fig. 7, despite the clear evidence of phthalate itself there.

A third explanation involving plasma chemistry (but not phthalates) would argue that aromatic species can be formed from linear species at sufficiently high energies. For example, in gas-phase reactions at high temperature one can expect such chemistry ("dehydrocyclization"), and the high energies in wire chambers might be sufficient to accomplish this even at moderate temperatures. However, this explanation is also inconsistent with the absence of aromatics on the field wire.

Presumably the answer lies with the sense wire itself, where condensed-phase chemistry is occurring in the presence of extremely strong electric fields. It may involve the phthalates, but this seems doubtful in view of the fact that quite a bit of the regular phthalates remain intact (e.g., the M = 149 ion detected by MS) under such conditions. Perhaps attention should be drawn to the metal itself. If the tungsten was exposed because of a porous or otherwise imperfect gold coating (see comments about gold coatings, below), certain catalytic reactions might occur. In petroleum refining, the "reforming" process converts linear hydrocarbons to aromatics by means of a solid metal catalyst (in that case, usually platinum). It may be possible for tungsten to exert a similar effect under these unusual conditions, especially if the high local fields cause field ionization at the surface.

AUGER ELECTRON SPECTROMETRY

Operation

The AES technique provides information about surface composition (sensitive to a depth of about 2-3 nm) at the elemental level, and thus is not useful in general for identification of molecular species. However, knowledge of the atomic composition of materials is useful for other purposes,

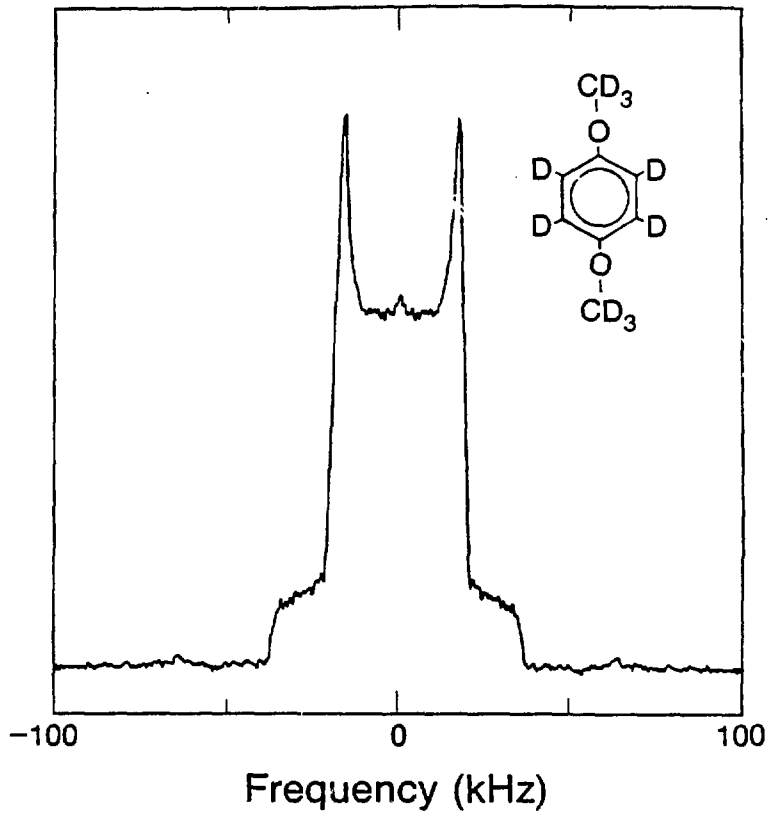

X8L 8512-4906

Figure 5.2). Quadrupolar Echo Spectrum of perdeuterated p-dimethoxybenzene. Ten shots were accumulated with dwell time(TI) of 5 μsec and recycle delay(RDLY) of 60 seconds. The echo was acquired in buffer 1 of the quadrature detection system thus allowing the clearing of buffer 2. This allows a $2^{1/2}$ increase in signal-to-noise in the frequency spectrum and was done in like manner for all powder patterns below. The splitting of the horns is 33.1 ± 1.0 kHz and the edges are separated by 73. ± 2 kHz. Blips due to horns of the aromatic deuterons are just above the noise and are separated by 126.9 ± 2 kHz.

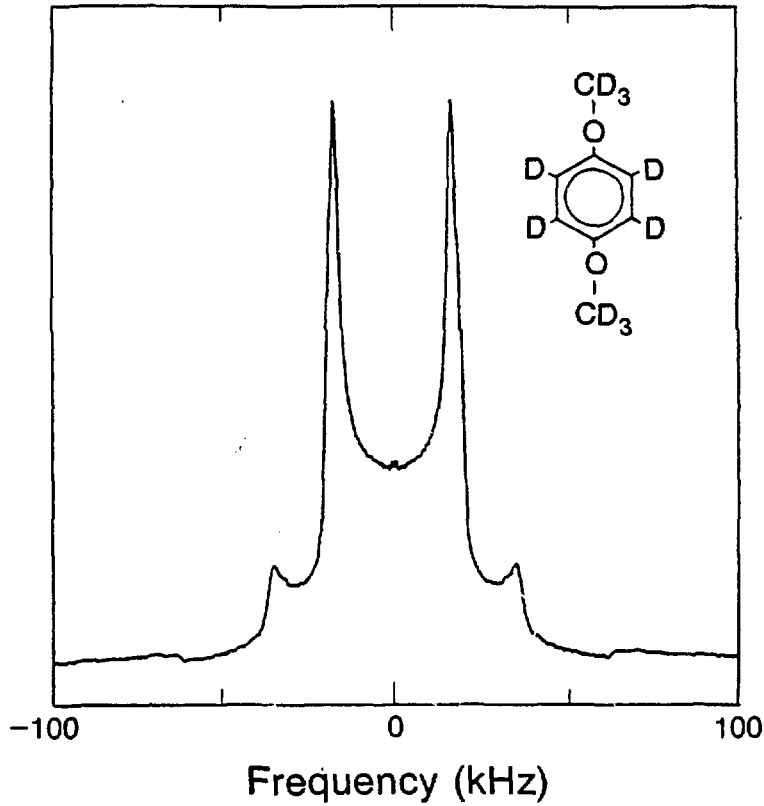

XBL 8512-4905

Figure 5.3). Five pulse compensated quadrupolar echo spectrum of perdeuterated dimethoxybenzene. The methyl horns and edges are quite sharp and separated by 34.5 ± 1. kHz and 70.3 ± 2 kHz respectively. The compensated sequence has resulted in significant distortion of the powder pattern, most likely due to a missetting of the rf phases or pulse lengths. The spectrum was acquired with an effective dwell time of 4 μsec and RDLY 60 seconds. Six hundred twenty-one phase-cycled shots were collected with an effective acquisition time of (621)(2)(1 minute) = 1242 minutes.

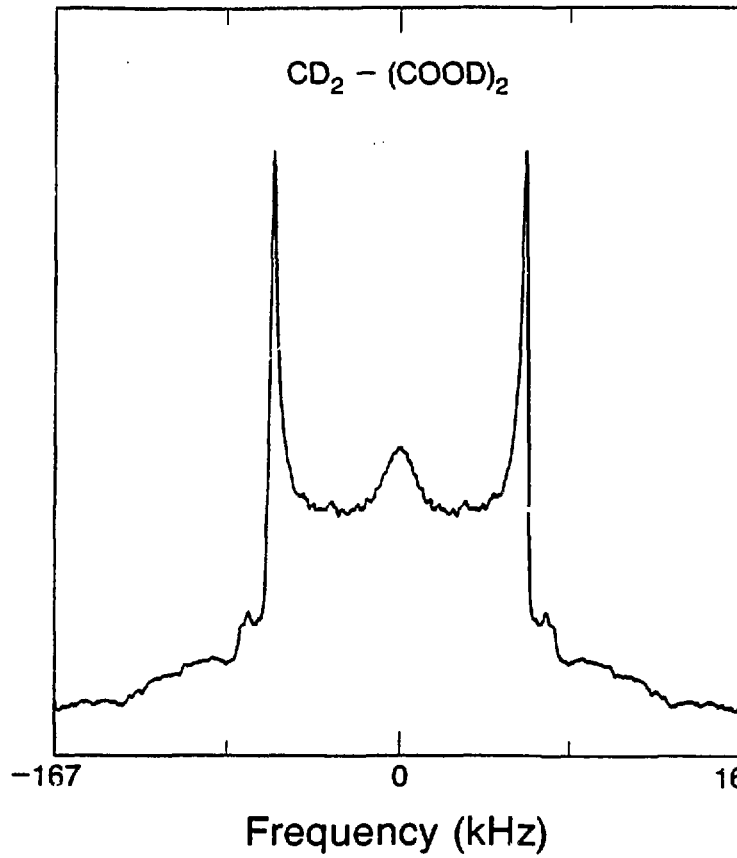

XBL 8512-4907

Figure 5.4). Compensated Echo Spectrum of perdeuterated malonic acid. The two major peaks are due to the superimposed horns of the carboxylic acid and methylene sites. The blips on the sides separated by 144 ± 3 kHz are the ν_2 shoulders stemming from the two inequivalent COOD sites(η_1=.112, η_2=.098).[6]

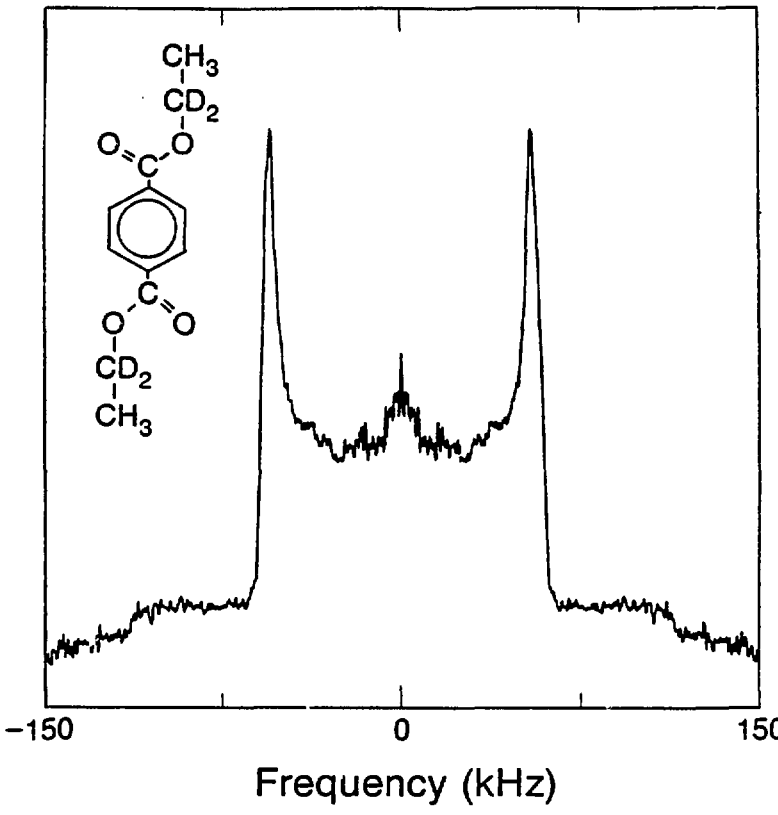

XBL 8512-4908

Figure 5.5). Diethyl terephthalate-d4 ($CH_3CD_2CO_2C_6H_4CO_2CD_2CH_3$) compensated quadrupolar echo spectrum. The methylene deuterons produce a spectrum with $\Delta\nu_1$ = 110. ± .7 kHz. A hint of a shoulder on the horns indicates $\eta \neq 0$; from this one can calculate $\eta \leq .13$ and e^2qQ/h=148.7 kHz. Zero field measurements[13] have shown the two methylene sites are characterized by $(e^2qQ/h)_1$=149.53 kHz, η_1=.042, $(e^2qQ/h)_2$=152.76 kHz, η_2=.049. The spectrum was obtained with dwell time of 3 μsec and RDLY of 60 sec and is the Fourier-transform of 1200 phase-cycled fids for a total acquisition time of (1200)(2)(1 minute) =2400 minutes.

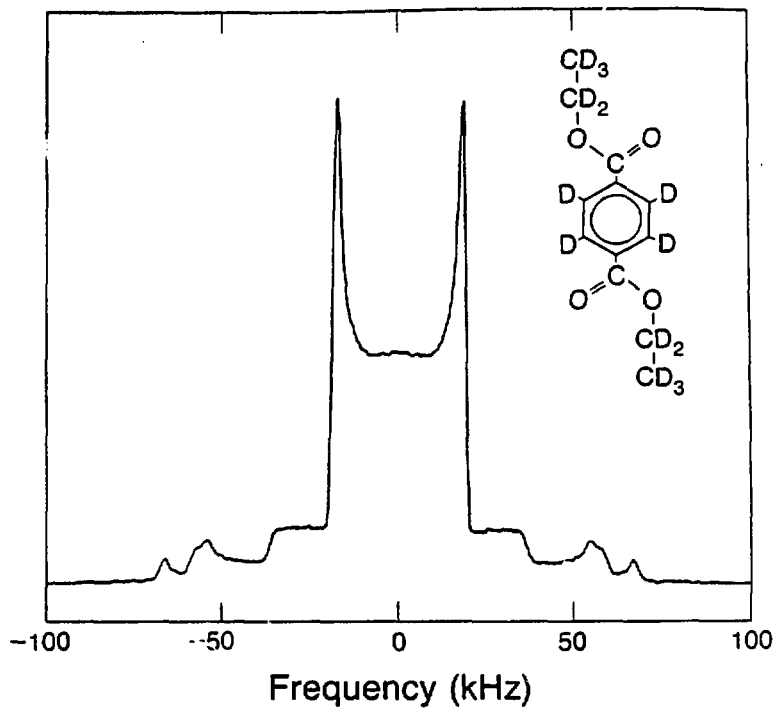

XBL 8512-4909

Figure 5.6). Perdeuterated diethyl terephthalate compensated quadrupolar echo spectrum. Most of the structure is due to the methyl group but horns due to the methylene and aromatic deuterons are also clearly visible. The methyl, methylene, and aromatic horns are separated by 35.8 ± .8, 111.2 ± 3.2 and 133.1 ± .8 kHz respectively. The irregular lineshape of the methylene horns accounts for the relatively high uncertainty in their separation. The spectrum was acquired using a dwell time of 4 μsec and a RDLY of 60 seconds. Three hundred phase-cycled shots were accumulated for an effective acquistion time of (300)(2)(1 minute)=600 minutes.

quadrupole parameters cannot be resolved, no quadrupole coupling constant can be assigned with an accuracy better than ± 1-2 kHz and small asymmetry parameters are impossible to detect. For many applications gross information is all that is required, e.g. motion in polymers, but if one is interested in small changes in EFG due to substituent effects, libration effects or in resolving the signal from similar sites, then powder spectra are simply not adequate. Another facet of this experiment is that the signal from a given site can be spread over 100's of kHz. One would expect a significant improvement in signal-to-noise with a technique such as the zero field experiment which can significantly reduce the linewidth and concentrate the signal from a given site into a small number of narrow lines.

II). Deuterium Zero Field NQR

A). Introduction.

In this section we shall present and discuss previously unpublished ^{2}H zero field NQR data and also discuss pertinent experimental details. The theory of time domain zero field NQR experiments[12-14] and the general theory of the various frequency domain NQR experiments[4,22,25] have been discussed in detail elsewhere. We shall confine ourselves here essentially to the application of existing zero field experiments to an assortment of samples.

B). Experimental Details.

The deuterium NQR spectra have been obtained using either the sudden[12] or indirect detection[13] experiments and are so indicated. Experimental parameters pertinent to the individual spectra are given

in the Table 5.1. More complete experimental details are given in the appendix and in the paper by Bielecki et al.[26] The sudden experiments employed an intermediate switching field of approximately 300-400 gauss. The indirect detection experiments employed intermediate fields and pulsed dc fields of 100 gauss. All samples were obtained from the laboratory of H. Zimmermann in Heidelberg with the following exceptions. The lithium sulfate monohydrate was recrystallized by us from an H_2O/D_2O mixture. The perdeuterated polyethylene was provided by Dr. R. Eckman of Exxon. The nonadecane-2,2'-d2 was loaned to us by Dr. R. Snyder of the H. Strauss research group. Deuteration levels were estimated from solution state NMR measurements, mass spec data, and in the very simplest cases, the method employed (i.e. dissolution in a 1:1 mixture of H_2O and D_2O). Quadrupole coupling constants and asymmetry parameters are reported with error limits correspnding to 95% confidence limits which have been estimated using procedures described elsewhere.[27]

C. Results

In this section we will discuss the zero field results obtained for a series of compounds. In addition we will discuss in detail the spectral assignments we have made. In general we shall display only the positive frequency half of experimental spectra since all spectra are even in the frequency. A summary of quadrupole parameters found in this work is given in Table 2.

1. Lithium Sulfate monohydrate (50% deuterated)

The water molecules of this hydrate execute rapid 180° flips about their C_2 axes in combination with librations about three perpendicular axes.[41] The resulting zero field spectrum, Figure 5.7,

TABLE 5.1 SPECTRAL PARAMETERS

sample	FIDS[a]	NFID[b]	TI[c] (μsec)	RDLY[d] (sec)	PSL	Method[f]	Fgs[g]
$Li_2SO_4 \cdot H_2O$; 50% D	2	1000	3	6	256	ZFID	7
nonadecane-2,2' D2	5	500	3	2	30	ZFID	8,9
Na propionate	2	500	2	6	15	ZFID	10
perdeuterated polyethylene	1	200	3	15	512	SUDDEN	11
benzoic acid (95% d5, 60% COOD)	1	350	3	60	256	ZFID	12
	9	220	10	50	256	ZFID	13
Terephthalic acid	1	228	3	100	256	ZFID	14
(98% d4; 60% COOD)	3	180	10	60	256	ZFID	15
toluic acid (75%	1	670	3	30	50	ZFID	16-18
deut CH_3, 90% COOD)	4	187	10	50	256	ZFID	19
diethyl terephthalate (perdeuterated)	4	799	3	10	2048	SUDDEN	20-21

[a] number of phase-cycled fids.

[b] number of points in each phase of the phase-cycled fid. Zero filling used to increase the number of points to power of two

[c] dwell time in the zero field evolution period (t_1).

[d] recycle delay time

[e] number of pulsed spin-locking acquired points in high field.

[f] ZFID = Zero Field Indirect Detection

[g] figures for which this information pertains

Table 5.2: Deuterium Quadrupolar Coupling Constants and Asymmetry Parameters[a]

		This work		literature[c]	
		e2qQ/h	η	e^2qQ/h	η
Aromatic carboxylic acids and esters					
diethylterephthalate (CD_2)*		149.53	0.042		
		152.76	0.049		
diethylterephthalate (ring)*		180.53	0.022		
		178.33	0.015		
terephthalic acid(ring)		177.3	0.033		
toluic acid	ring	173.74	0.028		
	ring	78.92	0.023		
	COOD	168.1	0.10		
benzoic acid[b]	ortho	177.80	0.040		
	meta	179.70	0.026		
	para	172.95	0.010		
	COOD			167.33[36]	.14
Alkanes					
nonadecane 2,2-d_2		74.03	0.39	72.7[29]	.36
polyethylene $(-CD_2-)_n$*		164.93	<.01	163.9[30]	NR
Carboxylic acid salts and amines					
α-glycine (CD_2)*		160.09[42]	0.042	159.99[7]	.043
		169.01	0.092	169.41[7]	.085
Na propionate (CD_2)		170.14	<.02		
Hydrates and metal sandwich compounds					
Li_2SO_4.HDO		123.05	0.81	123±3.[4]	.80±.02
$Ba(ClO_3)_2$.HDO*		2.7[13]	0.96	121.5±.4[44]	.976±.007
Ferrocene-d_{10}*		193.8[42]	<.01	198±2[45]	NR

[a]Error limits where quoted are those of the respective author(s).
[b]Ortho, meta and para assignments made as discussed in text.
[c]Reference for asymmetry parameter(where reported) is that of qcc.
*Denotes sudden experiment, all others are ZFID.
NR = Not reported

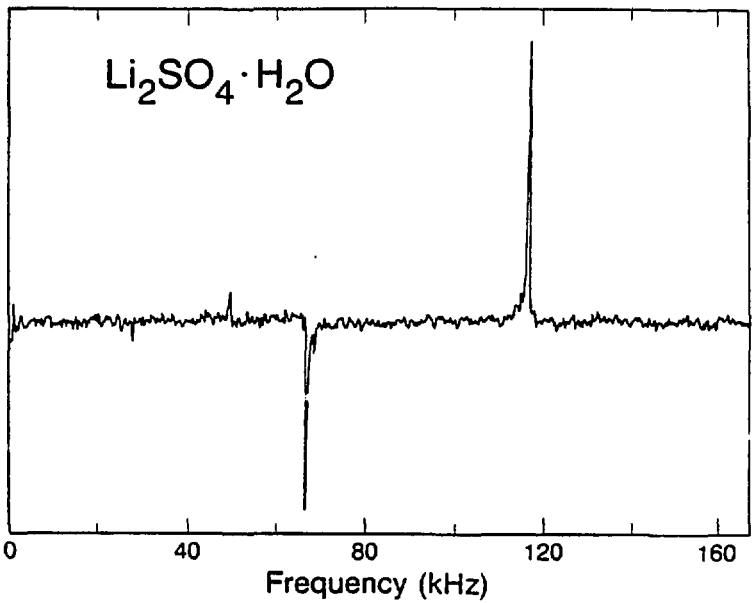

Figure 5.7). ^2H ZFID spectrum of 50% deuterated lithium sulfate monohydrate. The ν_+, ν_- and ν_o lines of the motionally averaged H_2O are clearly visible at 117.19, 67.38, and 50.13 kHz. Linewidths are ~.53 kHz. A small peak at 27.99 kHz is due to ^7Li.

shows three major peaks corresponding to the ν_+, ν_-, and ν_0 lines of the motionally averaged EFG tensor.[23] Calculation of the quadrupole coupling parameters from these lines yields eq^2Q/h=123.05±.06 khz and η=0.810±0.008. A small blip at 27.99 khz is most likely due to one of the inequivalent ^{7}Li sites(I=3/2). Direct detection zero field measurements of the lithium spectrum of this material[12] obtained lines at 21.7 and 27.8 kHz.

2. Nonadecane 2,2-d2.

Motional averaging in this material again produces a non-axially symmetric electric field gradient and reduces the effective quadrupole coupling constant to a value close to 1/2 that expected for a static C-D bond.[1,28] Figure 5.8 shows the three line deuteron spectrum characteristic of a single nonaxial site, superimposed on the broad hump due to the protons. Calculation of the quadrupolar parameters from these frequencies yields e^2qQ/h=74.03±0.10 kHz and η=0.39±0.02 in good agreement with high field powder measurements(e^2qQ/h = 72.7 kHz, η = 0.36).[29] Figure 5.9 shows the resulting zero field spectrum when the zero field fid is shifted by several μsec, leaving only ^{2}H signal.

3. Sodium propionate 2,2,-d2.

The zero field spectrum, Figure 5.10, consists essentially of lines centered at 122.27 kHz, 6.7 kHz and zero frequency. The asymmetric shape of the high frequency line indicates the possibility of a nonaxially symmetric EFG. From its linewidth of ~4.9 kHz one can say that

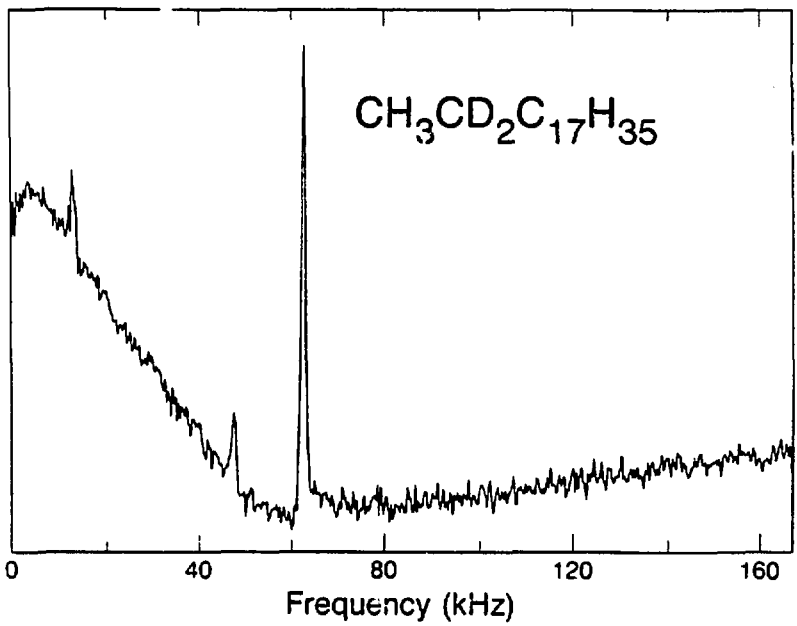

XBL 8511-11485

Figure 5.8). Nonadecane-2,2'-D2($CH_3CD_2C_{17}H_{35}$) Deuterium ZFID spectrum. It was found experimentally that the ν_o lines were better resolved by using DC pulses of ~450° rather than 360° (proton angles). The hump of the proton signal results. The ν_+, ν_- and ν_o lines of the motionally averaged CD_2 group are still clearly observed and appear at 62.7, 48.3 and 13.9 kHz, respectively. (sample courtesy of R. Snyder).

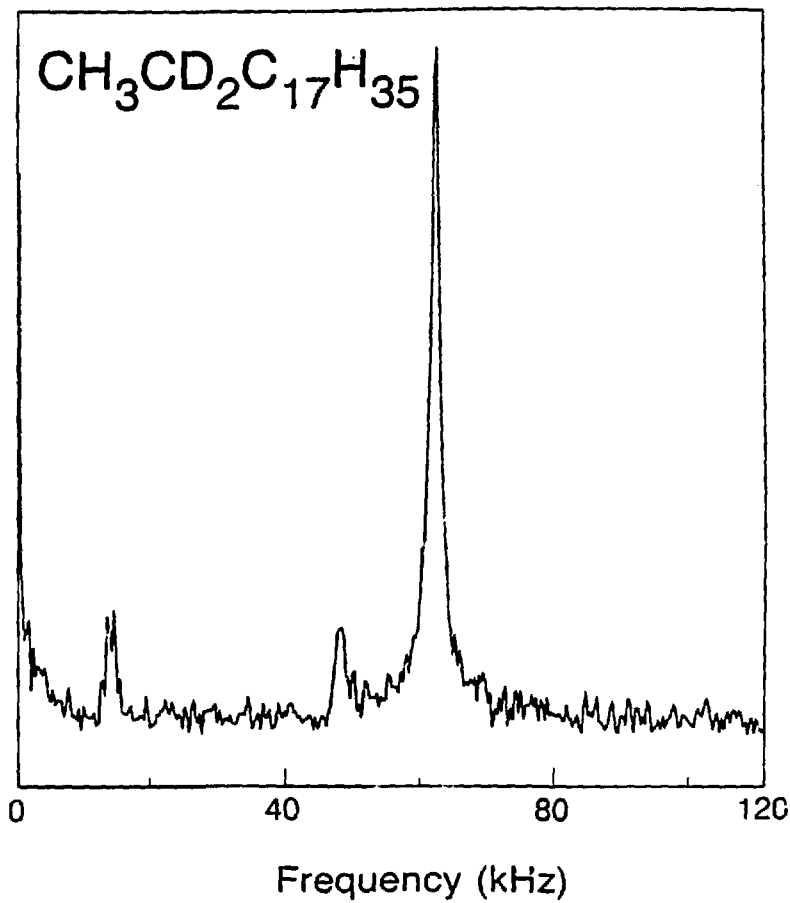

XBL 8511 11494

Figure 5.9). Nonadecane-2,2'-D2. Same fid as Figure 8, however fid was shifted to eliminate proton signal.

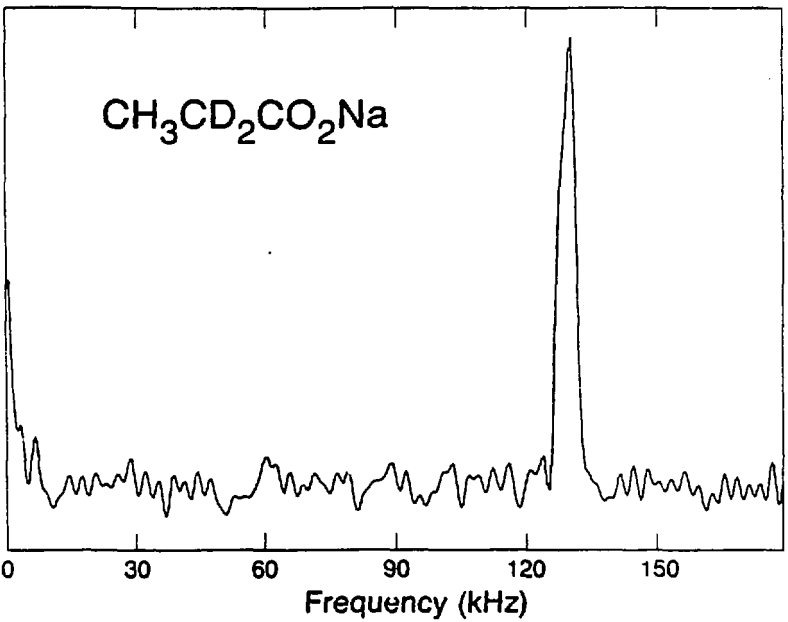

XBL 8511-11488

Figure 5.10). Deuterium ZFID spectrum of Sodium propionate-D2 ($CH_3CD_2CO_2Na$). From the width of the high frequency peak centered at 122.3 kHz, one can deduce the intermediate frequency peak at 6.7 kHz is not a ν_o line. Its origin is unknown, possibly due to an impurity. The width of 4.9 kHz suggests the line at 122.3 is simply the unresolved ν_+/ν_- lines and/or the superposition of lines from several sites.

$$\nu_+ - \nu_- \leq 4.9 \text{ kHz} \quad , \text{ or} \qquad (5.2)$$
$$\frac{3e^2qQ}{h}\frac{\eta}{2} \leq 4.9\text{khz}.$$

From the frequency of the high frequency line one can estimate the quadrupolar coupling constant by

$$\frac{3e^2qQ}{4h} \sim 122.77 \text{ kHz}, \quad \text{or} \qquad (5.3)$$
$$\frac{e^2qQ}{h} \sim 163.0 \text{ kHz}$$

which implies that $\eta \leq 0.06$. Equation (5.1) can also be expressed as $\nu_o \leq 4.9$ kHz. So the line at 6.7 kHz is ruled out as a possible ν_o line. The estimated quadrupole coupling constant is close to the value reported for a static C-D bond.

4. Perdeuterated polyethylene (80% crystalline).

This material has been the subject of considerable study by solid state NMR.[1,16,28,30] In general the material exists with an amorphous and a crystalline part, whose relative amounts vary depending upon method of production and treatment. The amorphous region (estimated to be 20% for this particular sample[34]) should not contribute to the zero field spectrum since its high field T_1 is expected to be on ~100 ms[16] and thus no magnetization should survive the zero field cycle. The sudden zero field spectrum of this material, Figure 5.11, consists of a 1 : 1.6 : 1 triplet in contrast to the 1:1:1 triplet expected for an $\eta \approx 0$ spin I=1 nucleus. Slightly asymmetric lines at ± 123.7 kHz are in agreement with wide line deuterium measurements which obtained $3e^2qQ/h = 123$ kHz.[30] The 4.0 kHz linewidth of the high frequency lines can in principle result from the deuteron-deuteron dipolar coupling

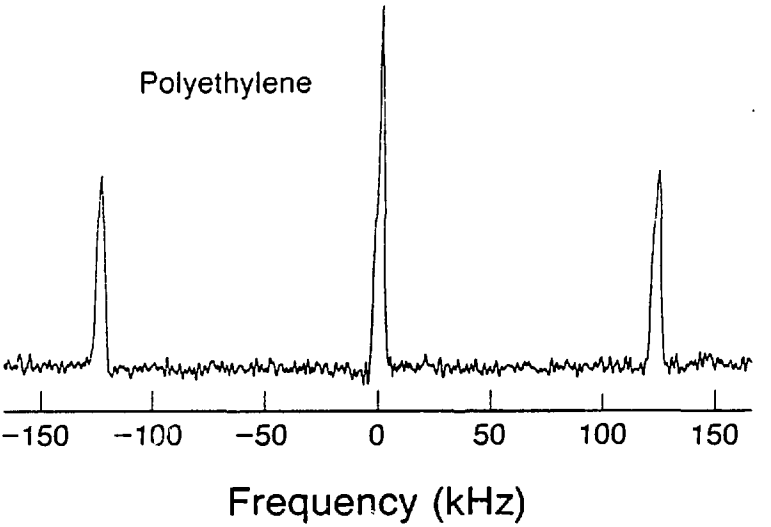

XBL 861-6116

Figure 5.11). ^{2}H ZFID spectrum of ~80% crystalline polyethylene. Both positive and negative frequencies are plotted to show the relative intensities of the zero frequency and ±123.7 kHz lines. (sample courtesy of R. Eckman)

and/or a distribution of quadrupole coupling constants.

We note Meir has performed simulations of the effect of low frequency librations on the deuterium zero field spectrum and found that even motions whose frequencies are ~1/100 that of the quadrupole frequency can have a significant effect on the observed spectrum.[32] These slow motions increase the intensity at zero frequency at the expense of the outer lines. Certainly this could explain the polyethylene results but verification of this hypothesis will require additional study. In this regard it would be especially nice to carefully characterize the sample's crystallinity (our value above is only an estimate), high field spectrum and zero field T_1.

5. Benzoic acid (95% deuterated ring, 60% COOD).

In the solid state, benzoic acid exists in a tetramolecular unit cell in which the molecules form centrosymmetric, nearly planar dimers.[34] All five of the ring protons are crystallographically inequivalent.[25,34] Formally this means that the molecular environments are not precisely the same, however this does not necessarily mean that there will be a strong enough perturbation of the EFG tensors of the inequivalent sites to allow their resolution. The zero field indirect detection spectra of a sample deuterated to ~95% on the ring and 60% COOD is shown in Figures 5.12 and 5.13. Figure 5.13 is a folded in version of Figure 5.12. Previous authors[37] have found the COOD produces ν_+ and ν_- lines at 131.5±.5 and 119.5±1.0 kHz respectively. From the absence of the latter we assume the observed spectrum contains no signal from the COOD and therefore represents signal only from the ring sites. This seems reasonable

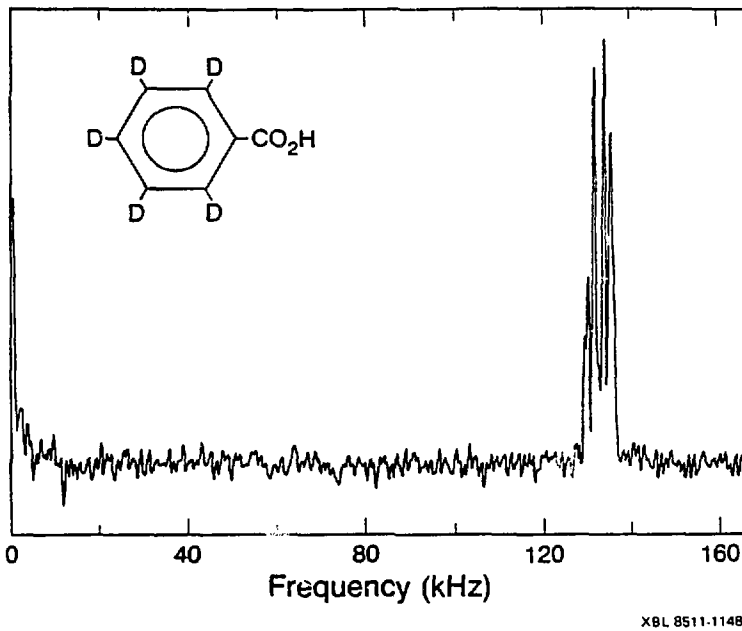

Figure 5.12). ^2H ZFID spectrum of benzoic acid (95% deuterated ring, 60% COOD). The aromatic sites produce four well resolved lines in the 130-140 kHz region and structure due to the ν_Q lines is visible around zero frequency. The inverted spike around 11.7 kHz is probably due to the proton signal of the rapidly exchanging COOH···HOOC.

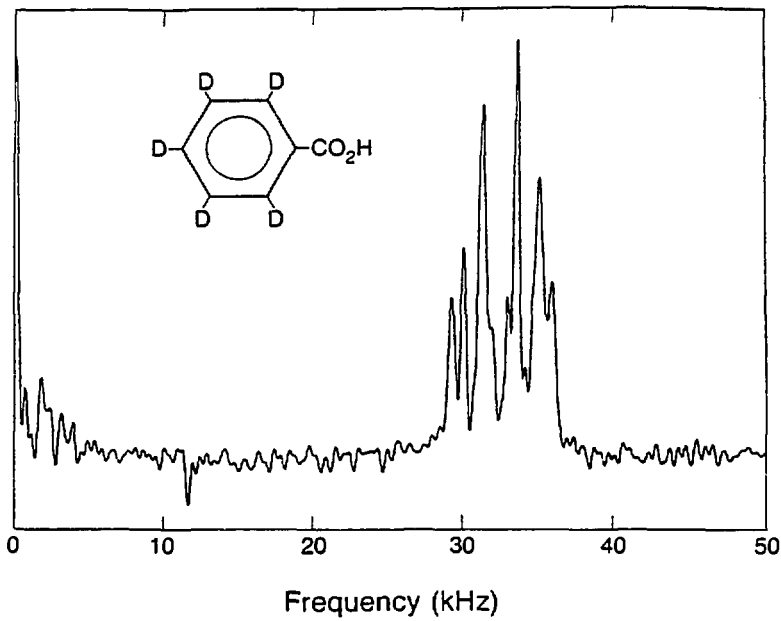

XBL 8511-11497

Figure 5.13). ZFID spectrum of benzoic acid (95% deuterated ring, 60% COOD). A narrower bandwidth was used to obtain this spectrum in which six lines are resolved in the aromatic region. Using the dipolar split lines in the ν_o region one can assign the spectrum to three resolvable sites.

since the dipolar coupling to adjacent protons is rather small for the carboxylic deuteron, therefore the efficiency of the level crossing is impaired compared to to that of the ring sites. Six major peaks are observed in the region 129-136 kHz., accompanied by some relatively minor splittings due probably due to the perturbative effect of deuteron-deuteron and deuteron-proton dipolar couplings.[35] A single line at 11.8 kHz is close in frequency to that expected for the COOD ν_o line.[36] From the crystal structure of this material and an estimate of r(C-H) =1.1 angstroms, one expects that pairs of adjacent ring protons should produce a signal at 11.6 kHz. On the other hand, the proton spectrum of toluic acid shows a peak centered at 12.5 kHz due to the motionally averaged dimer pair.(See Chapter VI.) Although this is ~.9 kHz greater than the line observed here, it seems like the most reasonable assignment.

The "ν_o" region of the observed spectrum shows resolved structure but must be interpreted with some caution since drift in the receiver, rf or dc pulse circuitry can lead to low frequency artifacts. On the basis of the spectrum in Figure 13 and repetition thereof we appear to resolve peaks at 0.93, 2.05, 3.42, and 4.2 kHz with a hint of a shoulder at approximately 2.5 kHz.

One can propose a tentative assignment on the basis of the observed spectrum by assuming that there are three resolvable sites and that the deuteron-deuteron dipolar splittings will result in relatively minor splittings in the ν_+ and ν_- lines. The simulations in Chapter IV of the NQR spectra of dipolar coupled deuterons on adjacent aromatic ring sites showed that the spectrum is still largely describable in terms of ν_+ and ν_- lines. Extra lines are produced but

the major lines still basically correspond to ν_+ of ν_- lines.

Simulations for several(>2) coupled deuterons have not been performed to date. We expect, however, in analogy with the above, that the further perturbation provided by the additional dipolar coupling will still leave the system describable in terms of $\nu_\pm$ lines.

From Figure 13 one has the following set of lines to be assigned.

ν_o .93, 2.05/2.54, 3.4/4.2 (kHz)

$\nu_\pm$ 129.3, 130.18, 131.45, 133.6, 135.2, 135.94

That is we have picked out the six major lines in the ν_+/ν_- region and furthermore assumed that the lines in the ν_o region represent three possibly dipolar split transitions. From this group, there is only one consistent assignment which is given in Table 5.3 below.

We can further assign these quadrupole parameters to specific

Table 5.3 Benzoic acid assignment

	ν_o	ν_-	ν_+	e^2qQ/h	η	site
I.	.9	129.3	130.2	173.0	.010	ortho
II.	2.0-2.5	133.6	135.9	179.7	.026	meta
III.	3.4-4.2	131.4	135.2	177.8	.040	para

sites of the ring with the following qualitative arguments. First, we expect the electronegative oxygens to increase the asymmetry parameters of the deuterons sites resulting in

$$\eta_{ortho} \geq \eta_{meta} \geq \eta_{para}$$

Secondly, it has been shown[37] that electron donating groups, such as -NH_2, increase the average quadrupole coupling constant relative to that observed in the unsubstituted benzene. By the same argument, one expects an electron withdrawing group, such as -COOH, to decrease the average quadrupole coupling constant of the ring. From the resonance arguments of basic organic chemistry[38] one expects the electron withdrawing effect to be greatest at the ortho and para sites. With these arguments we make the site assignments of Table 5.3.

6.Terephthalic acid. [Aldrich 98% d4-60%COOD]

X-ray diffraction has determined that this dicarboxylic acid exists in the solid state as infinitely long chains held together by hydrogen bonds on either end of each molecule.[39] Two polymorphic forms with closely related triclinic unit cell dimensions were found, differing in the relative displacements of the chains. At room temperature, however, Bailey and Brown report that one of the forms becomes "rarer on storage." We unfortunately did not pursue this aspect. If the space group of both forms of this material is $P\bar{1}$, as was assumed by the X-ray study, then each polymormorph should possess two crystallographically inequivalent deuterons.

Two indirect detection zero field spectra are shown in Figures 5.14 and 5.15. These differ in that the first is a relatively low resolution wide bandwidth spectrum and the second is a higher resolution narrow bandwidth spectrum. Using the two spectra together we observe major lines centered at 134.4, 131.3, 12.01, 11.42, and 2.9 kHz. In Figure 5.15 the lowest frequency line of these appears to be either dipolar split or split by noise. Also in Figure 5.15 the high

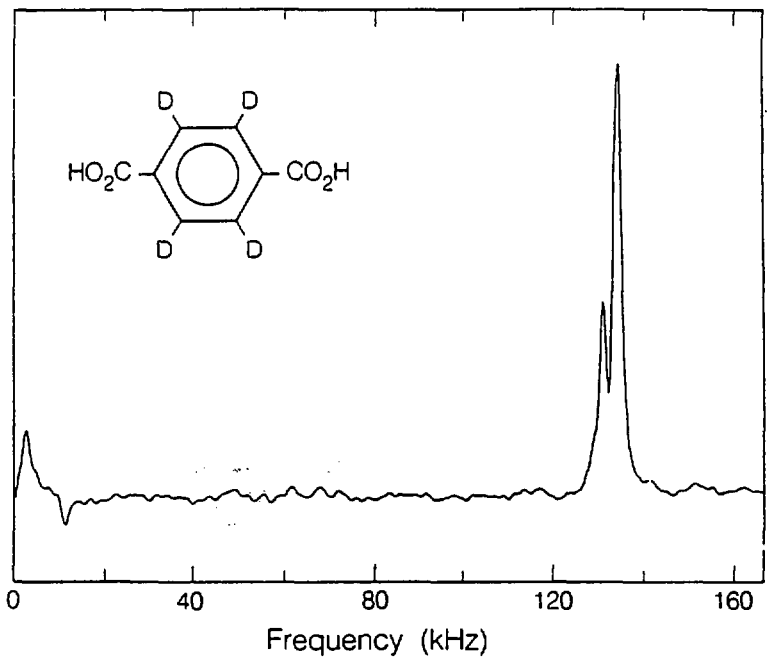

Figure 5.14). Terephthalic acid (98% d4, 60% COOD). Basically four lines appear in this spectrum, three of which are assigned to a simple η=0 site or possibly the superposition of more than one similar site. The by now familiar inverted line at -12 kHz is assigned to the protons of the carboxylic acid dimer.

Figure 5.15). A "folded" in spectrum of terephthalic acid (98% d4, 60% COOD). The aromatic peaks which appeared at 131.3 and 134.4 kHz in Figure 14 show up here at 31.2 and 34.4 kHz, respectively. Centered around 2.9 kHz is the ν_0 corresponding to the aromatic lines. At 5.0 kHz and 5.6 kHz are two "blips" which are unassigned, possibly artifacts due to spectrometer drift. At 11.4 and 11.95 kHz are two lines probably due to the exchanging carboxylic acid dimer protons. If this latter assignment is correct, this constitutes the best resolved spectrum to date of these dimer protons.

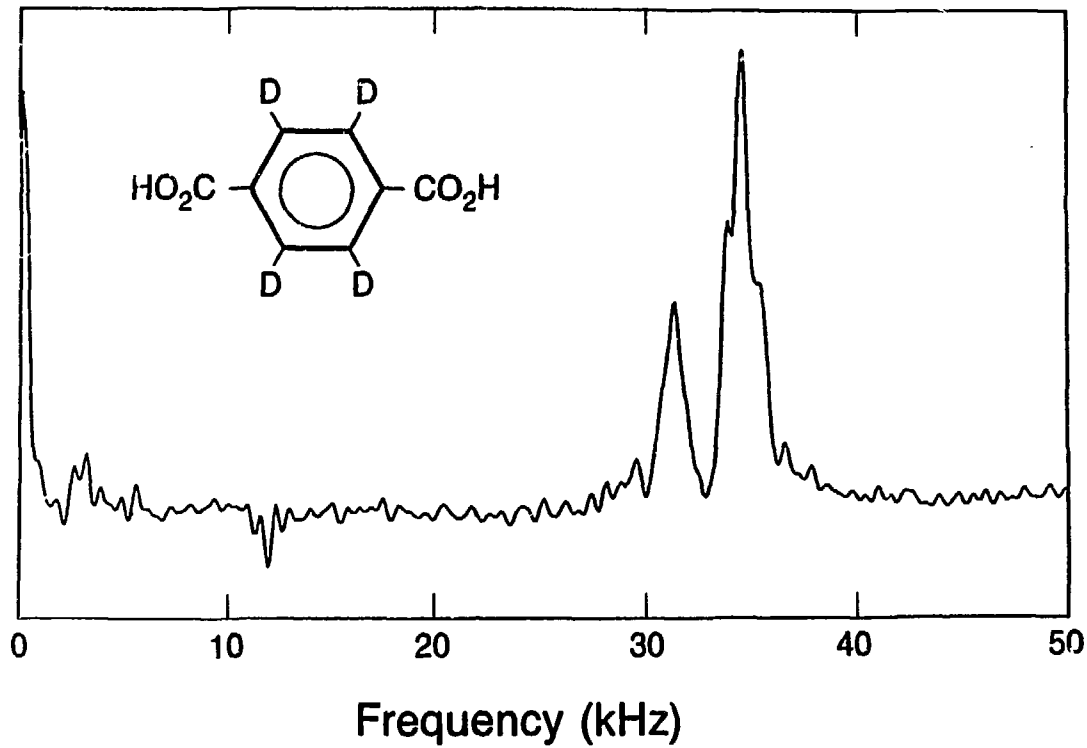

XBL 861-6111

frequency lines are seen to be quite asymmetric, suggesting perhaps a superposition of unresolved sites with similar quadrupolar coupling parameters. Lines appear at 129.49 and 136.5 kHz which seems qualitatively similar to the satellite lines seen in the simulations of dipolar coupled pairs of aromatic deuterons in Chapter V. With this in mind, the lines at 2.4, 131.5 and 134.4 suggest a ν_o, ν_-, ν_+ set. Assuming the frequencies of these lines are characterized to within $\pm W_{HM}$ one obtains e^2qQ/h=177.09±.17 kHz and η=0.35±.01. The line at 12.01 kHz is right where one would expect the ν_o line from the deuteron of a dimerized COOD group[36] and the line at 11.4 kHz is right where one would expect the proton signal for adjacent proton pairs on the aromatic ring. The low probability of finding adjacent protons on the 98% deuterated ring makes this latter assignment seem rather implausible. It is much more likely that the 11.4 and 12.0 kHz lines constitute the well resolved doublet due to the COOH···HOOC protons. In hindsight, we should have performed the sudden experiment on this sample to obtain the proton signal as a means of testing this assignment.

7. Toluic acid (75% random deuteration on methyls, 90% deuteration of aromatic sites).

In the solid state toluic acid exists as carboxylic acid dimers[40] of a type similar to those of benzoic acid.[34] Figure 5.16 shows the zero field indirect detection spectrum of a sample ~90% deuterated on the ring and carboxyic acid and 75% deuterated on the methyl group. Figure 5.17 is the corresponding time domain signal. Three distinct regions are present in the frequency spectrum, the carboxylic

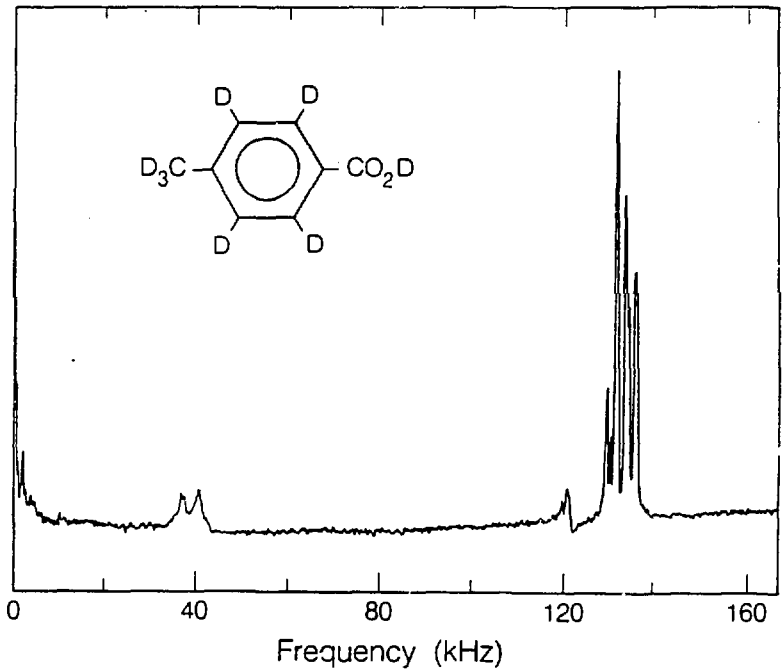

XBL 859 8997

Figure 5.16. ^2H ZFID spectrum of Toluic acid (~75% random deuteration of methyls, ~90% deuteration of aromatic sites). There are four main features of this spectrum; from right to left are the five line cluster of the aromatic lines (plus the GOOD ν_+ line), the slightly out-of-phase GOOD ν_- line, the superposition of CHD_2 and CH_2D signals around 40 kHz, and the ν_o region.

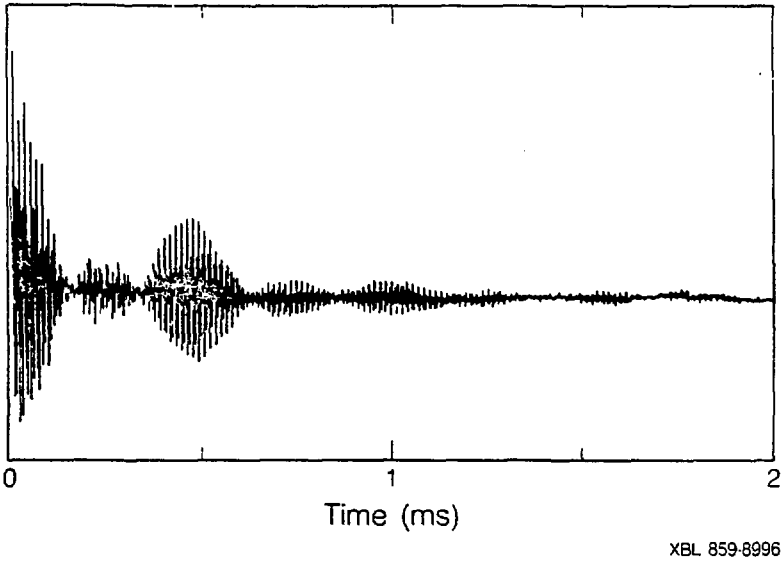

Figure 5.17. Time domain signal corresponding to Figure 16, toluic acid.

Figure 5.18. Expanded view of the toluic acid aromatic/ν_+/ν_- region of Figure 16.

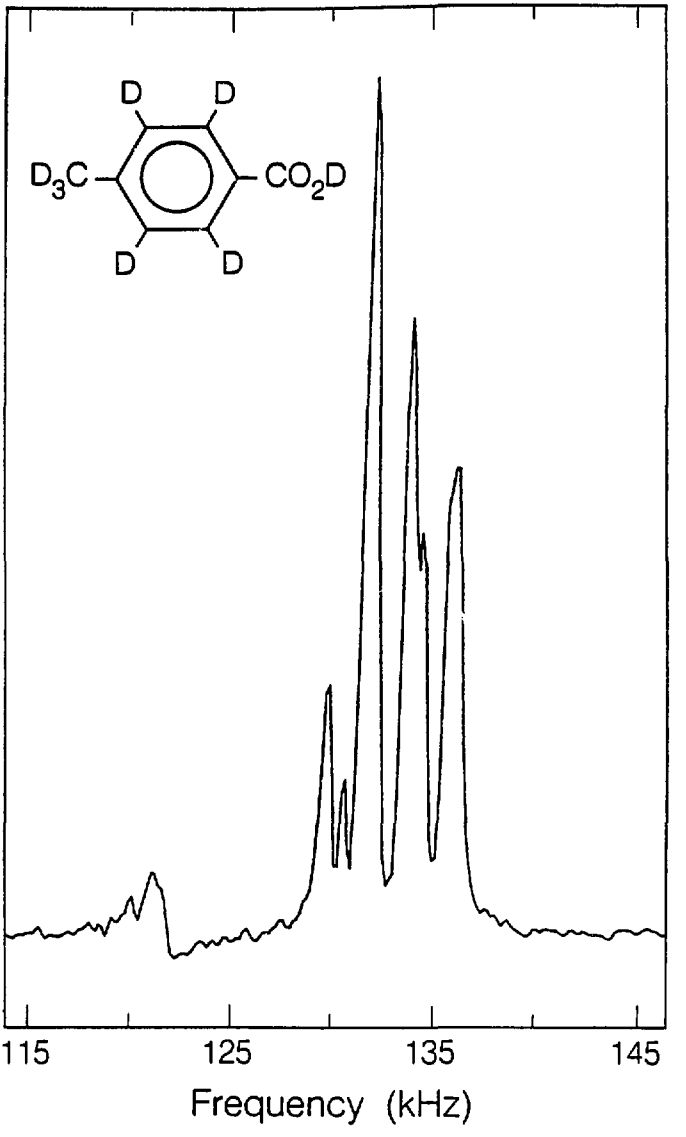

XBL 859-8998

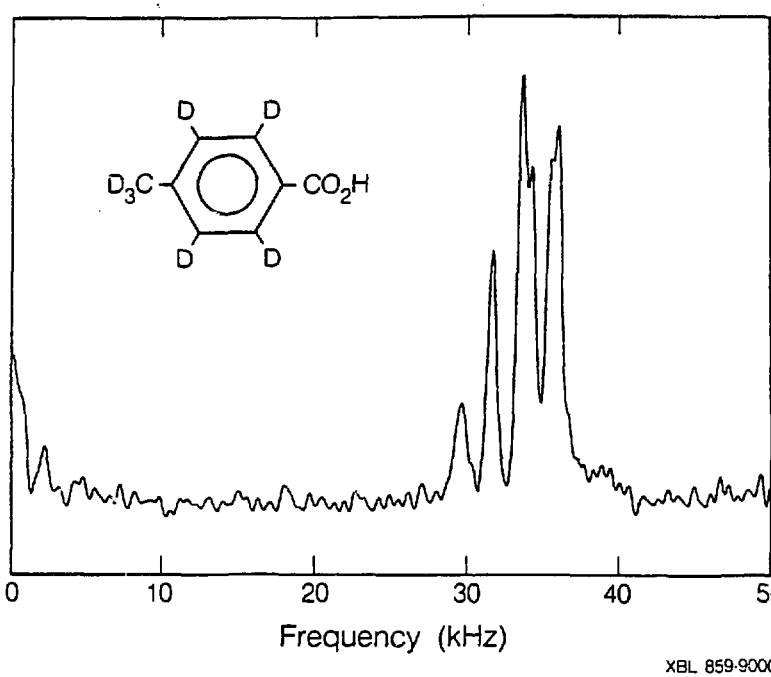

Figure 5.19. Deuterium ZFID spectrum of Toluic acid D7 (60% COOD). Comparison of Figure's 18 and 19 allows the unambiguous assignment of the COOD ν_+ and ν_- lines.

acid/aromatic site region(115-145 kHz), the methyl region(35-45 kHz) and the ν_0 region(0-10 kHz). Figure 5.19 shows the zero field indirect detection spectrum of another sample estimated to be 95% deuterated on the ring and methyl groups and 60% COOD. Here the bandwidth is reduced relative to Figures 5.16 and 5.18, but the frequencies can still be reliably assigned. From a comparison of the spectra of the two samples one can deduce the ν_+ and ν_- lines of the COOD occur at 130.5±.3 and 121.7±.3 kHz, respectively. Previous authors[36] have reported the ν_+ and ν_- lines at 131.5±0.5 and 119.5±1.0 kHz, respectively for the COOD in benzoic acid at room temperature.

The methyl region is cluttered by the superposition of CH_2D and CHD_2 signals. Induced asymmetries in the EFG tensors of the methyl deuterons due to the unbalanced methyl groups might produce contributions to the ν_0 region. There is a noticeable shoulder around the zero frequency peak and a reasonably strong peak at 2.4 kHz.

Exclusion of the COOD signal leaves 4 major peaks in the aromatic region, namely

1) 129.9 kHz 3) 133.8 kHz

2) 131.8 kHz 4) 136.1 kHz

A shoulder appears on peak 3) separated by ~.65 kHz.

We can make a tentative assignment of the aromatic sites of we assume the 2.4 kHz line is the ν_0 line of aromatic sites. In addition we assume the 4 lines above are all ν_+ or ν_- lines, i.e. none are satellite lines produced by dipolar coupling. This seems reasonable in light of the simulations of Chapter V.

Predictions of the quadrupolar parameters and ν_0 lines of the possible pairings of the aromatic lines are given in Table 5.4. We

Table 5.4 Possible Toluic acid assignments

Pairings		Predicted parameters					
$site_1$	$site_2$	ν_{o1}	ν_{o2}	e^2qQ/h_1	η_1	e^2qQ/h_2	η_2
1&2	3&4	1.9	2.3	174.5	.022	179.9	.026
1&3	2&4	3.9	4.3	175.8	.044	178.6	.048
1&4	2&3	6.2	2.0	177.3	.070	177.1	.023

see the first combination predicts ν_o lines at 1.9 and 2.3 kHz. Given the linewidths estimated from aromatic region to be between .7 and 1.0 kHz, it would seem quite reasonable to resolve only a single line at approximately their average. Furthermore, the asymmetry parameters predicted for the first combination are in line with the values seen earlier in this chapter for the aromatic sites in terephthalic acid, benzoic acid and diethyl terephthalate *(vide infra)*.

On the other hand, the second and third combinations listed in Table 4 require ν_o lines of higher frequencies than those observed experimentally and so we can rule those combinations out on that basis. Therefore the first entry seems reasonable at least as a tentative assignment.

8. Diethyl terephthalate(perdeuterated).

The well resolved spectrum, Figure 5.20, obtained by the sudden field cycle consists of four distinct regions corresponding to ring, methylene, and methyl deuterons, and a low frequency portion due to the ν_o lines. Expanded plots of the separate regions are shown in

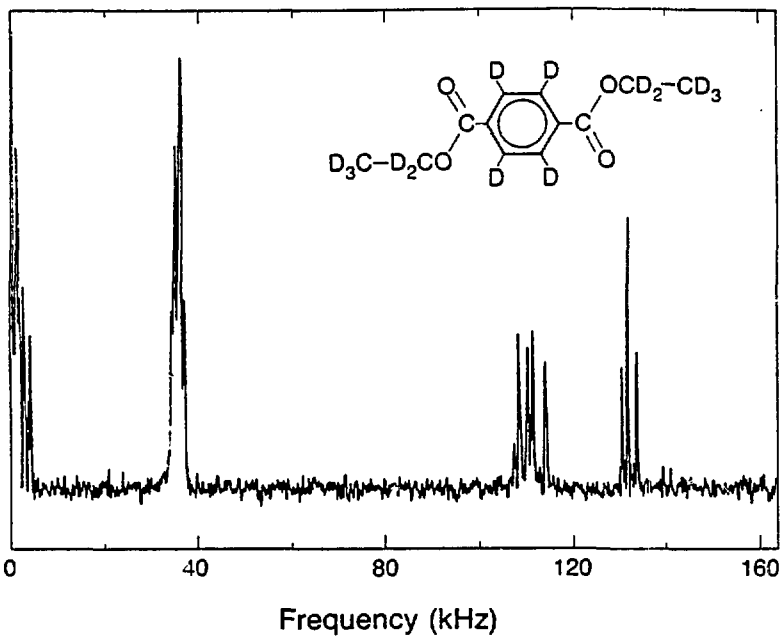

XBL 8511-11496

Figure 5.20. Sudden zero field NQR spectrum of perdeuterated diethyl terephthalate. Four regions are clearly evident; from right to left the three line aromatic region, the methylene region, the methyl region and the ν_o region.

Figure 5.21. Perdeuterated diethyl terephthalate. Expanded plots of the individual regions. The methyl group lineshape, indicative of an $\eta=0$ site should produce no contributions to the ν_o region. Since $\eta\neq 0$ for an aromatic site, the central line in (d) must consist of the superposition of the ν_+ and ν_- lines of two different sites. This requires ν_o lines at 1.3 and 2.0 kHz in agreement with (a). The deuteron-deuteron dipolar coupling in the CD_2 group produces the splittings observed in the ν_+/ν_- lines of (c) as well as in the ν_o lines seen in (a). Figure IV.14 illustrates this more clearly.

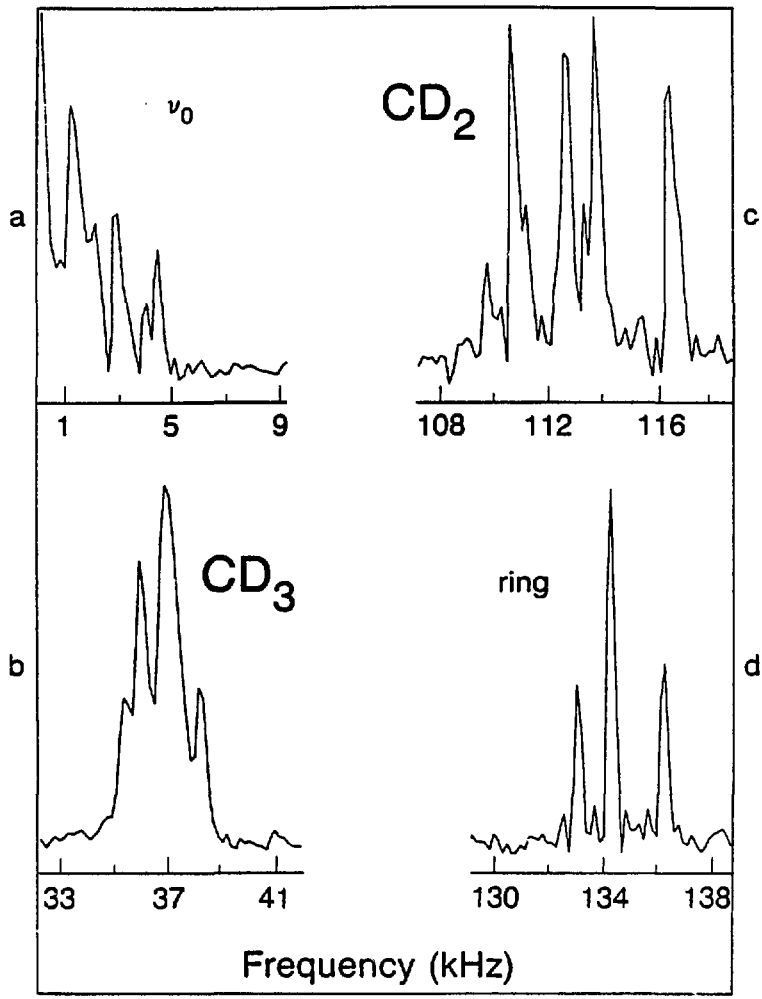

XBL 8511-11495

Figure 5.21. Comparison of the methyl group signal with spectra and simulations given elsewhere indicates a symmetric site with η equal to or very near to zero. Therefore the methyl group should make no contribution to the ν_o region signal. Deuteron dipolar couplings are evident in the splittings they produce in the CD_2 region(110-117kHz) and also in the ν_o region. Simulations and analysis based thereon of the aromatic and methylene signals are discussed in Chapter IV and will not be repeated here.

The aromatic region between 133 and 137 kHz shows three lines with ratio of intensities of ~1:2:1. Since η is not expected to equal zero for an aromatic site, the only possible assignment of the three lines is just

136.4 kHz	$\nu_{+,1}$
134.4	$\nu_{-,1}$; $\nu_{+,2}$
133.1	$\nu_{-,2}$

which predicts ν_o lines at 1.3 and 2.0 kHz. The larger intensity of the central line comes about by the accidental degeneracy of the $\nu_{-,1}$ and $\nu_{+,2}$ lines. The above assignment leads to $(e^2qQ/h)_1 = 180.53\pm.08$, $\eta_1=.022\pm.005$, $(e^2qQ/h)_2 = 178.33\pm.015$ and $\eta_2=.015\pm.005$.

D). Conclusions and Summary

We have presented results from a series of ^2H NQR experiments. The high resolution spectra obtained have allowed us to distinguish similar sites, for example the deuterons of the same methylene group or deuterons on adjacent aromatic ring sites. This latter aspect has allowed us to assign quadrupolar parameters to specific ring sites using substituent effect arguments. In addition, we have shown that one can can use the zero field NQR experiments to gain information

about the relative orientations of the EFG tensors of dipolar coupled deuterons. This technique should find application in other systems since one does not require single crystals.

IV.A Appendix - Error Limits of Zero Field NQR Experiments

The experimental error limits were estimated using the method outlined in Shoemaker et. al.[27] We estimate 95% confidence limits, λ, for the frequency of spectral lines as being equal to the width half maximum divided by two, i.e. $\lambda = W_{HM}/2$. The quadrupolar coupling constant and asymmetry parameters are calculated using the frequencies of the ν_+ and ν_- lines by

$$e^2qQ/h = \frac{2}{3}\left[\nu_+ + \nu_-\right] \text{ and} \tag{4}$$

$$\eta = \frac{3(\nu_+ - \nu_-)}{\nu_+ + \nu_-} \tag{5}$$

Assuming that $\lambda(\nu_+) = \lambda(\nu_-)$, then using formulas II.52 and II.53 of reference 27, we obtain

$$\lambda(q) = \frac{2\sqrt{2}}{3}\,\lambda(\nu_+) \qquad \text{and} \tag{6}$$

$$\lambda(\eta) = \sqrt{2}\,\delta\,\eta\left[\frac{1}{(\nu_+ - \nu_-)^2} + \frac{1}{(\nu_+ + \nu_-)^2}\right]^{1/2} \tag{7}$$

where $\delta = \lambda(\nu_+) = \lambda(\nu_-)$. For lines with W_{HM}=300 Hz, e^2qQ/h = 150.0 kHz and η = .05, we obtain $\lambda(q)$ = .14 and $\lambda(\eta)$ = .0028. We would then report $(e^2qQ/h)_{expt}$ = 150±.14 kHz and η_{expt} = .050±.003 within 95% confidence limits.

IV.B Appendix - Assorted Spectra

In this appendix we present several assorted unpublished spectra as a means of "archiving" them. Most of them are ^{2}H spectra, although one of them is an indirect detection ^{7}Li spectrum. All are of reasonably good quality but for one reason or another have not been included in the previous Chapters. Each spectrum is described in the following table and in its respective figure caption. The indirect detection experiments were performed by detection of ^{1}H signal in high field.

Table V.3 Spectral Parameters

	FIDS[a]	NFID[b]	TI[c]	RDLY[d]	Method[e]	Ref[f]	Nucleus
hexloxybenzoic acid	2	512	3	7	Sud	A3T50-52	^2H
per-d malonic acid	3	680	3	10	Sud	A7T54-55	^2H
per-d malonic acid	5	330	3	10	PD	J9M174	^2H
per-d dimethyl terephthalate	1	129	10	10	PD	J9M201 A6T148	^2H
dimethylnaphthalene	8	500	3	2	ZFID	J10M79	^2H
$Li_2SO_4 \cdot H_2O$	4	166	3	5	ZFID	J9M65	^7Li
4,4' dimethyl benzophenone	7	1024	10	7	Sud	GD	^2H
4,4' dimethyl benzophenone	1	599	3	180	Sud	GD	^2H
ferrocene (per-d))	1	1001	6	1	Sud	GD	^2H

[a]number of phase-cycled fids.

[b]number of points in each phase of the phase-cycled fid.

[c]dwell time in the zero field evolution period (t_1), in units of μs.

[d]recycle delay time (sec).

[e]ZFID = indirect detection, Sud = sudden transition, PD = pulsed experiment with direct detection

[f]Original notebook references. (JMM or AMT)

Figure 5.22. Perdeuterated hexyloxybenzoic acid. Sudden transition zero field ^{2}H spectrum.

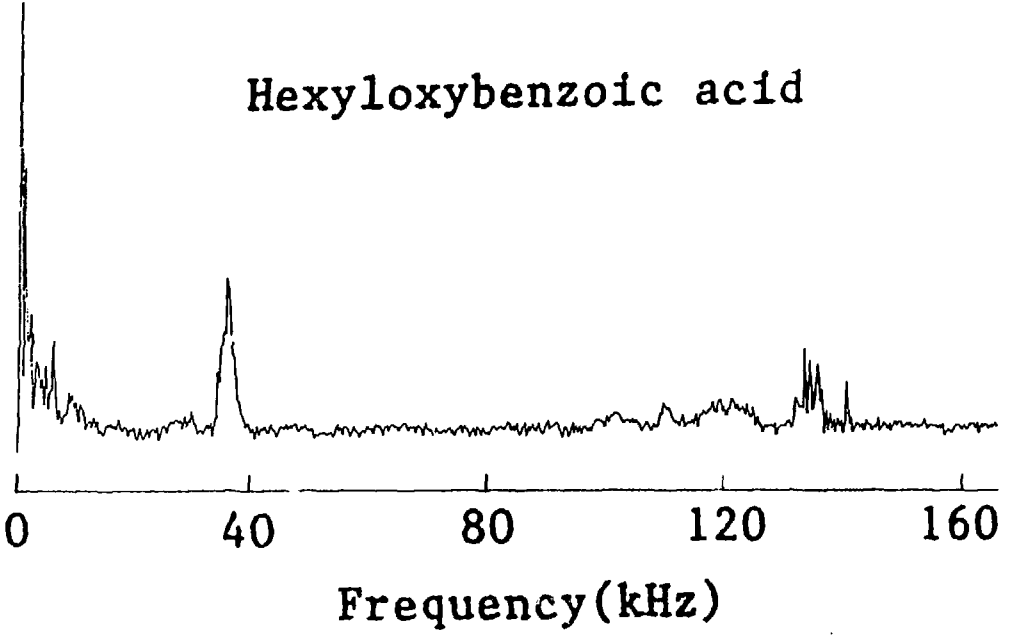
Hexyloxybenzoic acid
0
40
80
120
160
Frequency(kHz)

Figure 5.23. Perdeuterated malonic acid. Sudden transition zero field ^{2}H spectrum.

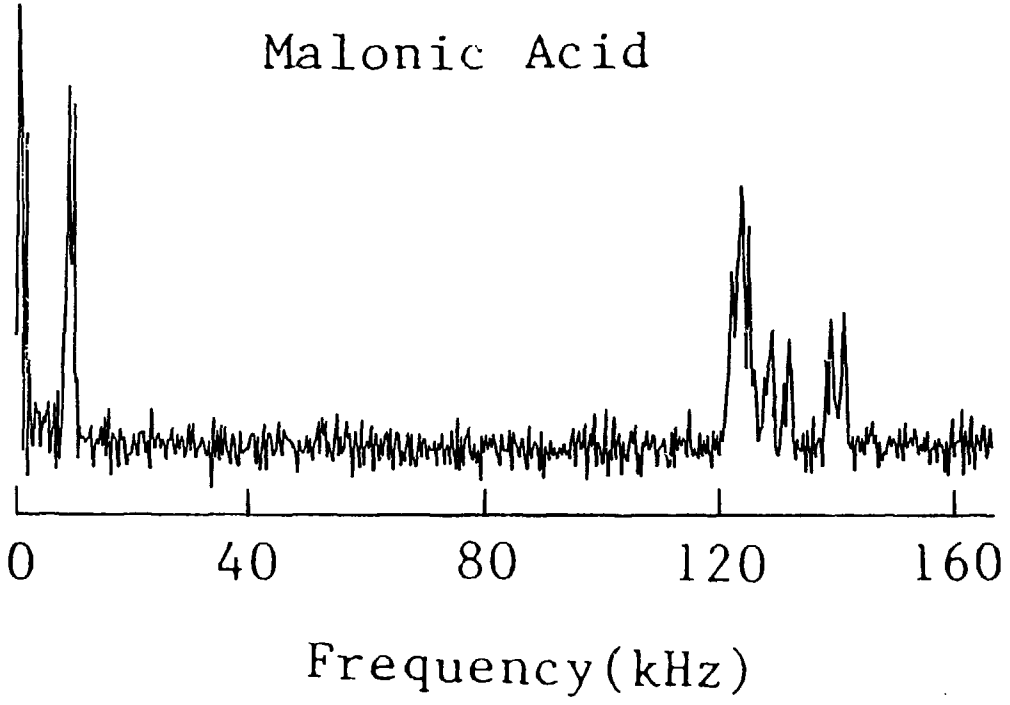
Malonic Acid
0
40
80
120
160
Frequency(kHz)

Figure 5.24. Perdeuterated malonic acid. Pulsed direct detection zero field ^{2}H spectrum.

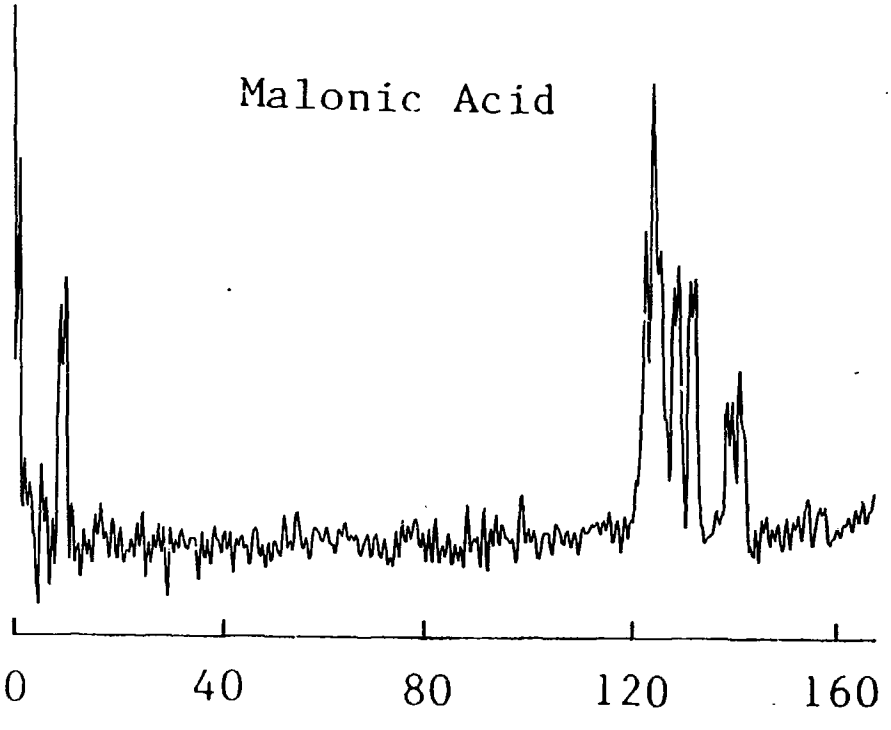
Malonic Acid
0
40
80
120
160

Figure 5.25. Perdeuterated dimethyl terephthalate. Pulsed direct detection zero field ^{2}H spectrum.

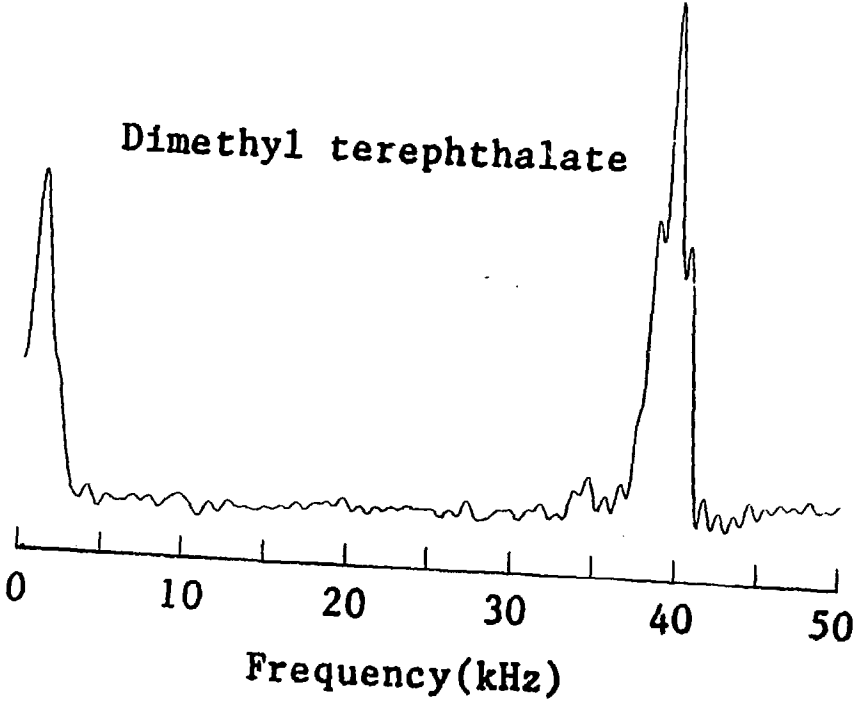
Dimethyl terephthalate
0
10
20
30
40
50
Frequency(kHz)

Figure 5.26. Ring deuterated dimethylnapthalene. Zero field indirect detection ^{2}H spectrum.

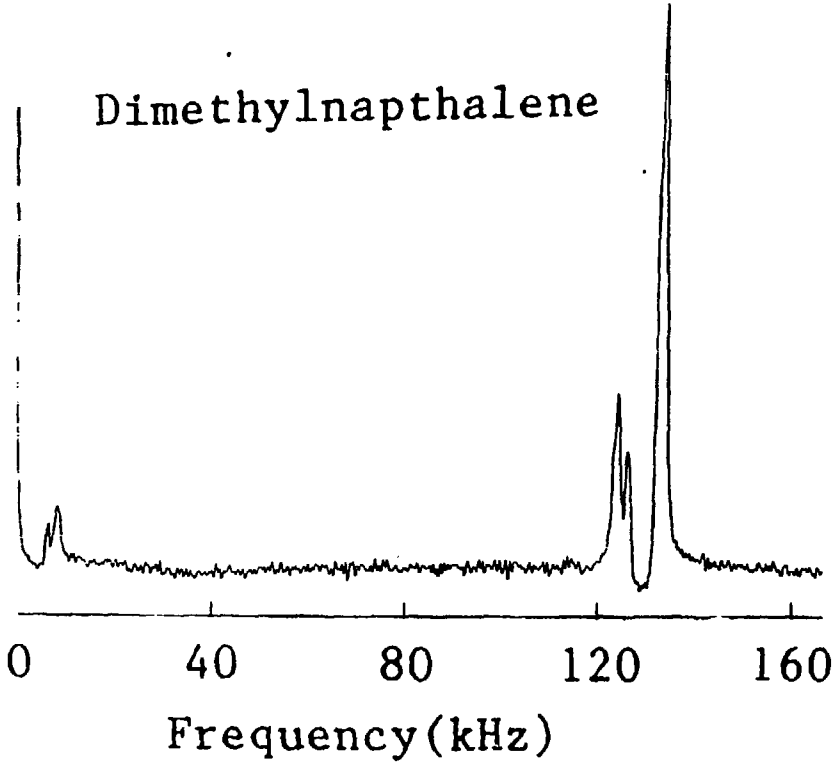
Dimethylnapthalene
0
40
80
120
160
Frequency(kHz)

Figure 5.27. Ring deuterated dimethylnapthalene. Expanded plots of previous figure, 5.26.

Dimethylnapthalene

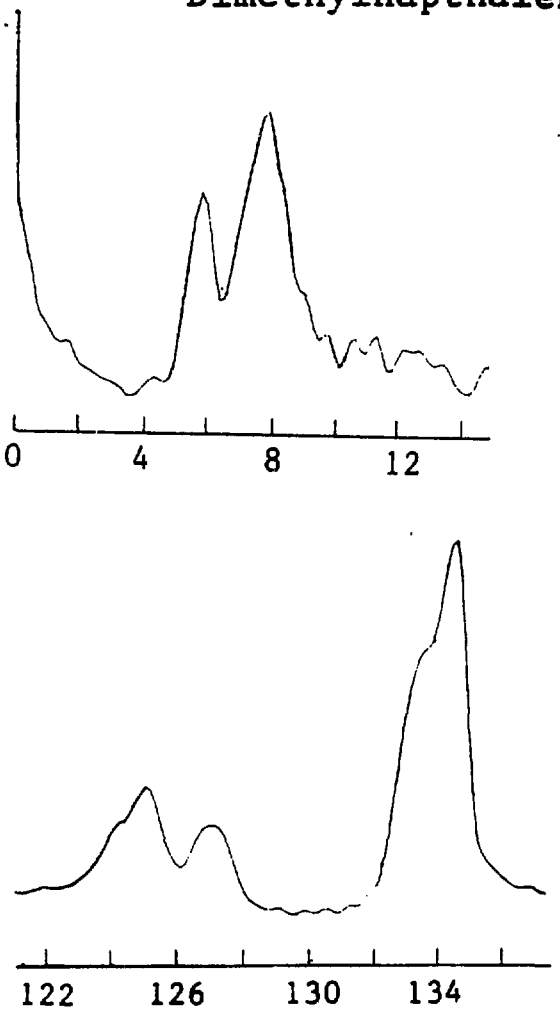

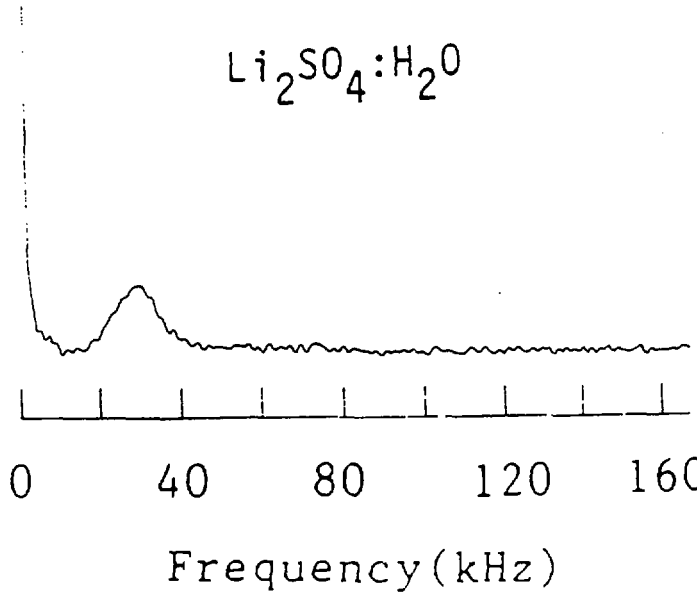

Figure 5.28. Lithium sulfate monohydrate. Zero field indirect detection ^{7}Li spectrum. Only one site appears to be resolved in contrast to the two found by Bielecki et al. Perhaps the sample is adversely affected by drying in hot oven (~70 C) as subsequent ^{1}H experiments gave completely different results as a function of sample history.

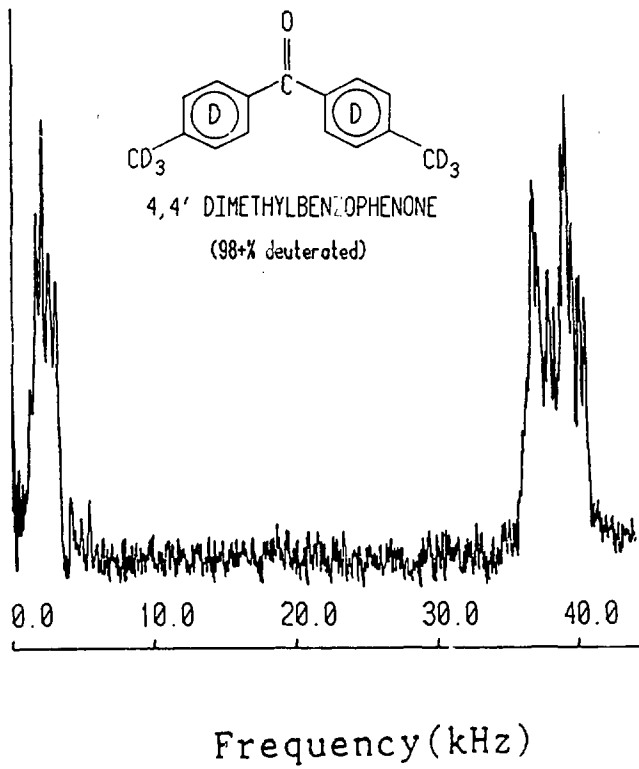

Figure 5.29. 4,4' Dimethylbenzophenone (>98% deuterated). Sudden transition zero field spectrum recorded using 7 second recycle delay. In this spectrum the aromatic signal, folded in to -28 kHz to 38 kHz, is buried in the the noise due to its long T_1 ($\geq$ 3 minutes). The sample spinlocked quite well; 2048 points of spinlocking signal were recorded in high field. (Courtesy of G. Davenport).

Figure 5.30. 4,4' Dimethylbenzophenone (>98% deuterated). Expanded plot of low frequency region of Figure 5.29.

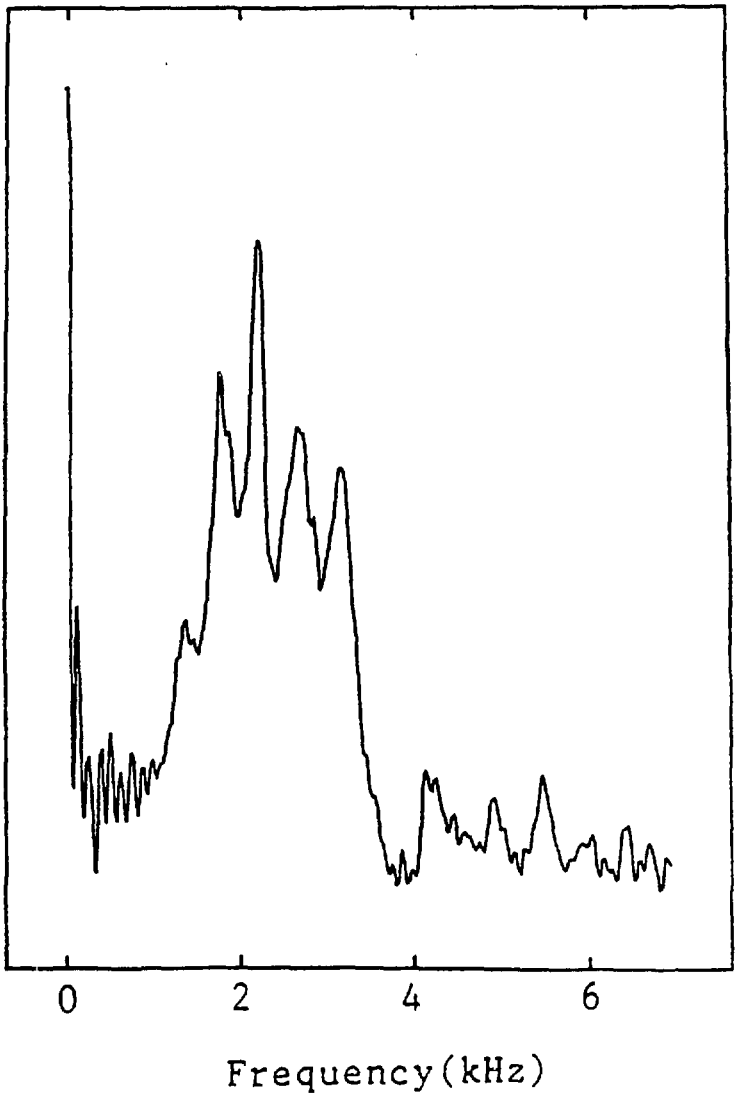
0
2
4
6
Frequency(kHz)

Figure 5.31. 4,4' Dimethylbenzophenone (>98% deuterated). Expanded plot of high frequency region of Figure 5.29.

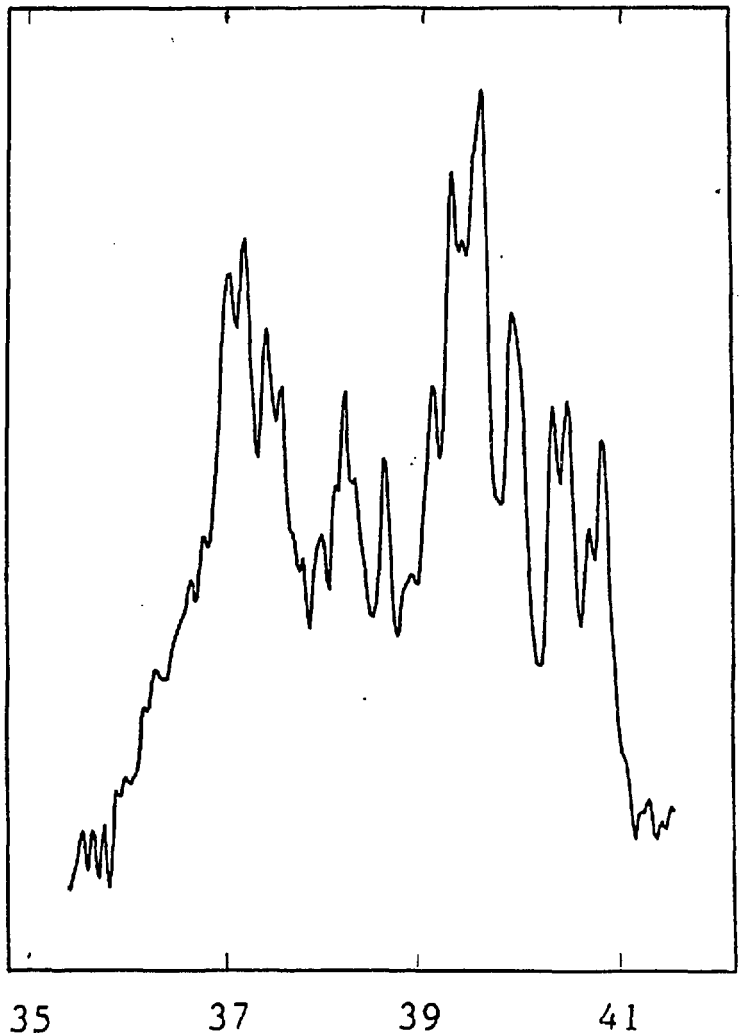
35
37
39
41
Frequency(kHz)

Figure 5.32. Expanded plot of 3 minute recycle delay version of deuterium sudden transition zero field spectrum of 4,4' Dimethylbenzophenone (>98% deuterated). Unfortunately a plot of the full spectrum did not exist at the time of this writing. Note this spectrum corresponds to eighth entry in Table V.3 on page 205 and is from a different run than Figures 5.29 - 5.31. (Courtesy of G. Davenport)

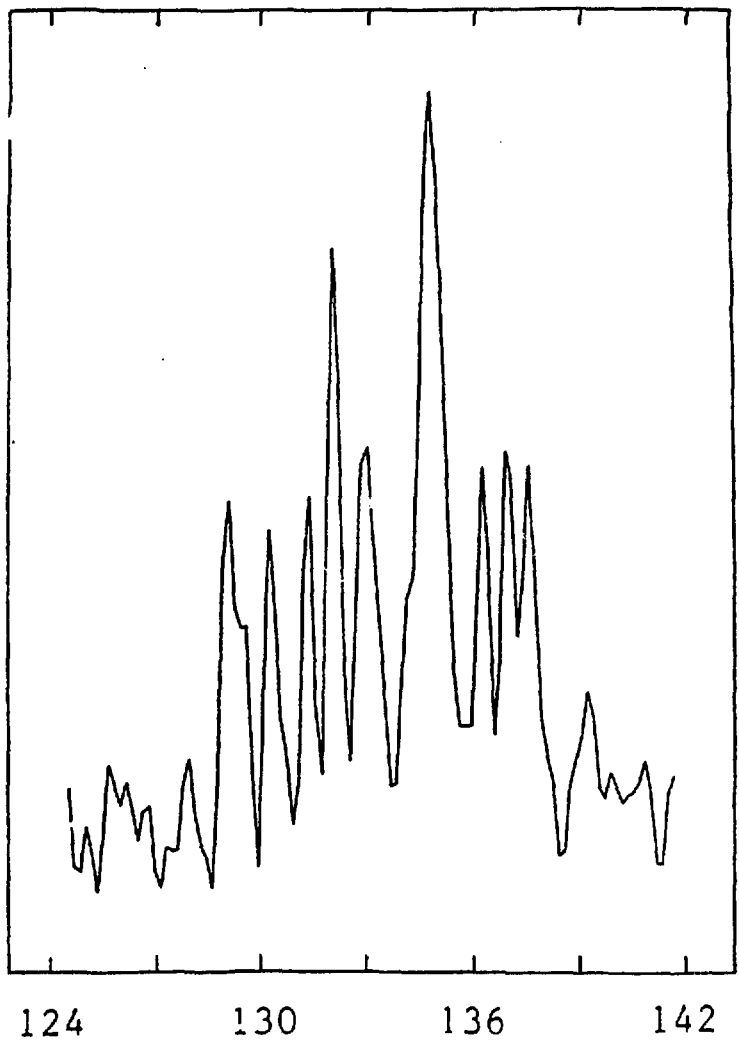
124
130
136
142
Frequency(kHz)

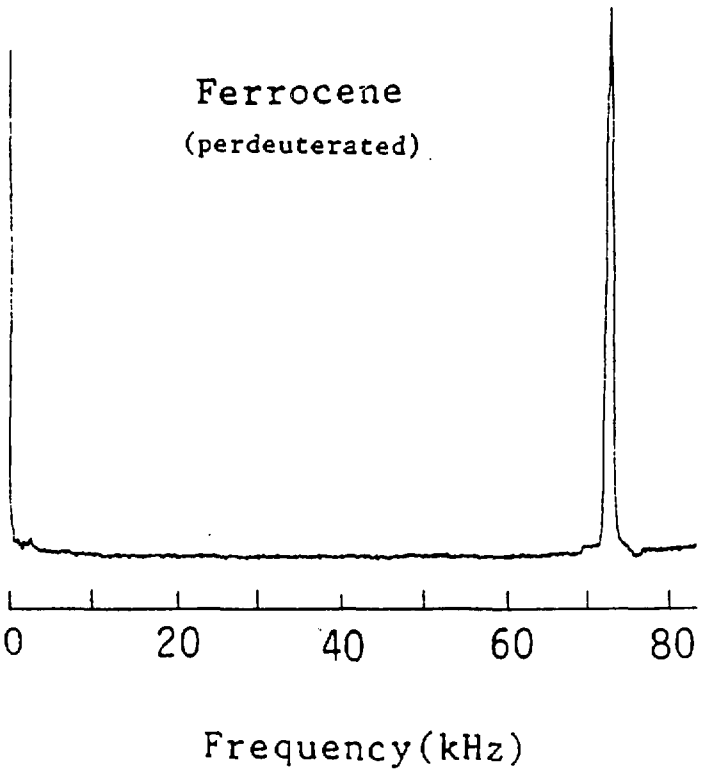

Figure 5.33. Sudden transition zero field spectrum of perdeuterated ferrocene. This spectrum was acquired using a recyle delay of one second and acquiring 1000 spinlocking points in high field. The major feature of the spectrum is a peak at 72.9 kHz with a shoulder at 72.5 kHz, which is better seen in the following Figure. (Courtesy of G. Davenport)

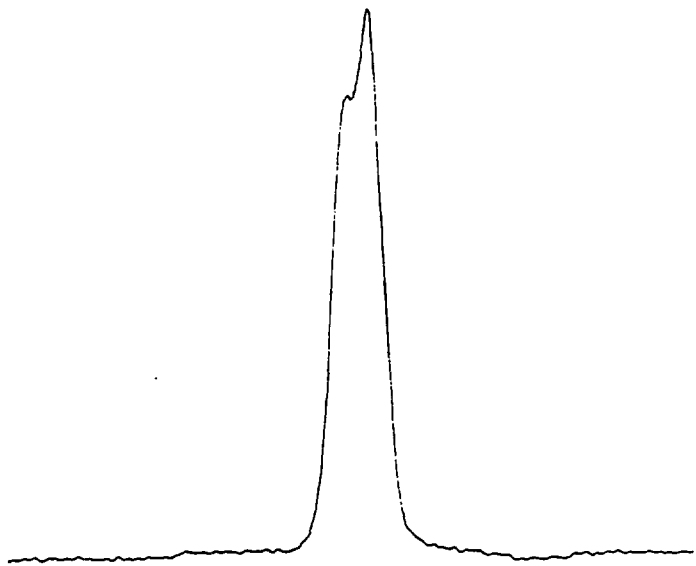

Figure 5.34. Expanded plot of high frequency region of Figure 5.34. Unfortunately the scale is unknown.

V. Chapter Five References

1. H.W. Spiess in "Advances in Polymer Sci," H.H. Kausch and H.G. Zachmann, editors, (Springer, Berlin, 1985) 66a, 23.
2. P.M. Henrichs, J.M. Hewitt and M. Linder, J.Magn.Reson. 60, 280(1984).
3. R. Hentschel and H.W. Spiess, J.Mag.Reson. 35, 157(1979).
4. D.T. Edmonds, Phys.Rep.C. 29, 233(1977).
5. R.E. Slusher and E.L. Hahn, Phys.Rev.Lett. 12, 246(1964); R.E. Slusher and E.L. Hahn, Phys.Rev. 166, 332(1968); A.G. Redfield, Phys.Rev. 130, 589(1963).
6. C. Muller, S. Idziak, N. Pislewski and U. Haeberlen, J.Magn.Reson. 47, 227(1982).
7. C. Muller, W. Schajor, H. Zimmermann, and U. Haeberlen, J.Magn.Reson. 56, 235(1984).
8. W. Derbyshire, T.C. Gorvin and D. Warner, Mol.Phys. 17,401(1969).
9. D.M. Ellis and J.L. Bjorkstam, J.Chem.Phys. 46, 4460(1967).
10. W. Derbyshire, T.C. Gorvin and D. Warner, Mol.Phys. 12, 299(1967).
11. G.M. Volkoff, H.E. Petch and D.W.K. Smellie, Can.J.Phys. 30, 279(1952).
12. A. Bielecki, J.B. Murdoch, D.P. Weitekamp, D.B. Zax, K.W. Zilm, H. Zimmerman, and A. Pines, J.Chem.Phys. 80, 2232(1984).
13. J.M. Millar, A.M. Thayer, A. Bielecki, D.B. Zax and A. Pines, J.Chem.Phys. 83, 934(1985).
14. D.B. Zax, A. Bielecki, K.W. Zilm, A. Pines, and D.P. Weitekamp, J.Chem.Phys. 83, 4877(1985).
15. R. Kreis, D. Suter and R.R. Ernst, Chem.Phys.Lett. 118, 120(1985).
16. D. Hentschel, H. Sillescu and H.W. Spiess, Macromolecules 14, 1607(1981).
17. R. Hentschel and H.W. Spiess, J.Magn.Reson. 35, 157(1979).
18. M.H. Levitt, D. Suter and R.R. Ernst, J.Chem.Phys. 80, 3065(1984).
19. J.G. Powles and J.H. Strange, Proc.Phys.Soc. 82, 6(1963).
20. J.H. Davis, K.P. Jeffrey, M. Bloom, M.I. Valic and T.P. Higgs, Chem.Phys.Lett. 42, 390(1976).
21. M. Mehring, High Resolution NMR in Solids, (Springer-Verlag, Berlin, 1983).

22. M.H. Cohen, Solid State Physics, F. Seitz and D. Turnbull, editors, (Academic, New York, 1958), 5.

23. R.G. Barnes in Advances in NQR, J.A.S. Smith, editor, (Heyden, London,1974), 1, 335

24. T. Chiba, J.Chem.Phys. 36, 1122(1962).

25. T. Das and E.Hahn in "Solid State Physics", F. Seitz and D. Turnbull, editors, (Academic, New York, 1958), Supplement I.

26. A. Bielecki, D.B. Zax, K.W. Zilm and A. Pines, in press, Rev.Sci. Instrum.

27. D. P. Shoemaker, C. W. Garland and J. I. Steinfeld; Experiments in Physical Chemistry (McGraw-Hill, 1962, New York) Third edition, p.52-53. 28. H.W. Spiess, Colloid and Polymer Sci. 261, 193(1983).

29. M.G. Taylor, E.C. Kelusky, I.C.P. Smith, H.L. Casal and D.G. Cameron, J.Chem.Phys. 78, 5108(1983).

30. D. Hentschel, H. Sillescu and H.W. Spiess, Makromol.Chem. 180, 244(1979).

31. S. Vega, Adv. Magn. Reson, J.S. Waugh, editor, (Academic, New York, 1968)6, 259.

32. P. Meier, private communication.

33. R. Eckman, private communication.

34. G.A. Sim, J.M. Robertson, and T.H. Goodwin, Acta. Cryst. 8, 157(1955)

35. D.T. Edmonds, M.J. Hunt and A.L. McKay, J.Magn.Reson. 11, 77(1973); D.T. Edmonds, M.J. Hunt and A.L. McKay, J.Magn.Reson. 20, 505(1975); D.T. Edmonds and A.A.L. White, J.Magn.Reson. 31, 149(1978).

36. T. L. Brown, L. G. Butler, D. Y. Curtin, Y. Hiyama, I. C. Paul, and R.B. Wilson, J. A. C. S. 104, 1172(1982).

37. M. Rinne and J. Depireux, Adv. in NQR, J.A.S. Smith, editor, (Heyden, London, 1974)1, 357.

38. R.T. Morrison and R.N. Boyd, Organic Chemistry, Third edition,(Allyn and Bacon, Boston, 1973), Chapter 11.

39. M. Bailey and C.J. Brown, Acta.Cryst. 22, 387(1967).

40. M.G. Takwale and L.M. Pant, Acta.Cryst. B27, 1152(1971).

41. D.F. Holcomb and B.Pedersen, J.Chem.Phys. 36, 3270(1962); L.W. Reeves in "Progress in NMR Spectroscopy," J.W. Emsley, J. Feeney

and L.Sutcliffe, editors, (Pergamon, Oxford, 1969) volume 4, 193.

42. J.M Millar, A.M. Thayer and A. Pines, submitted.

43. S. Ketudat and R.V. Pound, J.Chem.Phys. 26, 708(1957).

44. T. Chiba, J.Chem.Phys. 39, 947(1963).

45. P.L. Olympia, Jr.; I.Y. Wei and B.M. Fung, J.Chem.Phys. 51, 1610(1969).

Chapter VI. Zero Field NMR of Small Amplitude Vibrations in a Polycrystalline Solid

I. Introduction

NMR has been an excellent tool for the study of motion in condensed matter since one observes a time average over the motion resulting in an average chemical shift, quadrupolar coupling, or dipolar interaction. Because powder patterns[1] are insensitive to the relatively small perturbations of these motions one often resorts to single crystal measurements[2] or oriented liquid crystal measurements.[3] Zero field NMR offers an approach to this problem which is useful for polycrystalline or otherwise disordered materials since it has been demonstrated to provide sharp dipolar[4-6] and quadrupolar information[7-9] from such systems down to very low frequencies. Zero field NMR should be sensitive to small amplitude motions which result in splittings or extra lines in the frequency spectrum. Such motions typically do not result in observable changes in the high field NMR spectrum. In this report we present the first experimental results for the study of libration in a polycrystalline hydrate using proton and deuterium zero field experiments.

The proton zero field spectrum of a static water molecule would consist of lines at zero frequency and at $\pm\nu_d=3\gamma^2h/8\pi^2r^3$, where r is the internuclear distance of the two protons.[4] The characteristic motion of the waters in a typical hydrate are rapid 180° flips about their C_2 axes[10] and librations about three axes.[11,12] To a good approximation the librational modes correspond to rotations about the x, y, and z axes[12] of the molecular coordinate system shown in Figure

Figure 6.1. The three librational modes of the water molecules in barium chlorate monohydrate. In this molecular coordinate system the H_2O lies in the plane of the paper with its C_2 axis parallel to the z axis. From top to bottom these modes are referred to as waving, twisting, and rocking. Waving does not produce a reorientation of the internuclear vector, thus only twisting and rocking have an averaging effect on the dipolar tensor.

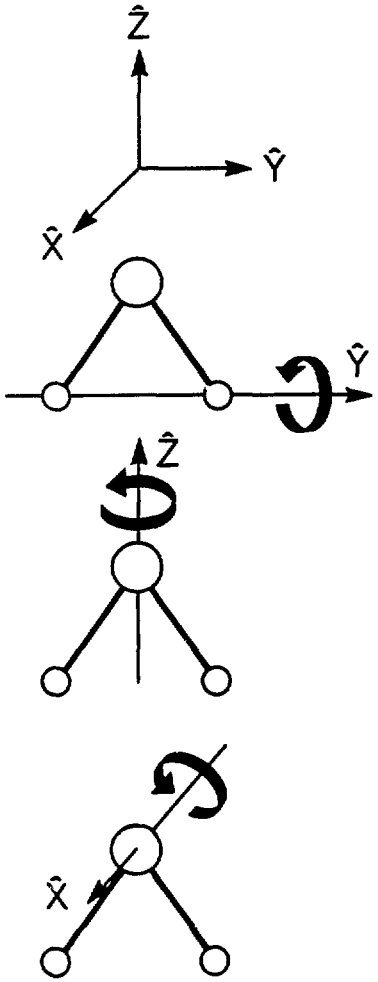

XBL 859-12121

6.1 and are commonly referred to as rocking, waving and twisting, respectively. The influence of the motion on the proton zero field spectrum is treated by calculation of its effect on the dipolar Hamiltonian, H_d, which is responsible for the zero field spectrum. The rapid 180° degree flips have no effect since they merely exchange the two protons. Waving has no effect since it leaves the orientation of the internuclear vector r invariant. The dipolar Hamiltonian is therefore motionally averaged by only two of the librational modes. The resulting motionally averaged Hamiltonian, H_d', is given in the molecular frame by

$$H_d' = \langle R_z(\theta_z)\cdot R_x(\theta_x)\cdot H_d\cdot R_x(\theta_x)^{-1}\cdot R_z(\theta_z)^{-1}\rangle$$

$$= \vec{I}_1\cdot\langle R_z(\theta_z)\cdot R_x(\theta_x)\cdot \underline{D}\cdot R_x(\theta_x)^{-1}\cdot R_z(\theta_z)^{-1}\rangle\cdot\vec{I}_2$$

$$= \vec{I}_1\cdot \underline{D}'\cdot \vec{I}_2 \qquad (6.1)$$

where θ_x and θ_z are the librational angles about the x and z axes respectively, and the brackets signify a time average over the motion. To second order in the angles θ_i characterizing the libration, we can write the motionally averaged tensor, $\underline{D}'$, in angular frequency units as[11,13]

$$\underline{D}' = d\begin{bmatrix} 1-3\langle\theta_z^2\rangle & 0 & 0 \\ 0 & -2+3\langle\theta_z^2\rangle+3\langle\theta_x^2\rangle & 0 \\ 0 & 0 & 1-3\langle\theta_x^2\rangle \end{bmatrix} \qquad (6.2)$$

where $d=\gamma^2h/2\pi r^3$. Application of the rotations in the reverse order of Equation 6.1 produces the same expression for $\underline{D}'$ to this order of

approximation. An unequal intensity in the amplitudes of the two librational modes produces a nonaxially symmetric average dipolar tensor. This is made more clear by defining $\Delta = D'_{22}$ and $\eta = (D'_{11} - D'_{33})/D'_{22}$ and rewriting Equation 6.2 as

$$\underline{D}' = \begin{bmatrix} -\Delta(1-\eta)/2 & 0 & 0 \\ 0 & \Delta & 0 \\ 0 & 0 & -\Delta(1+\eta)/2 \end{bmatrix} \qquad (6.3)$$

Calculation of the sudden experiment zero field spectrum for this case proceeds in a manner analagous to that described previously.[4,5] The normalized high field signal expected for a powder sample is given by

$$S(t_1) = \cos\{\tfrac{\Delta}{4}(3+\eta)t_1\} + \cos\{\tfrac{\Delta}{4}(3-\eta)t_1\} + \cos(\Delta\eta t_1/4) \qquad (6.4)$$

where t_1 is the evolution time in zero field. The effect of the motion is to split the lines of the static spectrum by an amount proportional to the asymmetry of the dipolar tensor. These motionally produced splittings or additional lines in the zero field spectrum are in sharp contrast with the shoulders on broad powder patterns which occur in the high field case.

The zero field spectrum of a motionally averaged spin one nucleus follows from a treatment similar to that above. Explicit expressions for the dependence of the quadrupole coupling constants and asymmetry parameter on the librational amplitudes have been calculated.[11,13] Both the quadrupole coupling constant and asymmetry parameter depend on all three librational modes as well as the exchange frequency characterizing the 180° flips. In barium chlorate at room

temperature, however, the frequency is sufficiently high that one need only consider an average over the two orientations.[10] The 180° flips average the static quadrupole tensor, which has its principal axis along the O-D bond, to one with its principal component either along the C_2 axis or perpendicular to the molecular plane of the water molecule.[14] The asymmetry parameter is also affected, its value near unity is a consequence of the motion.[15] One notes however that librational amplitudes are a function of the reduced mass of the molecule, hence the amplitudes and NQR frequencies will differ slightly in HDO and D_2O.

II. Zero Field Experiments

A). Proton zero field spectra

All spectra reported here were obtained at room temperature using a homebuilt 180 MHz proton frequency instrument that has been modified for the zero field experiments.[16]

The proton zero field spectrum of isotopic abundance barium chlorate has been published before.[4] Intermolecular dipolar couplings produce linewidths of approximately 7 kHz thus obscuring the splitting due to the motion. The effect of isotopic dilution by deuterium on the linewidth of the proton zero field spectrum is shown for a series of dilution levels in Figure 6.2. An increase in the amount of structure in the spectrum is seen as the level of protonation decreases. The spectrum from a 10% protonated sample, Figure 6.3, shows all three lines predicted by Equation 6.4 for the asymmetric dipolar tensor. By combining equations 6.2 through 6.4 one can use the experimental splittings to obtain the difference $\langle\theta_z^2\rangle$-

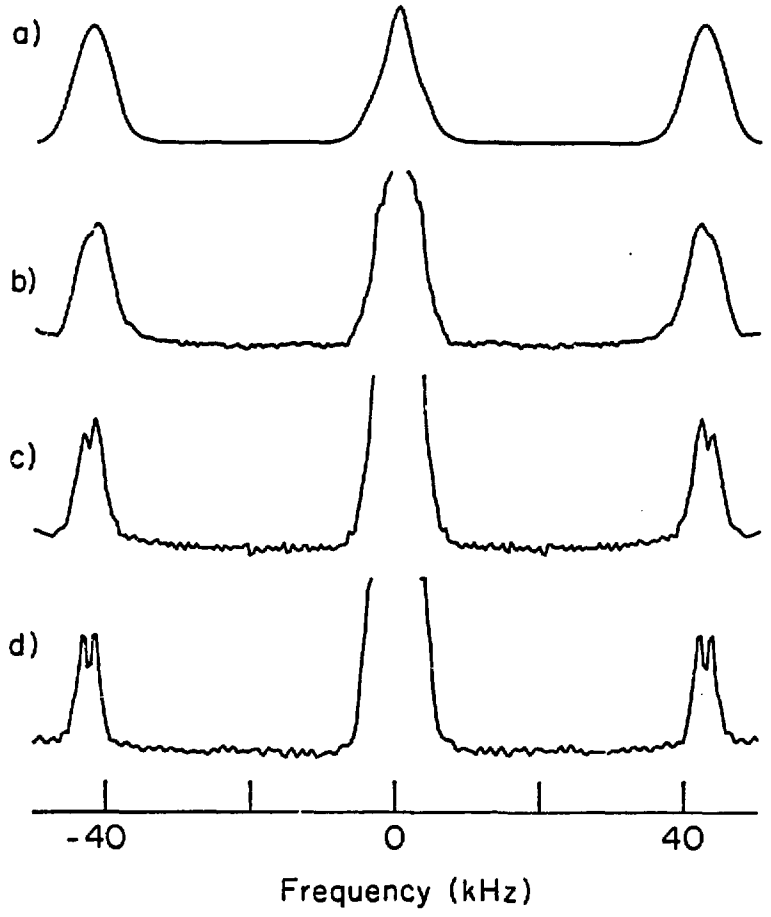

Figure 6.2. Proton sudden zero field spectra of barium chlorate monohydrate as a function of isotopic dilution by deuterium; a) isotopic abundance, b) 60% protons, c) 31% protons, d) 10% protons. Structure due to the asymmetric dipolar tensor of dilute water molecules is observed as the intermolecular contribution to the linewidth is reduced. Unpaired protons in the dilute samples contribute to the line centered at zero frequency.

Figure 6.3. a) Proton zero field spectrum of 90% deuterated $Ba(ClO_3)_2 \cdot H_2O$ obtained with the sudden experiment field cycle. The applied field, B_z, is shown schematically in the inset as a function of time. Zero field evolution is initiated by sudden switch-off of the field. After the t_1 evolution period the field is switched on suddenly and the sample returned to high field where the magnetization M_z is measured as a function of t_1. Here only the positive frequency portion of the spectrum is displayed. All three lines characteristic of the motionally averaged non-axially symmetric dipolar tensor are resolved, appearing at 1.37, 41.8, and 43.4 kHz with linewidths of approximately 2 kHz, considerably narrower than that obtained with the fully protonated material.

b) Zero field spectrum from the sudden field cycle with dc pulses. This cycle, shown in the inset, is identical to the sudden experiment except for the application of 90^o dc magnetic field pulses, P_x and P_x', at the initiation and termination of the zero field evolution period. These experiments employed a dc field of 0.010 Tesla oriented orthogonal to B_o. The spectrum obtained is essentially identical with that of the sudden experiment.

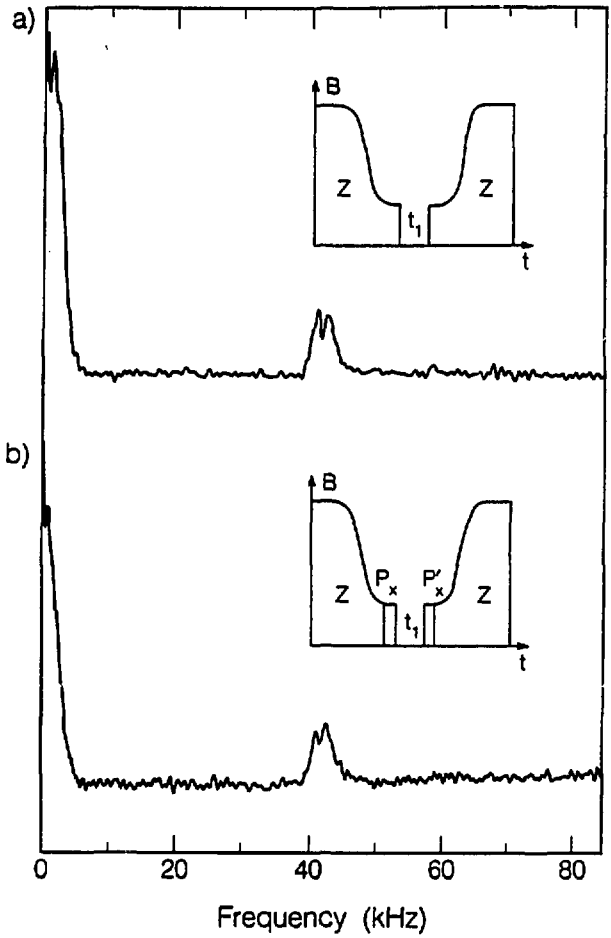

XBL 859-12123

$\langle\theta_x^2\rangle$=0.024. Using r=1.52 angstroms, a value obtained from neutron diffraction measurements[17], one can calculate $\langle\theta_x^2\rangle$=0.044 and $\langle\theta_z^2\rangle$=0.070 (radians^2).

A second experiment was performed to determine if the observed splittings could be due to residual magnetic fields present during the zero field evolution period. The field cycle is shown in the inset of Figure 6.3b. In this experiment a dc pulse calibrated to rotate the initial magnetization from the z axis to the x-y plane[8] was given immediately after the sudden switch-off of the intermediate field. In addition, an identical dc pulse was given at the conclusion of the t_1 period to store the effect of the zero field evolution. This sequence being identical with the sudden experiment in every other detail has the effect of simply changing the relative orientation of the stray field with the initial condition of the magnetization. The spectrum obtained with this sequence, Figure 6.3b, is essentially identical with that of the sudden experiment.

B) Effect of Stray Fields

Computer simulations of the zero field spectrum of a powder distribution of static pairs of protons in a stray nonzero field were performed as a means of further probing the effects of stray fields. The simulations assumed an internuclear distance of 1.6 angstroms and stray magnetic fields of varying strengths and directions. In the sudden experiment the magnetization at t_1=0 is along the lab z direction. The symmetry of a powder then requires only examination of stray fields with components along the z axis and a perpendicular axis which we define as the x axis. The results of these simulations, some of which are shown in Figure 6.4, bear little or no resemblance to the

Figure 6.4. Simulations of zero field spectra obtained using the sudden field cycle in the presence of variable residual fields for a powder sample of isolated pairs of protons where r~1.6 angstroms. The sudden experiment utilizes a field along the z direction which is suddenly switched off to initiate evolution. Simulations on the right correspond to the residual field aligned along the z axis and those on the right left the x axis of the lab frame. Magnitudes of the residual fields used in the simulations from top to bottom are: a,b) 0.35 gauss; c,d) 1.2 gauss; and e,f) 2.4 gauss. Additional simulations for general orientations of the residual field in the x-z plane are in qualitative agreement with those shown. In all cases quite large residual fields are required to produce splittings in the spectrum.

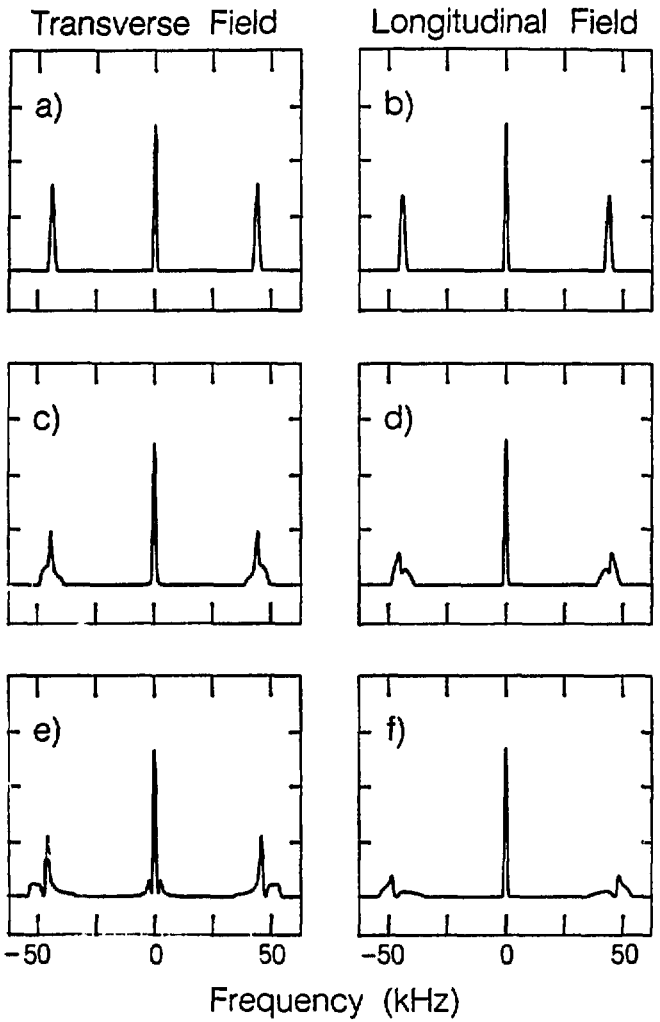
Transverse Field
Longitudinal Field
a)
b)
c)
d)
e)
f)
−50
0
50
−50
0
50
Frequency (kHz)

XBL 857-8935

experimental spectra and indicate that residual fields > 1 gauss are required to produce splittings comparable to those seen in Figure 6.1. Experimental measurements typically place an upper limit of 0.025 gauss on the magnitude of the stray field.

C) Deuterium spectra

Although the rapid C_2 flips do not manifest themselves in the proton spectrum, they are readily observable via their effect on the deuterium quadrupolar spectrum.[11,14,15] The deuterium zero field NQR spectrum of a 50% deuterated sample of barium chlorate was obtained at room temperature using the indirect detection method which is described in detail elsewhere.[8] Since room temperature deuterium low field T_1's are of the order of milliseconds, an indirect detection method is necessary. The indirect method is selective for the deuterons in that ideally only they are induced to evolve during the zero field evolution period and hence little or no signal is observed due to the proton pairs. In the spectrum, shown in Figure 6.5, the ν_+, ν_-, and ν_0 lines are all clearly resolved and from their frequencies one calculates e^2qQ/h =122.7 kHz and η=0.960 which is in good agreement with earlier work.[11] If we neglect differences in librational displacements due to reduced mass, we can estimate $\langle\theta_y^2\rangle$ by combining the zero field proton and deuterium data with the quadrupole coupling constants of the static molecule found by Chiba.[11] Using the explicit expressions for the field gradient tensor averaged by libration and the C_2 flipping, one obtains $\langle\theta_y^2\rangle$=0.123(radians^2). We note the librations have a relatively minor effect on the quadrupole spectrum, the value of η near unity is primarily a

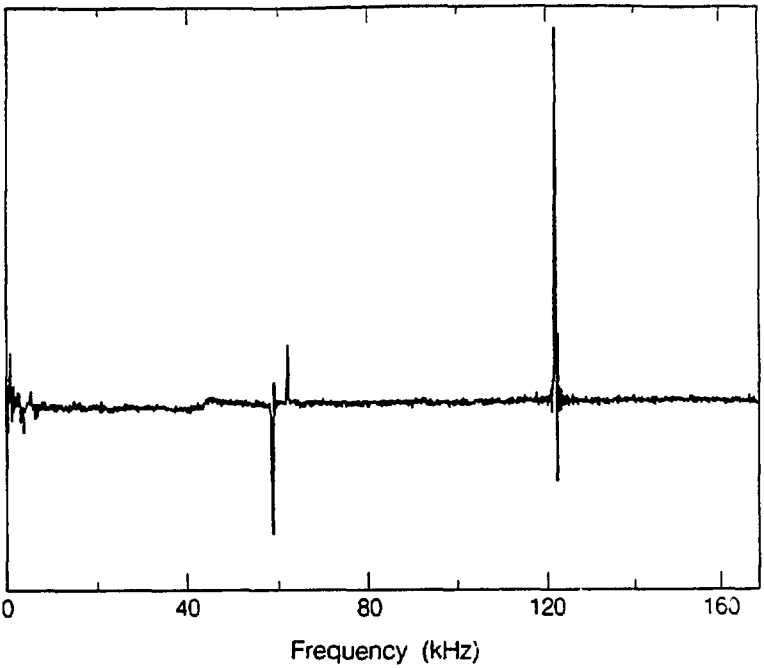

XBL 859-12122

Figure 6.5. Indirect detection zero field deuterium NQR spectrum of 50% deuterated barium chlorate monohydrate. All three lines expected are resolved from which one calculates e^2qQ/h=122.7 kHz and η= 0.96 in reasonable agreement with single crystal measurements of the perdeuterated material which obtained e^2qQ/h = 121.5 ± 0.4 kHz and η = 0.976 ±0.007.[11] The bump at approximately 40 kHz is due to proton pairs. Its small relative size gives an indication of the deuterium selectivity of the indirect experiment.

consequence of the C_2 flips.[15] An advantage of the dipolar measurements is that the static dipole interaction is inherently axially symmetric and any asymmetry is the direct result of motion.

III. Discussion

The non-axially symmetric dipolar tensor produced by libration is readily observable via the proton zero field spectrum. The excellent agreement between the results of the two versions of the zero field experiment, as well as the results of computer simulations, rule out the possibility of splittings due to residual fields. Our results for the mean square amplitudes of the librational modes are in reasonable agreement with earlier data,[11,18] especially when one considers that the exact librational modes might differ lightly from the inertial rotations assumed.[12] With the high resolution possible in the dipolar zero field experiment one has a sensitive measure of relatively small changes in the dipolar tensor.

The zero field NQR results for HDO demonstrate the high resolution of the experiment and the precision with which it can measure the asymmetry parameter. The parameters relating to the motion are underdetermined with a single NQR experiment since the quadrupolar frequencies are a function of the three librational modes, the rate of the 180° flips, as well as the values of $(e^2qQ/h)_o$ and η_o, the parameters of the static molecule. We note that these are the first room temperature deuterium NQR measurements of a hydrate, since these systems are usually inaccessible to frequency domain techniques because of their relatively short T_1's and low quadrupolar frequencies. In contrast to typical frequency domain NQR methods there is no power broadening[13] and ideally no signal due to protons.

This fact generally allows resolution of the ν_o lines, a tremendous aid in the assignment of the spectra.

In summary the zero field experiment has been demonstrated to provide information about the dipolar and electric field gradient tensors in a two spin system and thus provide information about its motional characteristics. In general these should provide complementary information since they possess unique principal axis systems and hence are affected differently by the different motions which occur in a system. The zero field measurements have the significant advantage of being made with a powder sample whereas the earlier measurements required a single crystal.[11] This aspect should allow study of subtle motions in systems inaccessible to single crystal measurements including amorphous and polycrystalline materials as well as biological samples.

IV. Appendix - ^{1}H Zero Field Studies of Motion in Toluic Acid

In the solid state , p-toluic acid forms a hydrogen-bonded dimer.[19] The internucear vector between the two acid protons of the dimer jumps between two conformations separated by an angle 2θ equal to 37.2°.[20] Consider an axis system where the internuclear vectors of both conformations lie in the xy plane and are symmetrically displaced about the y axis. Assuming an equal population of the two conformers one finds the dipolar tensor averaged by the jumping to be given by[15]

$$\underline{D} = d\begin{bmatrix} 1 - 3\sin^2\theta & 0 & 0 \\ 0 & 1 - 3\cos^2\theta & 0 \\ 0 & 0 & 1 \end{bmatrix} \quad \text{(Hz)} \qquad (6.5)$$

where $d = \gamma^2 h/((2\pi)^2 r^3)$. (Note units of the dipolar tensor are Hz in Equation 6.5, therefore d defined there differs by $1/2\pi$ from d appearing in equation 6.2.) Meier et al. experimentally found the motionally averaged tensor at room temperature to be given by

$$\underline{D} = \begin{bmatrix} 6.73 & & \\ & 9.67 & \\ & & -16.33 \end{bmatrix} \quad \text{(kHz)} \qquad (6.6)$$

where we have scaled the values found in their work by 2/3 to bring them into accord with our notation. Calculation of the zero field spectrum expected from this nonaxially symmetric tensor predicts lines at 1.48, 11.52 and 13.00 kHz. Figures 6.6 and 6.7 show the proton zero field spectrum obtained at room temperature from a sample in which all but the carboxylic acid protons were replaced with deuterons. The predicted low frequency line is not resolved most likely because of the relatively large zero frequency peak due to residual ring protons and also because of dipolar broadening from

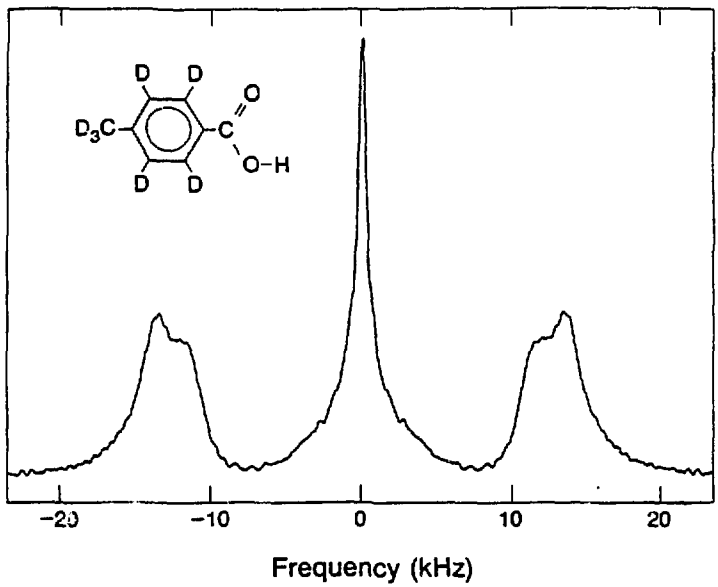

XBL 8511-11489

Figure 6.6. Proton sudden transition zero field spectrum of p-toluic acid D_3C-C_6D_4-COOH. The spectrum is the Fourier transform of two phase-cycled zero field fids of 155 points each acquired with a zero field dwell time of 15 μs and using a recycle delay of 45 seconds. The high field signal was obtained by averaging over 256 points of the spinlocking signal.

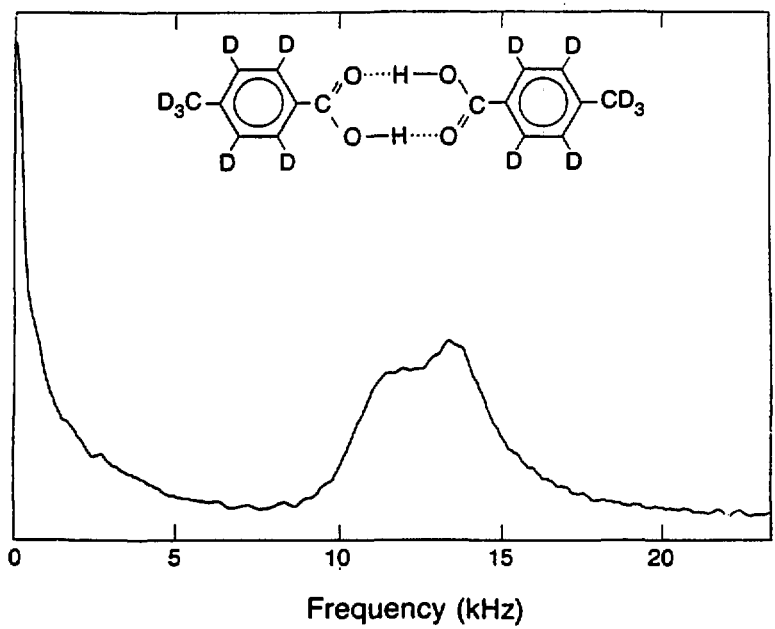

XBL 8511-11499

Figure 6.7. Proton sudden transition zero field spectrum of toluic acid D_3C-C_6D_4-COOH. This figure is simply the positive frequency regionof the previous figure.

neighboring acid pairs. However, the shoulder found in the high frequency line clearly shows evidence of the expected splitting and the frequencies of the two components of the observed line can be estimated to be 12.2 and 13.5 kHz, in good agreement with the predicted values. Later experiments using a sample perdeuterated on the ring and 60% COOD managed to resolve the high frequency lines a little better but still did not resolve the low frequency "difference" line.[21] Unfortunately, the resulting signal-to-noise in these latter experiments was noticeably degraded relative to that observed in Figures 6.6 and 6.7. The experiment was also performed on ring deuterated samples of terephthalic acid and benzoic acid. The zero field spectrum of both samples consisted of a featureless line centered at approximately 13 kHz, giving no indication of a splitting.

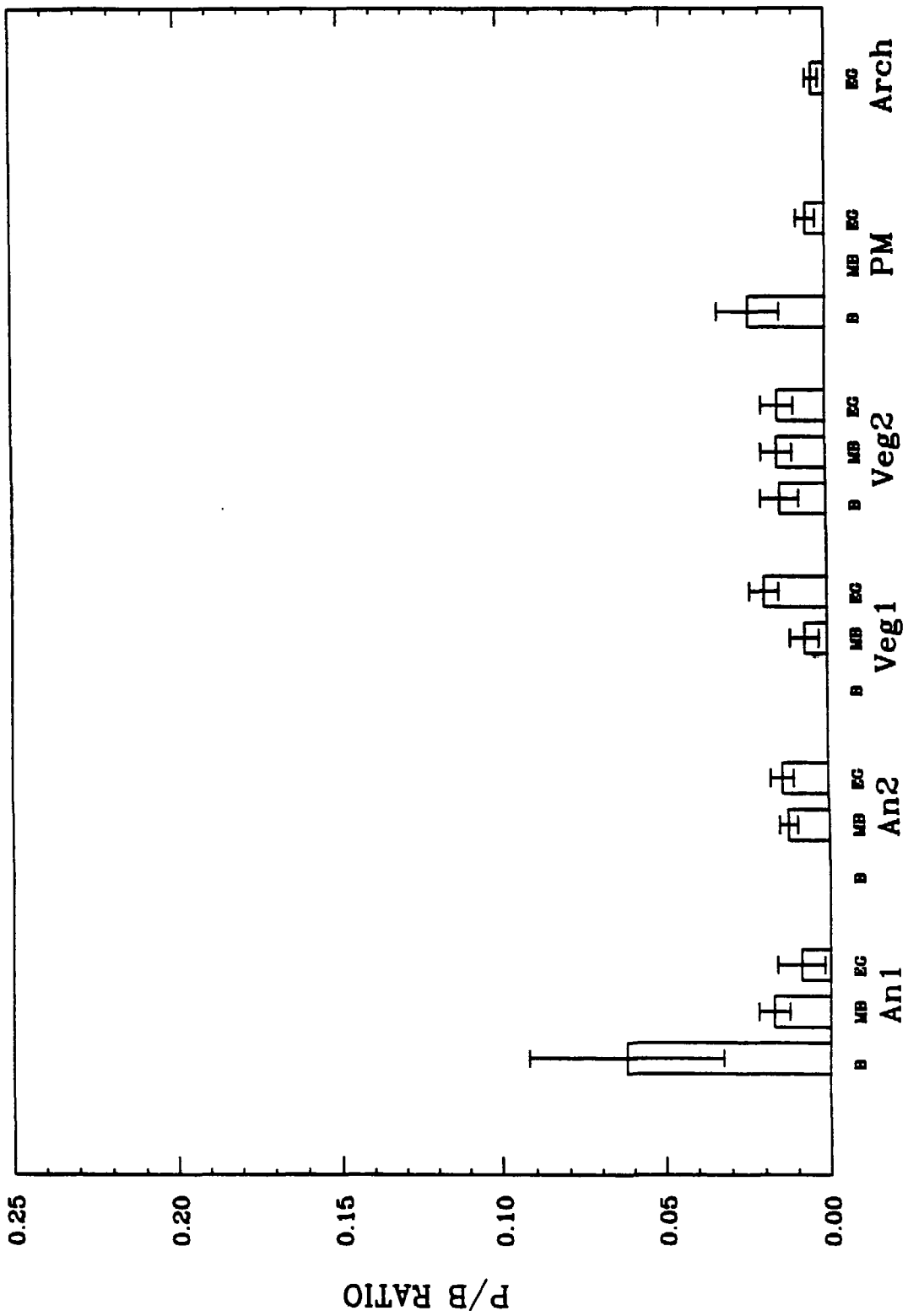
P/B RATIO
0.25
0.20
0.15
0.10
0.05
0.00
B
MB
EG
An1
An2
Veg1
Veg2
PM
Arch

18.B. Pedersen, J. Chem. Phys. 41, 122(1964).
19.M.G. Takwale and L.M. Pant, Acta Cryst B 27, 1152(1971).
20.B.H. Meier, F. Graf and R.R. Ernst, J.Chem.Phys. 76, 767(1982).
21.A.M. Thayer and T. Jarvie, private communication.

Chapter Seven. Zero Field NMR of a Nematic Liquid Crystal

I. Introduction

Nematic liquid crystals consist of long rod-like molecules whose average orientation is described by a director $\hat{n}$. In the absence of a magnetic field the average orientation of the director is determined by convection and interactions with walls and surfaces of the container of the sample[1]. In a macroscopic sample, $\hat{n}$ is a function of position throughout the sample owing to these effects. Since these materials have an anisotropic magnetic susceptibility defined by $\Delta\chi = \chi_{\parallel} - \chi$ they can be aligned by an applied magnetic field. Given a sample with positive $\Delta\chi$ in an applied field of sufficient magnitude, the system will be describable by a single director whose average alignment is along the field. Molecules of the liquid crystal will on the average be aligned with their long axes parallel to the director.

The magnetic field strength dependence of the alignment on a macroscopic scale has been studied by light scattering[2], optical[3] and magnetic[4] birefringence, and magnetic susceptibility[5] measurements. The unique feature of NMR is that it measures the alignment on a molecular scale. It has been suggested that the degree of ordering may differ on a macroscopic and molecular level in spite of the small energies of the order-director fluctuations.[6] The order parameter and fluctuations are important in relaxation of liquid crystal systems,[7] and it is thus instructive to directly measure the order parameter of a probe molecule in a nematic liquid crystal in high and low fields. The recent pulsed field cycling technique[8-10] of zero field NMR is ideally suited to this purpose. This Chapter presents the first

applications of zero field NMR to liquid crystals. A common approach to spectral simplification is to study the behavior of a solute dissolved in the liquid crystal[11,12] since the nematic phase causes the solute to acquire a preferred alignment with respect to the director.[11-13] The allowed motions of the solute reflect the anisotropic molecular tumbling in the uniaxial medium by characteristically averaging the dipolar interaction[14].

II. Experimental

The system chosen for study was composed of CH_2Cl_2 dissolved in p-pentyl phenyl 2-chloro-4-(p-pentylbenzoyloxy)benzoate (Eastman 11650). Samples were made homogeneous by thoroughly mixing after heating the liquid crystal/solute mixture to above its clearing point. The samples exhibited clearing points of ~65°±2°C and the CH_2Cl_2 concentration was estimated to be approximately 10-15 weight percent in the nematic. Samples were sealed and remained unchanged for several weeks. Precautions were taken to minimize the presence of bubbles in the samples.

Descriptions of the zero field NMR field cycling experiments have been presented elsewhere[8,9,15] and require little change when applied to liquid crystal samples aside from the application of orthogonal dc pulses in zero field. Field cycling schemes used in these experiments are shown in Figure 7.1. In the sudden experiment sequence of Figure 7.1a the zero field magnetization at t_1=0 is aligned along the laboratory z axis. In Figure 7.1b, dc pulses applied orthogonal to z rotate the initial magnetization to the x-y plane. The pneumatic shuttling system employed for translation of the sample from B_o to B_i

Figure 7.1. Schematics of zero field experimental field cycles. a) After demagnetization to an intermediate field, the zero field evolution period is initiated by the sudden switch-off of B_1. After a time t_1, the z component of magnetization is sampled by reapplication of the intermediate field and remagnetization to high field. The zero field interferogram, $S(t_1)$, is produced by repeated field cycles for incremented values of t_1. b) Sudden z/pulsed y field cycle. This field cycle is identical to (a) except for the application of pulsed dc magnetic fields corresponding to rotation angles given by $\theta=\gamma B_{dc} t_p$. For 90°_y pulses the density operator at the start of the t_1 period is now proportional to I_x in the lab frame. Detection of the transverse component is completed by the final P'_y pulse and application of a field in the z direction to trap the magnetization before remagnetization to high field. The magnitude of B_1 and the dc pulsed fields are typically on the order of 0.01 Tesla.

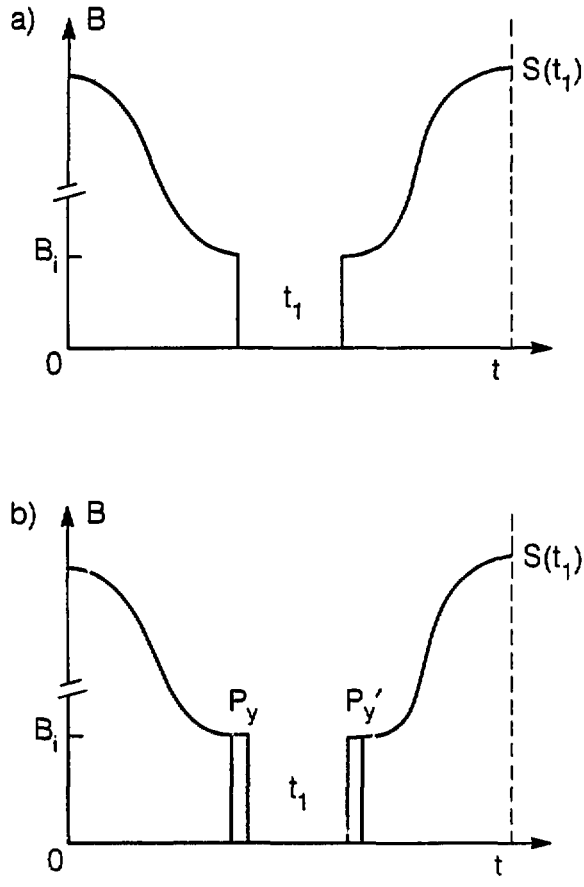

XBL 859-9009

as well as the electronics for production of the zero field have also been described[15]. Minimum air pressures were used to reduce the physical shock of shuttling the sample.

III. Results

The high field NMR spectrum of the CH_2Cl_2/11650 system was obtained using a 90_x-τ-180_y-τ echo sequence to reduce the effects of field inhomogeneities.[16] The signal intensity was measured as a function of τ. The minimum time for the incremented variable τ was chosen to echo only the solute signal and not that of the liquid crystal itself. The resulting dipolar spectrum is shown in Figure 7.2. The alignment of the proton-proton internuclear vector with respect to the director, $\hat{n}$, may be described by a single order parameter S=0.055±0.001 as calculated from the observed splitting.[14]

Previous work[9,17] has shown that polycrystalline samples of isolated proton pairs yield a three line frequency spectrum when subjected to the sudden experiment sequence of Figure 7.1a. The three lines are of equal intensity and occur at zero frequency and $\pm\nu_D=3\gamma^2h/8\pi^2r^3$. If this sudden experiment is applied to the CH_2Cl_2/11650 system using an echo as above to detect only the solute signal, one obtains the one line spectrum shown in Figure 7.3. This line at zero frequency corresponds to the central line of the triplet found in the polycrystalline case and yields no dipolar information on the solute.

The experiment was thus performed with the sequence of Figure 7.1b. Figure 7.4 presents the results of a series of these sudden z/pulsed y experiments. The angles of the dc pulses corresponding to

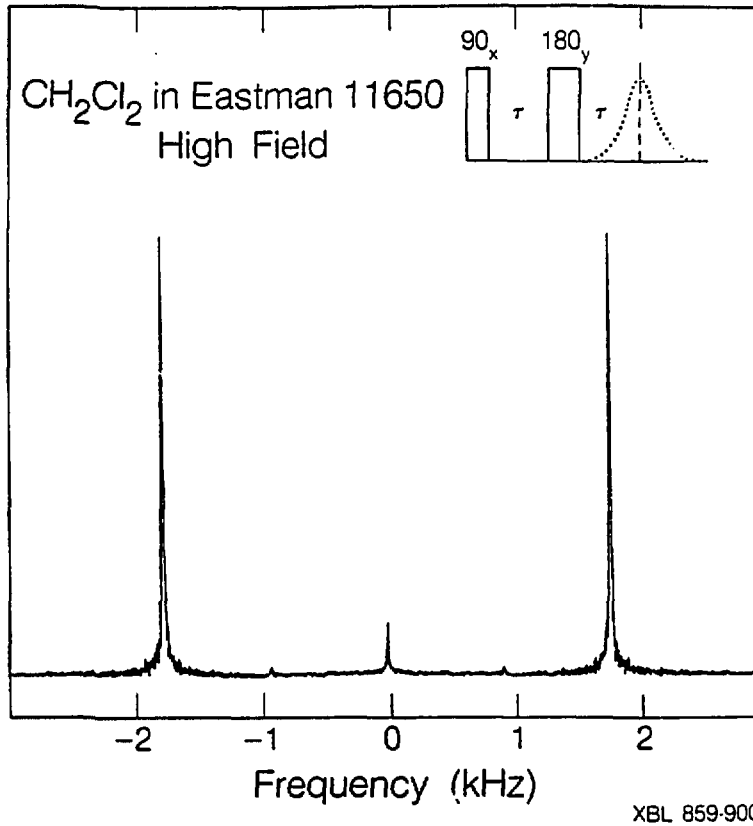

Figure 7.2. High field NMR spectrum of CH_2Cl_2 in Eastman 11650 taken as a function of τ with the pulse sequence shown at upper right. The molecular order parameter of the solute is calculated to be $S=0.055\pm0.001$ from the observed splitting.

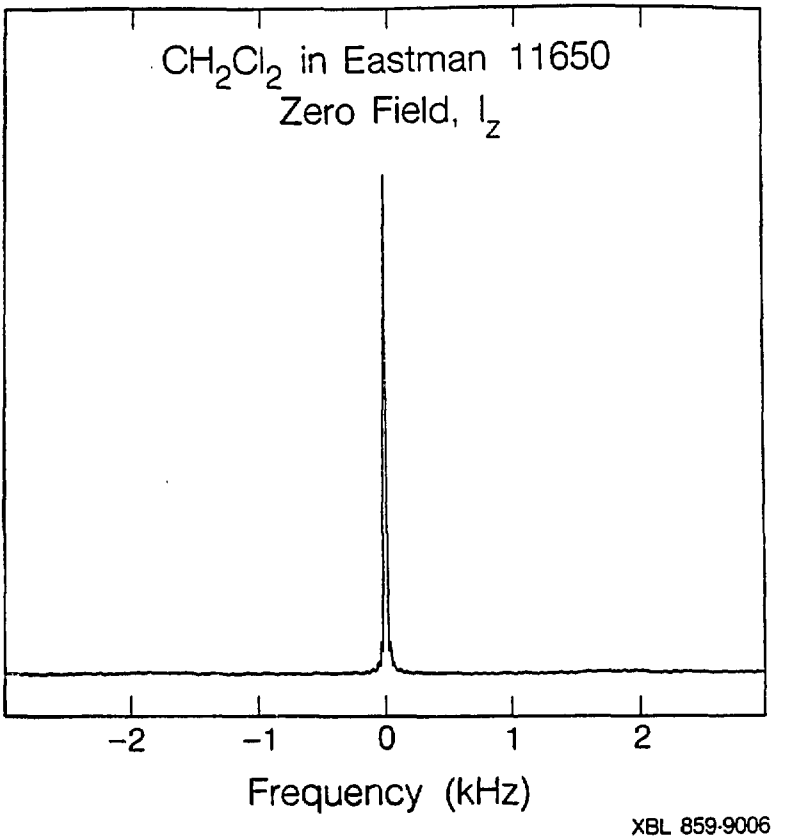

Figure 7.3. Spectrum of CH_2Cl_2 in Eastman 11650 using the field cycle of figure 1a. The single line at zero frequency indicates that no zero field evolution occured during the time t_1. The spectrum appears as expected for an ordered nematic in which the axis of quantization is the same in high as in low field.

Figure 7.4. Spectra of the CH_2Cl_2/11650 system obtained via the sudden z/pulsed y field cycle of Figure 7.1b. DC pulses used were (a)90°_y,270°_y and (b)180°_y,180°_y. The observed spectra show the same dependence on pulse angle as given by eq. [6], which was obtained assuming an ordered nematic liquid crystal in zero field. The molecular order parameter may be measured from the observed frequencies and was found to be S=0.054±0.001, which is unchanged from high field within an experimental error of 2%. Linewidths of ~45 Hz may be attributed to residual fields.

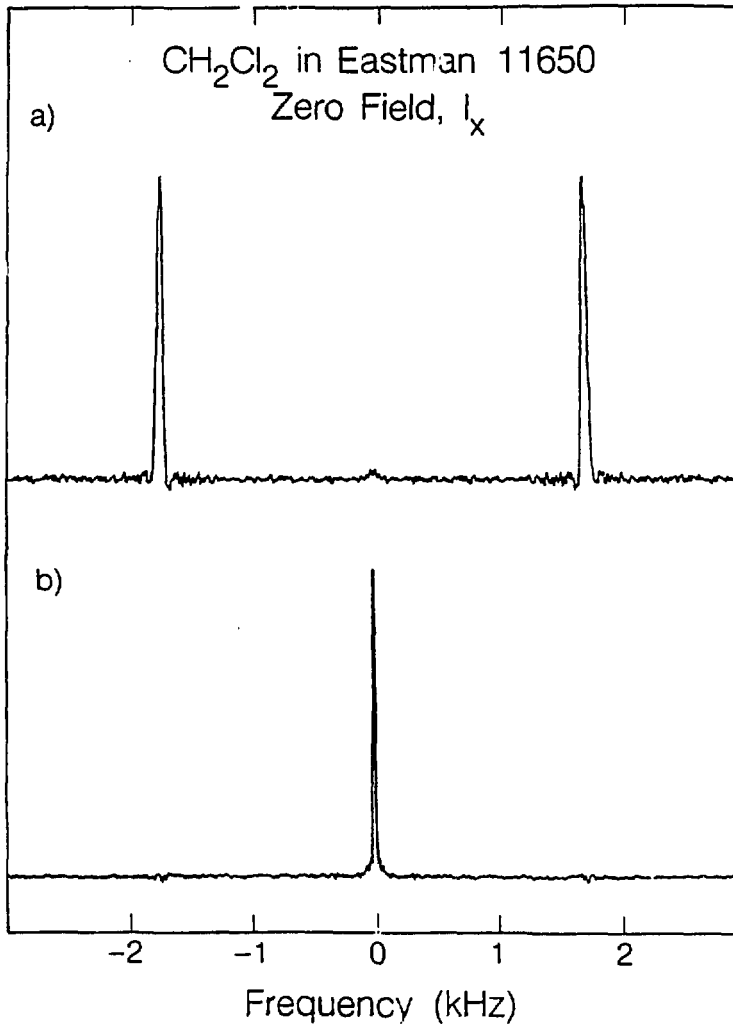
CH_2Cl_2 in Eastman 11650
Zero Field, I_x
a)
b)
−2
−1
0
1
2
Frequency (kHz)

XBL 859-9004

P and P′ in Figure 7.1b were determined by a calibration procedure described previously.[8] The spectra consist of 2 lines corresponding to either the zero frequency or $\pm\nu_D$ lines of the polycrystalline case. Calculation of the order parameter of the solute from the zero field spectrum yields S=0.054±0.001.

IV. Spin Hamiltonian in High Field

The behavior of the liquid crystal system in high and zero field experiments may be understood if one considers the Hamiltonian and the initial condition. The dipolar Hamiltonian in the average director frame may be written in spherical tensor notation as[18]

$$H_D = \sum_{m,m'=-2}^{2} (-1)^m T_{2,-m} A_{2,m'} < D^2_{m',m}(\Omega) > \qquad (7.1)$$

here $T_{2,m}$ and $A_{2,m'}$ represent director frame spin operators and principal axis system (PAS) spatial variables, respectively, and the $D^2_{m',m}(\Omega)$ effects the transformation between the two frames. The internuclear vector which is the z axis of the PAS frame is taken to be coincident with the z axis of the molecular frame. The brackets indicate a time average over the $D^2_{m',m}$ terms which accounts for fluctuations of the alignment of the molecular frame with respect to the director frame. Truncation of the spin part of the Hamiltonian by a large magnetic field leaves only the T_{20} term nonzero. Furthermore, only the m′=0 term of the traceless second rank tensor $A_{2,m'}$ is nonzero since the dipolar interaction is axially symmetric in the molecular/PAS frame. Therefore the effective high field dipolar Hamiltonian for a proton pair is given by[14,18]

$$H_D^o = T_{20}A_{20}S \qquad (7.2)$$
$$= \frac{\gamma_h^2}{4\pi^2 r^3} \cdot S(3I_{1z}I_{2z} - \vec{I}_1 \cdot \vec{I}_2)$$

where the order parameter S is given by

$$S = \langle D_{00}^2(\Omega) \rangle = 1/2 \langle \cos^2\beta - 1 \rangle \qquad (7.3)$$

and β is the instantaneous angle between the director and the proton-proton internuclear vector. The Hamiltonian of a dissolved solute will have the same form as that above. The NMR experiment then measures the degree of ordering of the solute molecular frame with respect to the average director orientation. In the presence of a large applied magnetic field, the director is aligned along the field and the director and lab frames coincide as illustrated in Figure 7.5a. The high field spectrum for a proton pair is then a two line spectrum due to the scaled dipolar coupling, and the order parameter of the solute, S, may be calculated from the observed splitting δ by $S=4\pi^2r^3\delta/3\gamma^2h$.[14]

V. Spin Hamiltonian in Zero Field

A) Aligned Systems.

The zero field director frame dipolar Hamiltonian for a molecule of the nematic is unchanged from that in high field and is equal to H_D^o of Equation 7.2. This is due to motional averaging about the average director which in an aligned system is oriented along the lab z axis, as in Figure 7.5b. Rotation about the long molecular axes and the uniaxial nature of the liquid crystal require that the indices m' and m in Equation 7.1 are both equal to zero.[19] In contrast to the high

Figure 7.5. Ordering in nematic liquid crystals. (a) The elongated molecules of the liquid crystal (ellipses) undergo rapid rotation about their long axes and fluctuations of these axes, thus having an average alignment with the director. In the presence of a magnetic field, B, the average orientation of the director (shown by the arrow) will be aligned along the magnetic field direction, B. (b) Order in the nematic remaining immediately after removal of the field. The sample maintains its average alignment along the laboratory z axis. Due to the rotational motions and symmetry of the liquid crystals, the dipolar Hamiltonian will also be truncated with respect to the z axis in the absence of a magnetic field. (c) Dealigned system showing local domain structure. The alignment of the local directors is no longer in the laboratory z direction. The average orientation of the molecules is described by the local directors. The dipolar Hamiltonian of a local domain is now truncated with respect to the local director.

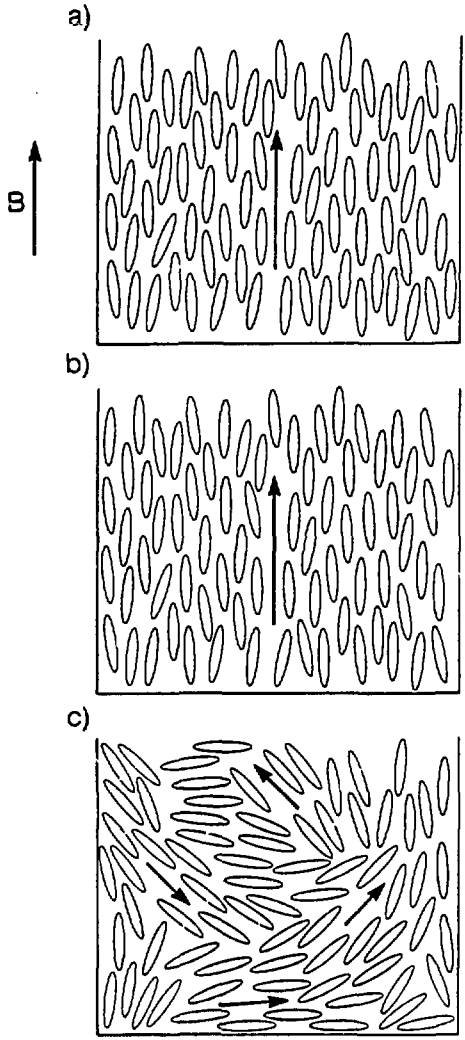

XBL 8510-9011

field case, the truncation is accomplished through the spatial terms of the Hamiltonian. Again the solute Hamiltonian will have the same form as that above since the nematic environment imposes a preferred orientation and motion.

The sudden experiment results reported above can now be interpreted.[6] Even in the absence of an applied field, a monoaligned sample with $\hat{n}$ aligned along the lab z direction, Figure 7.5b, will have a zero field Hamiltonian equal to the truncated lab frame dipolar Hamiltonian. The sudden switch-off of the intermediate field in the zero field experiment of Figure 7.1a initiates zero field evolution only if $[\rho_o, H_{zf}] \neq 0$. Since ρ_o is proportional to I_z before the transition, this condition is not met. No evolution occurs in zero field and the resulting spectrum for an ordered sample in zero field is simply a line at zero frequency.

The zero field spectrum of an aligned sample can still be obtained by use of a pulsed dc magnetic field to effectively change the initial condition from ρ_o proportional to I_z to some other operator that does not commute with H_D^o. In this case a pulse can be used to rotate the initial magnetization to the x-y plane of the laboratory frame. Given a magnetization along some axis in zero field, a dc magnetic field pulse of duration t_p applied perpendicular to that axis will rotate the magnetization by an angle θ given by[8]

$$\theta = \gamma B_{dc} t_p \tag{7.5}$$

If we define the direction of the dc field as the lab frame y and transform the initial density operator given above with a $\theta = \pi/2$ pulse

then the density operator will be proportional to I_x. Since $[H_D, I_x] \neq 0$ evolution is initiated. Exact calculation of the zero field interferogram for a two proton rod-like sample oriented in a liquid crystal subjected to the sudden z/pulsed y field cycle yields the normalized signal

$$S(t_1) = \cos^2\theta + \sin^2\theta \cos\omega_D t_1 \tag{7.6}$$

where θ is the angle of the dc pulse and for a liquid crystal system we define $\omega_D = 2\pi\nu_D$ by

$$\omega_D = S \cdot \frac{3h\gamma^2}{4\pi r^3} \tag{7.7}$$

in analogy with the polycrystalline case.[9,17] Resulting spectra obtained with the sudden z/pulsed y sequence may be seen in Figure 7.2 for different dc pulses. The molecular order parameter can be measured in zero field and is the same as that in high field within an experimental error based on the linewidths and small scale temperature fluctuations which may occur in the course of the experiment. The intensities in the experimental spectra have the same dependence on pulse angle as predicted by Eq. [7.6] for an ordered sample.

B)Dealigned Systems. The physical removal of the sample to low or zero fields might be expected to alter the alignment of the liquid crystal molecules. We consider the case where local ordering within a domain remains the same, while the alignment of the local directors of

these domains changes orientation, Figure 7.5c. If it is assumed that the locally allowed motions and fluctuations within a domain are the same in zero field as in the high field monodomain, then the director frame order parameter of the solute will be the same in high and zero fields since the director frame Hamiltonian is unchanged. The distributions of director orientations will manifest themselves as changes in the intensities and/or frequencies of the zero field lines. Thus ordered and disordered nematics may be distinguished by the characteristic appearance of their zero field spectra since the relative intensities of the zero field lines will be indicative of the degree of disordering. As shown earlier, molecules initially aligned along the z axis of the lab frame with ρ_o proportional to I_z produce only a central line in the zero field dipolar spectrum. When the magnetization is rotated to the x-y plane, as with a dc pulse, only the outer lines of the zero field spectrum result. General orientations will produce contributions of different intensities to the three lines. In the limit of an isotropic distribution of the local directors, the normalized zero field signal for the sudden experiment or the sudden z/pulsed y version with both dc pulses equal to 90° is given by

$$S(t_1) = 1/3[1 + 2\cos\omega_D t_1] \qquad (7.8)$$

which is the same form as that predicted for the proton pairs in a polycrystalline hydrate[9,17].

VI. Other Pulsed Zero Field Experiments

A) Demagnetization Experiments.

Further studies were also performed to observe the effect of complete demagnetization on the liquid crystal system. The field cycle, shown in Figure 7.6a, consists of demagnetization to zero field combined with a pulsed version of the experiment.[8,9] A spin temperature argument suggests that the density operator describing the initial demagnetized state in an aligned sample should be proportional to I_z since the motionally averaged dipolar and Zeeman Hamiltonians commute[20]. This predicts the zero field signal will be described by Eq. [7.6]. This is confirmed experimentally since spectra produced with the same dc pulses appear identical to those in Figure 7.4. Thus the resulting state is not one characteristic of a demagnetized sample. If the demagnetization were to produce an initial condition other than I_z then one expects an entirely different functional dependence for $S(t_1)$.

B) Echo Experiments.

The effects of residual z fields on the linewidths can be decreased in any of the zero field experiments described by employing a transverse dc π pulse to form a zero field echo. Figure 7.7 shows the results of a 180° refocussing pulse applied in the middle of the evolution period which is illustrated in the demagnetization sequence of Figure 7.6b. As expected this variation of the Hahn spin echo experiment[21] yields decreased linewidths which are measured here as ~15 Hz. Lines at one half the zero field frequency appear as artifacts in this echo spectrum and can be accounted for by imperfections in the dc pulses.

C) Dipolar and Double Quantum Order in Zero Field

Figure 7.6. Other zero field experimental field cycles used in the study of liquid crystals. a) After demagnetization to zero field, dc pulses are used to initiate and terminate the zero field evolution period t_1. The zero field interferogram $S(t_1)$ is collected after remagnetization to high field. (b) Same field cycle as (a) except that the t_1 period is now divided by a 180° refocussing pulse. This pulse removes the effect of residual field inhomogeneities in the z direction. (c) Zero field dc pulse sequence for the production of dipolar order in zero field. The directions of the dc pulsed fields are shown. The sequence 90_x-τ-45_y takes the initial state of I_z to one of dipolar and double quantum order in the lab frame. After the delay Δ, the 45_y pulse transforms the state into observable transverse magnetization. Application of a 90_x pulse and the z field allows for observation of this evolution as a function of t_1 in high field.

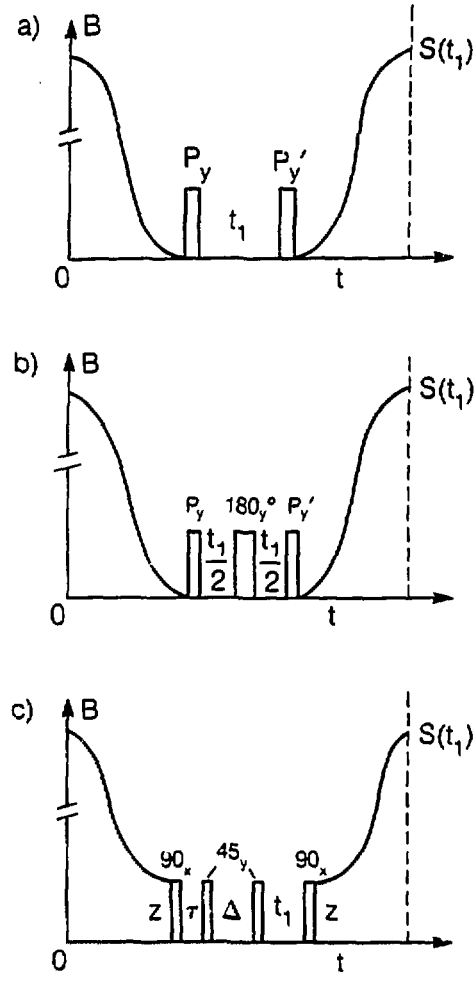
a)
B
$S(t_1)$
P_y
P_y'
t_1
0
t
b)
B
$S(t_1)$
P_y
$180_y°$
P_y'
$\frac{t_1}{2}$
$\frac{t_1}{2}$
0
t
c)
B
$S(t_1)$
90_x
45_{y_1}
90_x
z
τ
Δ
t_1
z
0
t

XBL 859-9008

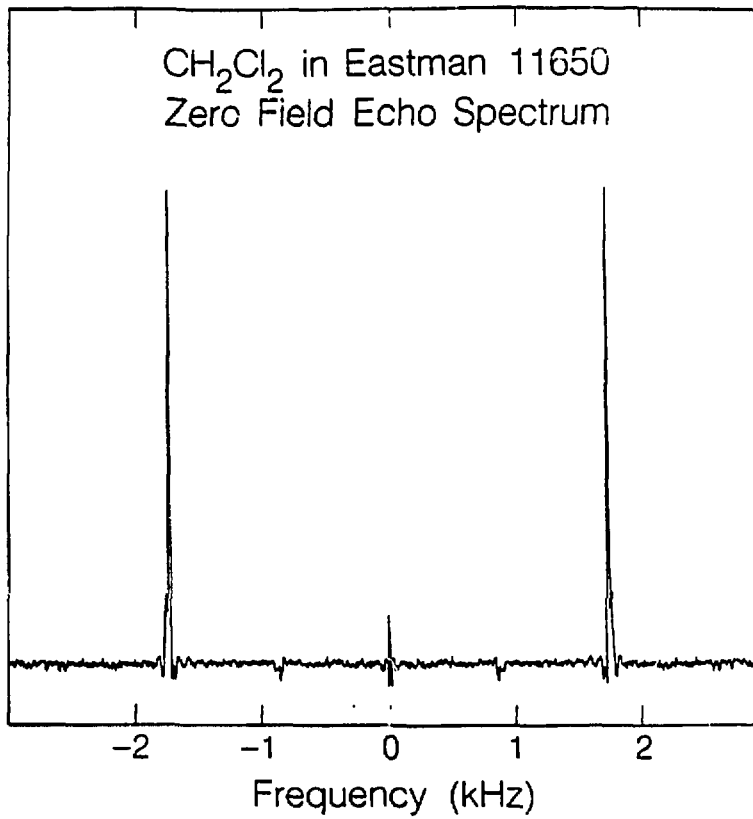

XBL 859-9007

Figure 7.7. Zero field echo spectrum of CH_2Cl_2/11650. The zero field spin echo sequence, figure 6b, removes the effect of residual fields. Shown is the spectrum using the dc pulse sequence 90°_{x}-$\tau_1/2$-180°_{x}-$\tau_1/2$-270°_{x}, where all pulses are applied along the laboratory y axis. A linewidth of ~15 Hz is obtained. The lines at one half the dipolar frequency and zero frequency are artifacts due to dc magnetic field pulse imperfections.

The zero field Hamiltonian in the laboratory frame is identical to that of the secular dipolar Hamiltonian in a high field rotating frame at resonance. With this understanding of the Hamiltonian and behavior of an aligned nematic in zero field, we have attempted application of multiple dc pulse sequences in zero field. A zero field version of the Jeener-Brokaert[22] sequence was performed, but unlike high field NMR techniques, separate coils were used for each orthogonal pulse direction. Using the field cycle of Figure 7.6c, the sample was demagnetized to an intermediate field then suddenly demagnetized to zero field where the pulse sequence 90_x-τ-45_y-Δ-45_y-t_1-90_x was applied. Immediately after the final 90_x dc pulse the sample was remagnetized suddenly and the high field signal recorded as a function of t_1. The preparation part of the sequence (up until the first 45_y) has the effect of creating a density operator given by

$$\rho = \rho_{H_D} + \rho_{DQ} \tag{7.9}$$

which contains both a dipolar order term and a double quantum term[23]. Methods for the separation of the dipolar order and double quantum (10)terms have been devised for high field versions of the Jeener-Brokaert experiment,[24] and these phase cycling techniques can in principle be extended to zero field as well. Here the delay Δ used in the sequence was chosen to be long enough to allow the double quantum coherence to decay to zero. Accumulation of the high field magnetization as a function of t_1 yields the interferogram of Figure 7.8a. As expected the signal arising from the created dipolar order grows in sinusoidally in t_1. Fourier transformation of the signal produces the spectrum shown in Figure 7.8b.

Figure 7.8. Interferogram from the zero field version of the Jeener-Brokaert[22] experiment using the pulse sequence shown in Figure 7.6c. The τ used in the preparation of dipolar order was 160 μsec and the delay Δ was chosen to be 20 msec to allow for the decay of any double and single quantum coherences. The sinusoidal appearance of the interferogram, $S(t_1)$, is as expected for the conversion by a 45°_{y} pulse of the dipolar order to observable single quantum coherence. Fourier transformation of the interferogram yields the dispersive zero field spectrum shown below consisting of lines of centered at $\pm\nu_D$. The linewidths and splittings of the zero field lines may be attributed to dc pulse imperfections and residual fields.

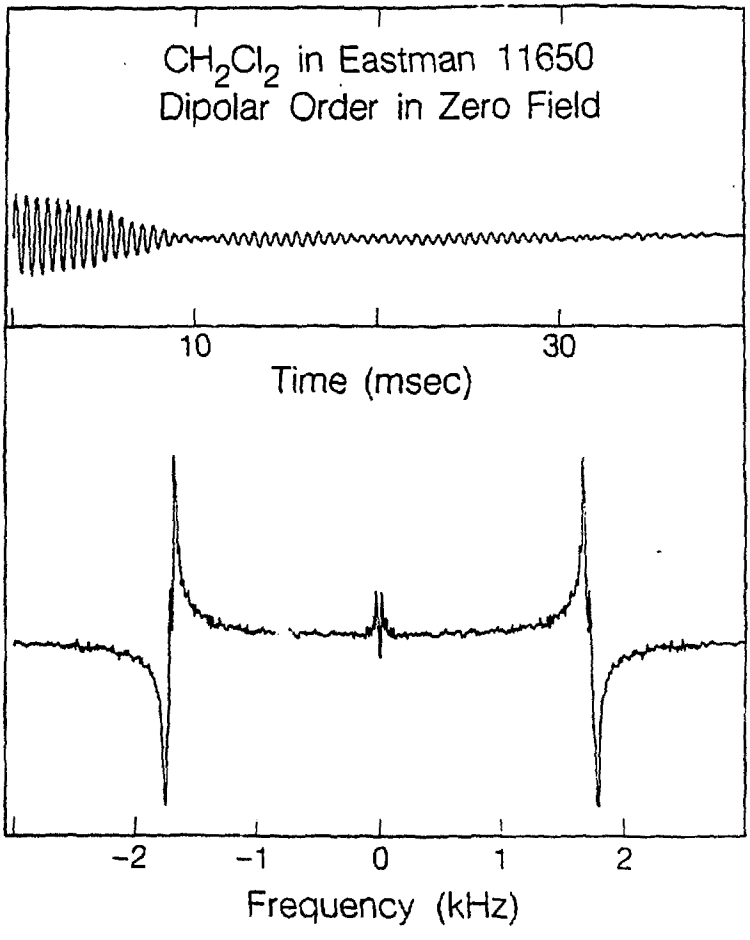
CH_2Cl_2 in Eastman 11650
Dipolar Order in Zero Field
10
30
Time (msec)
−2
−1
0
1
2
Frequency (kHz)

XBL 859-9003

VII. Conclusions

The molecular order parameter of a CH_2Cl_2/11650 nematic liquid crystal sample has been measured in high and zero field and has been found to be the same in both cases and does not differ by more than an experimental error of 2%. Several conclusions can be reached based on the frequencies and intensities in the zero field spectra, and the apparent dependence of the signal on the dc pulses used. Due to the short duration and relatively low fields used for the dc magnetic field pulses, only the spin states are perturbed and not the spatial ordering of the liquid crystal molecules. Most notably, we observe that the CH_2Cl_2/11650 system studied does not disorder in low ($\leq$200 G) or zero fields in times on the order of 10-500 msec. The zero field spectra are indicative of an aligned system and show no change in the order parameter from high field. Experimental evidence[25] suggests that fields of the order of 1 kG need be applied to change the alignment of the molecules in a time on the order of seconds. On that basis nematic liquid crystals may be expected to remain aligned in zero field on relatively long timescales, unless some perturbation such as the application of an appropriately large field causes more rapid reorientation of the sample.

We note as an experimental verification of the stability of the sample under field cycling conditions that no appreciable change was found in the high field spectrum and order parameter after demagnetization and immediate remagnetization. The possibility of complete disordering and subsequent reordering in the time of the field cycle is ruled out by the results of these zero field experiments.

In general, demagnetization experiments of nonoriented samples are expected to produce initial conditions other than I_z. However, due to the unchanged ordering and molecular motions of the CH_2Cl_2/nematic system in the demagnetization experiment, the magnetization remains quantized along the lab z axis. Thus demagnetization experiments on the nematic system produce an initial condition no different than that in experiments utilizing an intermediate field to maintain the spin order. DC pulses applied along various directions of the laboratory frame may then be successfully used to produce a new spin order. This encourages further applications of composite pulses[26], decoupling sequences and other multiple pulse techniques in zero field. Extensions are under way to use zero field NMR for the study of more complex systems such as smectics, discotics and lyotropics which do not order uniformly in an applied field. High field studies of these materials are hindered due to orientational disorder and thus might be usefully studied in zero field.

VIII. References

1. G. Meier, E. Sackman, and J.G. Grabmaier, Applications of Liquid Crystals (Springer Verlag, Berlin, 1975).
2. I. Haller and J. D. Litster, Phys. Rev. Lett. 25, 1550(1970); I. Haller and J. D. Litster, Mol. Cryst. Liq. Cryst. 12, 277(1977).
3. E. G. Hanson and Y. R. Shen, Mol. Cryst. Liq. Cryst. 36, 193(1976); W.H. de Jeu and P. Bordewijk, J. Chem. Phys. 68, 109(1978).
4. T. W. Stinson and J. D. Litster, Phys. Rev. Lett. 25, 503(1970).
5. J. C. Powell, W. D. Phillips, L. R. Melby and M. Panar, J. Chem. Phys. 43, 3442(1965); H. Gasparoux, B. Regaya and J. Prost, C. R. Acad. Sci.B. 272, 1168(1971).
6. M. Warner, Mol. Phys. 52, 677(1984).
7. P. R. Luyten, J. Bulthuis, W. M. M. J. Bovee, and L. Plomp, J. Chem.Phys. 78, 1712(1983).
8. J. M. Millar, A. M. Thayer, A. Bielecki, D. B. Zax and A. Pines, J. Chem.Phys. 83, 934(1985).
9. D. B. Zax, A. Bielecki, K. W. Zilm, A. Pines and D. P. Weitekamp; in press J. Chem. Phys.
10. R. Kreis, D. Suter and R. R. Ernst, Chem. Phys. Lett. 118, 120(1985).
11. P.Diehl and C.L. Khetrapal, NMR Basic Principles and Progress (1969), Volume 1; C.L. Khetrapal A. C. Kunwar, A. S. Tracey and P. Diehl, NMR Basic Principles and Progress, (1975), Volume 9.
12. J.G. Snijder, C.A. de Lange and E.E. Burnell, Isr. J. Chem. 23, 269(1983).
13. A. Saupe and G.Englert, Phys. Rev. Lett. 11, 462 (1963).
14. P.G. de Gennes, The Physics of Liquid Crystals (Clarendon Press, Oxford,1974).
15. A. Bielecki, D.B. Zax, K.W. Zilm and A. Pines, submitted to Rev. Sci.Instr.
16. A. Kumar, J. Magn. Reson. 30, 227(1978).
17. D.P. Weitekamp, A. Bielecki, D. Zax, K. Zilm and A. Pines, Phys. Rev.Lett. 50, 1807 (1983).
18. U. Haeberlen, High Resolution NMR in Solids, Selective Averaging,

Advances in Magnetic Resonance, Supplement 1, (Academic, New York, 1976); M. Mehring, Principles of High Resolution NMR in Solids, (Springer, Berlin, 1983).

19. J. W. Doane, Magnetic Resonance of Phase Transitions, F. J. Owens, C. P. Poole and H. A. Farach, editors, (Academic Press, New York, 1979)
20. M. Goldman, Spin Temperature and Nuclear Magnetic Resonance in Solids (Oxford, London, 1970).
21. E.L. Hahn, Phys. Rev. 80, 580 (1950).
22. J. Jeener and P. Brokaert, Phys. Rev. A 157, 232 (1969); J. Jeener, H. Eisendrath and R. van Steenwinkel, ibid, 478, 133 (1974).
23. S. Vega, J. Chem. Phys. 68, 5518 (1978).
24. S. Emid, J. Konijnendijk, J. Smidt and A. Pines, Physica B 100, 215 (1980).
25. R. A. Wise, A. Olah and J.W. Doane, J. de Phys. C1, 36, 117 (1975).
26. M. H. Levitt and R. Freeman, J. Magn. Reson. 43, 65(1981).